Pair-mixing induced Time-reversal-breaking superconductivity

Saswata Mandal¹ and Chao-Xing Liu*¹

¹Department of Physics, The Pennsylvania State University, University Park, Pennsylvania 16802, USA (Dated: November 19, 2025)

Experimental evidences of spontaneous time-reversal (TR) symmetry breaking have been reported for the superconducting ground state in the transition metal dichalcogenide (TMD) superconductor $4H_b$ -TaS₂ or chiral molecule intercalated TaS₂ hybrid superlattices, and is regarded as the evidence of the emergent chiral superconductivity. However, the T_c of these TMD superconductors is at the same order as pristine 1H or 2H-TaS₂ that does not show any signature of TR breaking and is believed to be conventional Bardeen–Cooper–Schrieffer superconductors. To resolve this puzzle, we proposed a new type of pair-mixing states that mix the dominant conventional s-wave pairing channel with the subdominant chiral p-wave pairing channel via the finite Cooper pair momentum based on the symmetry analysis of the Ginzburg-Landau theory. Our analysis shows the fourth order terms in the chiral p-wave channel can lead to a variety of pair-mixing states with spontaneous TR breaking. These TR-breaking superconducting states also reveal zero-field junction-free superconducting diode effect that is observed in chiral molecule intercalated TaS₂ superlattices.

Introduction— In the Bardeen-Cooper-Schrieffer (BCS) theory, the conventional s-wave spin-singlet pairing state preserves time-reversal (TR) symmetry. Spontaneous TR breaking in superconductors (SCs) when observed, is widely considered as a hallmark of unconventional superconductivity. Experimental evidence of TR breaking has been reported in a variety of superconducting (SC) materials, including Sr₂RuO₄[1, 2], $LaNiC_2[3, 4]$, $LaNiGa_2[5, 6]$, $UTe_2[7-10]$, other heavyfermion SCs [11-16], cuprates [17-20], iron based SCs [21–24] and others[25–28]. More recently, experimental evidence of TR breaking, including non-zero μ SR signal below $T_c[29]$, the existence of magnetic memory below T_c [30], π -phase shift in Little-Parks effect and zero-field superconducting diode effect (SDE)[31, 32], has been identified in a class of transition metal dichalcogenide (TMD) SCs, notably 4Hb-TaS₂[29, 33–39] and chiral molecule intercalated TaS₂ hybrid superlattices[31]. These experimental observations motivate theoretical speculation regarding the potential existence of chiral superconductivity in TaS_2 compounds[29–32, 40–45]. However, spontaneous TR breaking has not been observed in the pristine 1H or 2H-TaS₂ films, which are generally considered conventional s-wave BCS SCs[30, 46–48] with Ising-type of spin-orbit coupling, similar to other TMD SCs [49–51]. 4Hb-TaS₂ consists of alternating 1H and 1T TaS₂ layers and exhibits the transition temperature T_c around 2.7 K [29, 40, 41]. This value is comparable to $T_c \sim$ 2.2 K observed in 2H-TaS₂ [52, 53], implying that superconductivity in 4Hb-TaS₂ is likely to originate from the 1H TaS₂ layers. Similarly, superconductivity in chiral molecule intercalated TaS₂ hybrid superlattices should also originate from 1H-TaS₂ layers[31]. This raises a fundamental question: whether the pairing state in 4Hb-TaS₂ and chiral molecule intercalated TaS₂ belongs to the conventional Ising type of BCS state, or the unconventional TR-breaking chiral SC state.

We note that, compared to the pristine 1H or 2H- TaS_2 films, 1T- TaS_2 layers in 4Hb- TaS_2 and chiral molecule intercalation layers lower the local symmetry of 1H- TaS_2

layer. In 4Hb-TaS₂, a chiral charge density wave exists in the 1T-TaS₂ layers[54], accompanied with lattice distortion that cause the distances between the 1H-TaS₂ layer and its two adjacent 1T-TaS₂ layers to become unequal[55], which breaks the local mirror symmetry along the z-axis. Similarly, in Ref. [31], the intercalation of chiral molecules between 1H-TaS₂ layers also breaks any local mirror or inversion symmetry. As different pairing channels in SCs can be classified by irreducible representations (irrep) of the crystal symmetry group [56], lowering crystal symmetry will allow the mixing of different pairing channels [57–64]. This motivates us to explore the possibility of the pair-mixing between BCS state and chiral SC state in these TaS₂ systems.

In this work, based on the analysis of Ginzburg-Landau (GL) theory, we theoretically propose a finitemomentum-assisted pair-mixing state with dominant conventional s-wave pairing channel belonging to the A irrep and a secondary multi-component chiral pairing channel belonging to the E irrep of the magnetic point group (MPG) 31' [65-67] in 4Hb-TaS₂ and chiral molecule intercalated TaS₂. We demonstrate that the sub-dominant multi-component E pairing can induce TR breaking via the finite orbital angular momentum of the Cooper pairs. As an example, we discuss the TR-breaking vortex-antivortex phase and TR-preserving rotation-breaking stripe phase, and identify the SC phase diagram for these two SC phases as a function of GL parameters. We also demonstrate the existence of the SDE in the TR-breaking vortex-antivortex phase. Our theory illustrates the complex interplay between chiral structures that lower local crystal symmetry and spontaneous TR breaking in such SC compounds.

Pair-mixing states with a finite Cooper pair momentum - Instead of 3D TaS₂ systems, we consider a minimal model of a 1H-TaS₂ SC monolayer sandwiched by two insulating layers in this work, as depicted in Fig.1(a). Here the insulating layers correspond to 1T-TaS₂ layer with the chiral CDW in 4Hb-TaS₂ [29, 30] or the chiral molecule intercalation layer[31]. The insulating layers

break all mirror symmetries of $1H \text{ TaS}_2$ monolayer and thus are dubbed "chiral layers" below.

We first consider the symmetry classification of pairing channels for this sandwich structure. The 1H-TaS₂ monolayer is described by MPG $\bar{6}m2.1'$, including D_{3h} point group and TR symmetry [29]. The chiral layers are expected to break all mirror symmetries, and thus reduce the symmetry group to MPG 31' with only C_{3z} and TR [65–67]. Table I lists the irrep for different pairing channels of MPG 31'. Similar to other TMD SCs, experiments on pristine TaS₂ have revealed s-wave pairings with TR symmetry [29, 31, 47], naturally belonging to the A irrep in Table I. In $4H_b$ TaS_2 and chiral molecule intercalated TaS₂, a variety of experiments have revealed the evidence of spontaneous TR breaking [29-32] or nematic phases [40], necessitating the presence of multicomponent order parameter [28, 68–70]. In Table I, only the pairing channel with the ${}^{1}E^{2}E$ irrep (called E-irrep below) is two-dimensional and can host both the chiral and nematic phases. As a comparison, we also discuss the pairing symmetry classification for MPG $\bar{6}m2.1'$, as well as the compatibility relation, in SM [71] Table II and III.

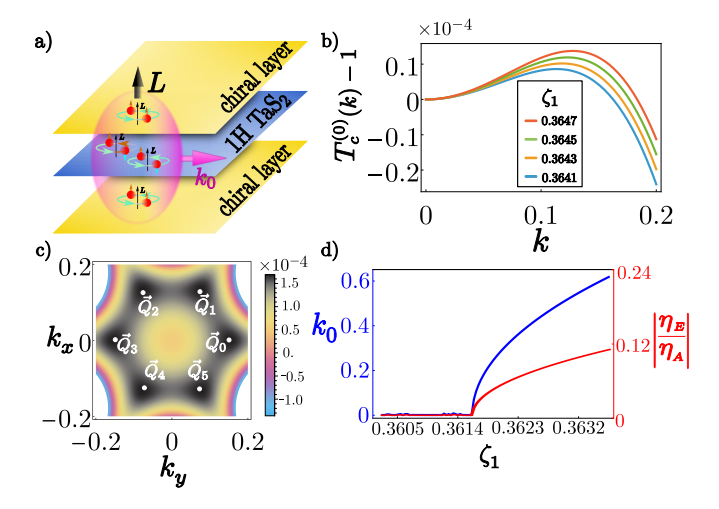


FIG. 1. (a) Schematics of 1H-TaS₂ layer sandwiched between chiral layers formed by either 1T-TaS₂ layer or chiral molecule layers. The s-wave singlet pairing in 1H-TaS₂ layer are mixed with p-wave triplet pairing in chiral layers at a finite momentum \mathbf{k}_0 . (b) $T_c^{(0)}(k)-1$ as a function of k with $T_{c,A}=2.7K, T_{c,E}=2K, \gamma_A=0.076, \gamma_E=0.01$ at different values of ζ_1 . (c) Color denotes $T_c(\mathbf{k})-1$ as a function of \mathbf{k} with $\zeta_2=\zeta_4=0.13,\ \zeta_1=0.3643,$ and all other parameters set to be same as (b). \mathbf{Q}_n with $n\in\mathbb{Z}_6$ labels six momenta for the maximal $T_c(\mathbf{k})$. (d) The blue and red curves depict the k_0 and the ratio $\left|\frac{\eta_E}{\eta_A}\right|$ as a function of ζ_1 , respectively, with the parameters to be the same as (b). All quantities above have been regularized to be dimensionless.

We search for possible pair-mixing between BCS (A) and chiral pairing (E), as schematically shown in Fig.1(a). At zero Cooper pair momentum $(\mathbf{k} = 0)$, crystal symmetry forbids the mixing between the pair-

ing channels that belong to different irreps. However, this obstacle can be overcome by considering a finite center-of-mass Cooper pair momentum \mathbf{k} . Table I also lists the irreps for k-polynomials, in which we notice $i\{k_+^{3n+1},k_-^{3n+1}\}$ and $\{k_+^{3n+2},k_-^{3n+2}\}$ for any integer n also belong to the E irrep. Since $E\otimes E=2A\oplus E$, we can construct pair-mixing terms invariant under MPG 31' as

$$\mathcal{F}_{A-E} = \sum_{\mathbf{k}} \eta_A^* (i\zeta_1^* k_- + \zeta_2^* k_+^2 + \zeta_4^* k_-^4) \eta_{E,+}$$

$$+ \eta_A^* (i\zeta_1 k_+ + \zeta_2 k_-^2 + \zeta_4 k_+^4) \eta_{E,-} + h.c.$$
(1)

up to k^4 orders, where η_A and $\eta_{E,\pm}$ denote the SC order parameters for the A-irrep channel and two components of E-irrep channel, respectively [56], ζ_n is the parameter of the k_{+}^{n} term for n=1,2,4. To be more concrete, we consider s-wave spin-singlet pairing (is_y) for the A channel η_A and p-wave spin-triplet pairing $(p_{\pm}(s_z \pm s_0))$ for the E channel $\eta_{E,\pm}$ in MPG 31'. For these pairing channels, we note that the pair-mixing terms \mathcal{F}_{A-E} in Eq.(1) cannot exist for MPG $\bar{6}m2.1'$ due to the mirror symmetry M_z along the z axis. As discussed in SM[71] Sec.A, the p-wave triplet pairing, order parameter $\eta_{E,\pm}$ is odd under M_z , whereas the spin-singlet pairing η_A and any momentum polynomial of k_{\pm} are even under M_z . Therefore, the existence of \mathcal{F}_{A-E} in Eq.(1) requires to break M_z symmetry in MPG $\bar{6}m2.1'$. Up to the quadratic terms, the GL free energy is written as $\mathcal{F}^{(2)} = \mathcal{F}_A^{(2)} + \mathcal{F}_E^{(2)} + \mathcal{F}_{A-E}^{(2)}$, where $\mathcal{F}_A^{(2)}$ and $\mathcal{F}_E^{(2)}$ are the standard quadratic terms for the A and E channels, respectively (See SM[71] Sec.A for details). From $\frac{\partial \mathcal{F}^{(2)}}{\partial \eta_{\Gamma}(\mathbf{k})^*} = 0$ with $\Gamma = A, E+, E-$, the linearized GL-equation can be derived as

$$(\tilde{T} - M(\mathbf{k}))\Psi(\mathbf{k}) = 0,$$

$$M(\mathbf{k}) = \begin{pmatrix} t_E & -\mu_1^*(\mathbf{k}) & 0\\ -\mu_1(\mathbf{k}) & t_A & -\mu_2(\mathbf{k})\\ 0 & -\mu_2^*(\mathbf{k}) & t_E \end{pmatrix}$$
(2)

where $t_{\Gamma=E,A} = \tilde{T}_{c,\Gamma} - \tilde{\gamma}_{\Gamma}\tilde{k}^2$, $\mu_1(\mathbf{k}) = i\tilde{\zeta}_1^*\tilde{k}_- + \tilde{\zeta}_2^*\tilde{k}_+^2 + \tilde{\zeta}_4^*\tilde{k}_-^4$, $\mu_2(\mathbf{k}) = i\tilde{\zeta}_1\tilde{k}_+ + \tilde{\zeta}_2\tilde{k}_-^2 + \tilde{\zeta}_4\tilde{k}_+^4$ and $\Psi(\mathbf{k}) = \{\eta_{E,+}(\mathbf{k}), \eta_A(\mathbf{k}), \eta_{E,-}(\mathbf{k})\}^T$ is the eigen-vector. We have rescaled all the parameters with tilde to be dimensionless by $\tilde{T} = T/T_{c,A}$, $\tilde{\gamma}_{\Gamma} = \frac{\gamma_{\Gamma}}{\tilde{\alpha}_{\Gamma}}$, $\tilde{\mathbf{k}} = \frac{k}{\sqrt{T_{c,A}/\tilde{\gamma}_A}}(\cos\theta, \sin\theta)$, $\tilde{\zeta}_1 = \frac{\zeta_1}{\sqrt{\tilde{\alpha}_A\tilde{\alpha}_E\tilde{\gamma}_AT_{c,A}}}$, $\tilde{\zeta}_2 = \frac{\zeta_2}{\tilde{\gamma}_A\sqrt{\tilde{\alpha}_A\tilde{\alpha}_E}}$, $\tilde{\zeta}_4 = \frac{\zeta_4T_{c,A}}{\tilde{\gamma}_A^2\sqrt{\tilde{\alpha}_A\tilde{\alpha}_E}}$. The rescaling quantities $\tilde{\alpha}_{\Gamma}$ and $T_{c,\Gamma}$ are defined from the coefficient of the quadratic term in $\mathcal{F}^{(2)}$ before rescaling, namely $\alpha_{\Gamma} = \tilde{\alpha}_{\Gamma}(T - T_{c,\Gamma})$ (See Eq.(A28) in SM Sec.A). Below we always choose the dimensionless quantities after rescaling and have dropped the notation of tilde for all the parameters in Eq.(2). The nonzero solution of linearized GL-equation requires $\mathrm{Det}(T\mathbb{I} - M(\mathbf{k})) = 0$, which gives rise to (See SM[71] Sec.A for details)

$$T_c(\mathbf{k}) = T_c^{(0)}(k) + \Delta T^{(1)}(k, \theta),$$
 (3)

where $T_c^{(0)}(k)$ is the isotropic part and $\Delta T^{(1)}(k,\theta)$ de-

pends on the momentum angle θ . We have already chosen the largest solution when solving $T(\mathbf{k})$. The critical temperature T_c is determined from the maximal value of $T(\mathbf{k})$ with respect to \mathbf{k} in Eq.(3), i.e. $T_c = \max_{\mathbf{k}} T_c(\mathbf{k})$. For the isotropic part $(\zeta_2 = \zeta_4 = 0)$, Fig.1(b) shows $T_c^{(0)}(k)$ as a function of k for different values of ζ_1 . The maximum of $T_c^{(0)}(k)$ appears at k = 0 for a small ζ_1 , while with increasing ζ_1 above the critical value ζ_{1c} , the maximum of $T(\mathbf{k})$ is shifted to a finite momentum, denoted as k_0 . The dependence of k_0 with respect to ζ_1 is shown by the blue curve in Fig.1(d). In the isotropic case $(\zeta_2 = \zeta_4 = 0)$, the eigenvector solution $\Psi^{(0)}(\mathbf{k})$ can be analytically solved as

$$\Psi^{(0)}(\mathbf{k}) = \begin{pmatrix} \eta_{E,+}^{(0)}(\mathbf{k}) \\ \eta_{A}^{(0)}(\mathbf{k}) \\ \eta_{E,-}^{(0)}(\mathbf{k}) \end{pmatrix} = \frac{1}{\sqrt{N(\mathbf{k})}} \begin{pmatrix} i\zeta_{1}k_{+} \\ T_{c}^{(0)}(k) - T_{c,E} - \gamma_{E}k^{2} \\ i\zeta_{1}^{*}k_{-} \end{pmatrix},$$

where $N(\mathbf{k})$ is the normalization factor. We next consider the first order correction of the anisotropic ζ_2 and ζ_4 terms, which acts on $\Psi^{(0)}(\mathbf{k})$ and gives rise to $\Delta T^{(1)}(\mathbf{k})$. $\Delta T^{(1)}(\mathbf{k})$ splits the T_c for different θ values and results in six momenta, namely $\{\mathbf{Q}_n =$ $k_0\cos(2n\pi/3)\hat{e}_x + k_0\sin(2n\pi/3)\hat{e}_y; \forall n \in \mathbb{Z}_6$ related by C_{3z} and \mathcal{T} of MPG31', for the critical temperature $T_c(\mathbf{Q}_n)$. A typical **k** dependence of $T_c(\mathbf{k})$ is shown in Fig.1(c) with six \mathbf{Q}_n labelled by the white dots. Strikingly, for $\zeta > \zeta_{1c}$, the SC ground state is a mixture of the A and E pairing channels due to non-zero k_0 , as shown by the blue curve in Fig.1(d), $\underline{\text{and t}}$ he ratio $|\eta_E/\eta_A|$ with $|\eta_E| = \sqrt{|\eta_{E,+}^{(0)}(\mathbf{Q}_n)|^2 + |\eta_{E,-}^{(0)}(\mathbf{Q}_n)|^2}$ also becomes non-zero, as exhibited by the red curve in Fig.1(d). The pairing states at six \mathbf{Q}_n are degenerate for $\mathcal{F}^{(2)}$ and thus we need to consider the fourth-order terms to identify the possible SC ground states below.

TABLE I. Representation $(\mathcal{D}_{\mathcal{S}}^{\Gamma})$ table and basis functions for the symmetry operator \mathcal{S} in the little group at Γ of MPG31'. Here s_0 and τ_0 are 2-by-2 identity matrices while $s_{x,y,z}$ and $\tau_{x,y,z}$ are Pauli matrices. s is for Cooper pair spin while τ is for the basis of the 2D E irrep. $p_{\pm} = p_x \pm i p_y$ is the relative momentum of Cooper pair, whereas $k_{\pm} = k_x \pm i k_y$ is the center-of-mass momentum.

$\operatorname{Irrep}(\Gamma)$	Basis functions	\mathcal{D}_E^Γ	$\mathcal{D}^{\Gamma}_{C_{3z}}$	$\mathcal{D}^{\Gamma}_{\mathcal{T}}$
A	$is_y, is_x, i^{\frac{1\pm1}{2}} \{ p_+(s_0 - s_z) \pm p(s_0 + s_z) \}$	1	1	1
$^{1}E^{2}E$		$ au_0$	$e^{i\frac{2\pi}{3}\tau_z}$	$ au_x$

Time-Reversal-Breaking Pair-Mixing States - For $\zeta > \zeta_{1c}$, the eigen-states $\Psi^{(0)}(\mathbf{Q}_n)$ at six \mathbf{Q}_n span the U(6) subspace and the general form of this projected SC state should be a linear superposition of the eigen-vectors

within this subspace

$$\Psi_{\alpha}(\mathbf{r}) = \sum_{n \in \mathbb{Z}_6} P_{\mathbf{Q}_n} \Psi_{\alpha}^{(0)}(\mathbf{Q}_n) e^{i\mathbf{Q}_n \cdot \mathbf{r}}, \tag{5}$$

where $P_{\mathbf{Q}_n}$ is the expansion coefficient of the eigenstate $\Psi^{(0)}(\mathbf{Q}_n)$ and $\alpha=2$ for the A component and $\alpha=1,3$ for the E components of the pair function. Based on the MPG 31' and U(1) gauge invariance, the fourth-order terms within the U(6) subspace can be constructed as (See SM[71] Sec.B1) [72]

$$\mathcal{F}^{(4)} = c_0 \left[\left(\sum_{i \in \mathbb{Z}_6} |P_{\mathbf{Q}_i}|^2 \right)^2 \right] + c_1 \left[\sum_{i \in \mathbb{Z}_6} |P_{\mathbf{Q}_i}|^2 |P_{\mathbf{Q}_{i+1}}|^2 \right]$$

$$+ c_2 \left[\sum_{i \in \mathbb{Z}_6} |P_{\mathbf{Q}_i}|^2 |P_{\mathbf{Q}_{i+2}}|^2 \right] + c_3 \left[\sum_{i \in \mathbb{Z}_6} |P_{\mathbf{Q}_i}|^2 |P_{-\mathbf{Q}_i}|^2 \right]$$

$$+ c_4 \sum_{i \in \mathbb{Z}_6} P_{\mathbf{Q}_i} P_{-\mathbf{Q}_i} \left(P_{\mathbf{Q}_{i+1}}^* P_{-\mathbf{Q}_{i+1}}^* + P_{\mathbf{Q}_{i+2}}^* P_{-\mathbf{Q}_{i+2}}^* \right)$$

with five independent parameters c_i (i=0,...,4). Here c_0 is the isotropic term that does not split the U(6) subspace and we choose $c_0 \gg |c_i|$ (i=1,...,4) to ensure the positive definiteness of the GL free energy. To simplify the problem, we below consider $c_4=0$, and all the other terms $(c_{0,1,2,3})$ in the free energy only rely on the amplitude of $P_{\mathbf{Q}_n}$.

We first search for all possible local minima of the free energy $\mathcal{F} = \sum_n [T - T_c(\mathbf{Q}_n)] |P_{\mathbf{Q}_n}|^2 + \mathcal{F}^{(4)}$ by solving the GL equation $\frac{\partial \mathcal{F}}{\partial |P_{\mathbf{Q}_n}|} = 0$ with $n \in \mathbb{Z}_6$. The solution ansätze can be labelled by the vector $\mathcal{P}_{\lambda} = (P_{\mathbf{Q}_0}^{\lambda}, \cdots, P_{\mathbf{Q}_5}^{\lambda})^T$ with λ denoting different local minima. After obtaining all possible solutions, we can compare their minimal free energy $\mathcal{F}_{min,\lambda}$ and the lowest energy solution determines the SC ground state. Depending on different values of the c_i parameters (i = 0, 1, ..., 4), we find in total 9 possible inequivalent solutions for the SC ground state, denoted by $\lambda \in \{1, 2a, 2c, 3a, 3d, 4a, 4b, 5, 6\}$. In SM[71] Sec.B2, we provide a complete discussion on the vector form, physical meaning and symmetry properties of all these possible SC ground states.

Next we consider **phase 2c** and **3d** as an example. With the choice of the parameters $c_0 = 1, c_1 = c_2 < 0, c_4 = 0$, we find either **phase 2c** or **3d** to be the SC ground state, separated by the phase boundary at $c_3 = \frac{2c_2}{3}$ (See SM[71] Sec.B3 for detailed derivation), as shown in Fig.2(a). We also calculate the minimal free energies $\mathcal{F}_{min,2c}$ and $\mathcal{F}_{min,3d}$ for **phase 2c** and **3d**, as depicted by the blue and yellow lines in Fig.2(b), respectively, which are plotted along the dotted path shown in Fig.2(a). The energy crossing between these two phases suggests a first-order phase transition. **Phase 2c** is described by the vector $\mathcal{P}_{2c} = \frac{e^{i\theta}\Delta_0}{\sqrt{2}}(e^{i\phi_1},0,0,e^{-i\phi_1},0,0)^T$, where Δ_0 is the pairing strength, while θ and ϕ_1 are overall and relative phase factors, respectively. **Phase**

2c preserves \mathcal{T} but breaks C_{3z} and is a stripe phase with an oscillating order parameter amplitude shown in Fig.2(c). In contrast, **Phase 3d** is characterized by the vector $\mathcal{P}_{3d} = \frac{e^{i\theta}\Delta_0}{\sqrt{3}}(e^{i\phi_1}, 0, e^{i\phi_2}, 0, e^{-i(\phi_1 + \phi_2)}, 0)^T$, which preserves C_{3z} but breaks \mathcal{T} . The order parameter of Phase 3d forms a hexagonal lattice of vortex-antivortex pairs, thus dubbed vortex-antivortex phase [73, 74], as shown in Fig.2(d). The black hexagon in Fig.2(d) shows one unit cell of the hexagonal lattice with the order parameter amplitude dropping to a minimal value at six corners of the hexagon. The red arrows in Fig.2(d) reveal the local supercurrent flows that wind clockwise and counter-clockwise around each black hexagon corner (see the cyan and yellow small hexagons), thus leading to the formation of vortices and antivortices, respectively. The spontaneous TR breaking of Phase 3d can be exhibited by the z-directional orbital angular momenta for the p-wave components (E-irrep) of the order parameter [75– 77], $L_z(\mathbf{r}) = |\Psi_1(\mathbf{r})|^2 - |\Psi_3(\mathbf{r})|^2$, where $|\Psi_{1,3}(\mathbf{r})|$ denotes the real space E component of the order parameters, as defined in Eqs.(4) and (5) (See SM[71] Sec.B4). A nonzero $L_z(\mathbf{r})$ implying $\Psi_1(\mathbf{r}) \neq e^{i\alpha}\Psi_3(\mathbf{r})$ breaks TR since $\Psi_1(\mathbf{r})$ is changed to $\Psi_3(\mathbf{r})$ under \mathcal{T} . In Fig.2(e), the peak (red color) and dip (blue color) of $L_z(\mathbf{r})$ appear at six corners of the unit cell (black hexagon), suggesting that the p-wave components (E-irrep) of order parameter emerges when the s-wave component (A-irrep) is suppressed in the vortex cores.

Since our system contains chiral layers and thus is non-centrosymmetric, spontaneous TR breaking can potentially lead to zero-field junction-free SDE[31, 78–81]. Thus, we evaluate critical current $J_c(\theta)$ as a function of the angle θ of the current direction. Fig.2(f) depicts the normalized critical current $\mathcal{J}(\theta) = J_c(\theta)/J_c(0)$ for Phase 3d, which reveals a strong anisotropy with threefold rotation symmetry. Consequently, the SDE coefficient η , defined by $\eta = \frac{1-\mathcal{J}(\pi)}{1+\mathcal{J}(\pi)}$, jumps from zero in **Phase** 2c due to TR symmetry, to a large non-zero value in Phase 3d across the phase transition, as depicted by the red line in Fig.2(b). Non-zero η is also found in other TRbreaking phases, including Phase 2a, 3a, 4a and 4b, as discussed in SM[71] Sec.C. We note that the zero-field junction-free SDE has been reported in chiral molecule intercalated TaS₂[31], consistent with our TR-breaking phases. We further propose to distinguish different TRbreaking phases via examining the angular dependence of normalized critical current $\mathcal{J}(\theta)$ in SM[71] Sec.C.

Conclusion and Discussion - In this work, we proposed a pair-mixing mechanism for unconventional superconductivity with spontaneous TR breaking. This TR breaking SC phase is featured by a finite Cooper pair momentum and can be probed through the zero-field junction-free SDE. Although our theory is formulated for the 2D TaS_2 monolayer sandwiched between two chiral layers in Fig.1(a), we would expect similar physics occurs in bulk 4Hb- TaS_2 [29] and chiral molecule intercalated TaS_2 hybrid superlattices [31] once differ-

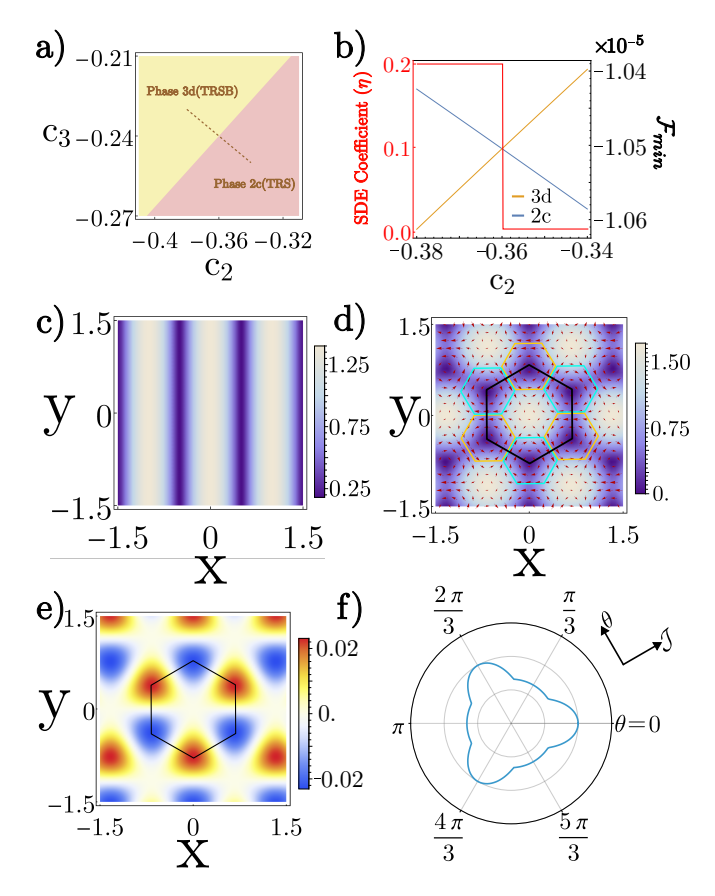


FIG. 2. (a) Phase diagram showing the stripe and vortexantivortex phases for $c_1 = c_2 < 0, c_0 = 1, c_4 = 0$. (b) Minimal free energy \mathcal{F}_{min} for **phase 2c** (blue curve for $\mathcal{F}_{min,2c}$) and **phase 3d** (yellow curve for $\mathcal{F}_{min,3d}$) across the dotted path in (a). Here \mathcal{F}_{min} is in units of $T_{c,A}$. The red curve represents the SDE coefficient η across the dotted path in (a). (c) and (d) represent the real space distribution $|\Psi(\mathbf{r})|$ of pair function for the Phase 2c and 3d, respectively. In (d), the black hexagon denotes the unit cell of vortex-antivortex lattice for Phase 3d, the red arrows depict the direction and magnitude of local supercurents, and the cyan and orange hexagons show the regions for vortcies and antivortices, respectively. (e) Distribution of $L_z(\mathbf{r})$ for **Phase 3d**. (f) Distribution of normalized critical current $\mathcal{J}(\theta)$ as a function of angle θ . Here we choose $\zeta_1 = 0.3647$ and all other parameters are same as Fig.1(b). All in-plane coordinates $\{x,y\}$ are in units of π/k_0 .

ent 1H TaS₂ layers in the bulk are decoupled, revealing quasi-2D SC behaviors. We also noticed that π -phase shift in Little-Parks experiments has also been observed in both TaS₂ systems[31, 32], providing another evidence of TR breaking, similar to that in superconductor/ferromagnet hetero-junctions [82–84]. The TR-breaking vortex-antivortex phase has also recently been proposed in rhombohedral graphene [74, 85]. However, there is one substantial difference. TR-breaking in rhombohedral graphene is from orbital magnetism and already exists above T_c , while TR-breaking only occurs spontaneously below T_c in our pair-mixing mechanism. This

pair-mixing mechanism also provides a new path for realizing TR breaking superconductivity via engineering the local chemical environment of conventional SC layers.

Acknowledgment - We would like to acknowledge D.

- F. Agterberg and H. Miao for the helpful discussions. SM and CXL acknowledge the support from the NSF-MERSEC (Grant No. MERSEC DMR 2011750).
- G. M. Luke, Y. Fudamoto, K. M. Kojima, M. I. Larkin, J. Merrin, B. Nachumi, Y. J. Uemura, Y. Maeno, Z. Q. Mao, Y. Mori, H. Nakamura, and M. Sigrist, Time-reversal symmetry-breaking superconductivity in Sr2RuO4, Nature 394, 558 (1998).
- [2] J. Xia, Y. Maeno, P. T. Beyersdorf, M. M. Fejer, and A. Kapitulnik, High resolution polar kerr effect measurements of sr₂ruo₄: Evidence for broken time-reversal symmetry in the superconducting state, Phys. Rev. Lett. 97, 167002 (2006).
- [3] A. D. Hillier, J. Quintanilla, and R. Cywinski, Evidence for time-reversal symmetry breaking in the non-centrosymmetric superconductor lanic₂, Phys. Rev. Lett. 102, 117007 (2009).
- [4] G. Csire, B. Újfalussy, and J. F. Annett, Nonunitary triplet pairing in the noncentrosymmetric superconductor lanic2, The European Physical Journal B 91, 217 (2018).
- [5] A. D. Hillier, J. Quintanilla, B. Mazidian, J. F. Annett, and R. Cywinski, Nonunitary triplet pairing in the centrosymmetric superconductor laniga₂, Phys. Rev. Lett. 109, 097001 (2012).
- [6] S. K. Ghosh, G. Csire, P. Whittlesea, J. F. Annett, M. Gradhand, B. Újfalussy, and J. Quintanilla, Quantitative theory of triplet pairing in the unconventional superconductor laniga 2, Physical Review B 101, 100506 (2020).
- [7] S. Ran, C. Eckberg, Q.-P. Ding, Y. Furukawa, T. Metz, S. R. Saha, I.-L. Liu, M. Zic, H. Kim, J. Paglione, et al., Nearly ferromagnetic spin-triplet superconductivity, Science 365, 684 (2019).
- [8] K. Ishihara, M. Roppongi, M. Kobayashi, K. Imamura, Y. Mizukami, H. Sakai, P. Opletal, Y. Tokiwa, Y. Haga, K. Hashimoto, et al., Chiral superconductivity in ute2 probed by anisotropic low-energy excitations, Nature Communications 14, 2966 (2023).
- [9] L. Jiao, S. Howard, S. Ran, Z. Wang, J. O. Rodriguez, M. Sigrist, Z. Wang, N. P. Butch, and V. Madhavan, Chiral superconductivity in heavy-fermion metal ute2, Nature 579, 523 (2020).
- [10] T. Metz, S. Bae, S. Ran, I.-L. Liu, Y. S. Eo, W. T. Fuhrman, D. F. Agterberg, S. M. Anlage, N. P. Butch, and J. Paglione, Point-node gap structure of the spin-triplet superconductor ute 2, Physical Review B 100, 220504 (2019).
- [11] E. Schemm, W. Gannon, C. Wishne, W. Halperin, and A. Kapitulnik, Observation of broken time-reversal symmetry in the heavy-fermion superconductor upt3, Science 345, 190 (2014).
- [12] K. E. Avers, W. J. Gannon, S. J. Kuhn, W. P. Halperin, J. Sauls, L. DeBeer-Schmitt, C. Dewhurst, J. Gavilano, G. Nagy, U. Gasser, et al., Broken time-reversal symmetry in the topological superconductor upt3, Nature Physics 16, 531 (2020).
- [13] R. Heffner, J. Smith, J. Willis, P. Birrer, C. Baines,

- F. Gygax, B. Hitti, E. Lippelt, H. Ott, A. Schenck, et al., New phase diagram for (u, th) be 13: A muon-spin-resonance and h_{C1} study, Physical review letters **65**, 2816 (1990).
- [14] E. Schemm, R. Baumbach, P. Tobash, F. Ronning, E. Bauer, and A. Kapitulnik, Evidence for broken timereversal symmetry in the superconducting phase of URu₂ Si₂, Physical Review B **91**, 140506 (2015).
- [15] Y. Aoki, A. Tsuchiya, T. Kanayama, S. R. Saha, H. Sugawara, H. Sato, W. Higemoto, A. Koda, K. Ohishi, K. Nishiyama, and R. Kadono, Time-reversal symmetry-breaking superconductivity in heavy-fermion pros₄sb₁₂ detected by muon-spin relaxation, Phys. Rev. Lett. 91, 067003 (2003).
- [16] A. Maisuradze, W. Schnelle, R. Khasanov, R. Gumeniuk, M. Nicklas, H. Rosner, A. Leithe-Jasper, Y. Grin, A. Amato, and P. Thalmeier, Evidence for time-reversal symmetry breaking in superconducting PrPt₄Ge₁2, Physical Review B—Condensed Matter and Materials Physics 82, 024524 (2010).
- [17] S. F. Zhao, X. Cui, P. A. Volkov, H. Yoo, S. Lee, J. A. Gardener, A. J. Akey, R. Engelke, Y. Ronen, R. Zhong, et al., Time-reversal symmetry breaking superconductivity between twisted cuprate superconductors, Science 382, 1422 (2023).
- [18] R. Kaur and D. Agterberg, Broken time-reversal symmetry and superconducting states in the cuprates, Physical Review B 68, 100506 (2003).
- [19] H. Weber, D. Weitbrecht, D. Brach, A. Shelankov, H. Keiter, W. Weber, T. Wolf, J. Geerk, G. Linker, G. Roth, et al., Evidence for broken time reversal symmetry in cuprate superconductors, Solid state communications 76, 511 (1990).
- [20] M. Simon and C. Varma, Detection and implications of a time-reversal breaking state in underdoped cuprates, Physical review letters 89, 247003 (2002).
- [21] K. Matsuura, M. Roppongi, M. Qiu, Q. Sheng, Y. Cai, K. Yamakawa, Z. Guguchia, R. P. Day, K. M. Kojima, A. Damascelli, et al., Two superconducting states with broken time-reversal symmetry in fesel- x s x, Proceedings of the National Academy of Sciences 120, e2208276120 (2023).
- [22] V. Grinenko, P. Materne, R. Sarkar, H. Luetkens, K. Kihou, C. H. Lee, S. Akhmadaliev, D. V. Efremov, S.-L. Drechsler, and H.-H. Klauss, Superconductivity with broken time-reversal symmetry in ion-irradiated ba_{0.27}k_{0.73}fe₂as₂ single crystals, Phys. Rev. B 95, 214511 (2017).
- [23] L.-H. Hu, P. Johnson, and C. Wu, Pairing symmetry and topological surface state in iron-chalcogenide superconductors, Physical Review Research 2, 022021 (2020).
- [24] N. Zaki, G. Gu, A. Tsvelik, C. Wu, and P. D. Johnson, Time-reversal symmetry breaking in the fe-chalcogenide superconductors, Proceedings of the National Academy of Sciences 118, e2007241118 (2021).

- [25] S. K. Ghosh, P. K. Biswas, C. Xu, B. Li, J. Z. Zhao, A. D. Hillier, and X. Xu, Time-reversal symmetry breaking superconductivity in three-dimensional dirac semimetallic silicides, Phys. Rev. Res. 4, L012031 (2022).
- [26] S. K. Ghosh, M. Smidman, T. Shang, J. F. Annett, A. D. Hillier, J. Quintanilla, and H. Yuan, Recent progress on superconductors with time-reversal symmetry breaking, Journal of Physics: Condensed Matter 33, 033001 (2020).
- [27] I. Maccari and A. Ramires, Tuning macroscopic phase frustration in multiorbital superconductors (2025), arXiv:2510.16843 [cond-mat.supr-con].
- [28] G. Csire, J. F. Annett, J. Quintanilla, and B. Újfalussy, Magnetically textured superconductivity in elemental rhenium, Physical Review B 106, L020501 (2022).
- [29] A. Ribak, R. M. Skiff, M. Mograbi, P. K. Rout, M. H. Fischer, J. Ruhman, K. Chashka, Y. Dagan, and A. Kanigel, Chiral superconductivity in the alternate stacking compound 4hb-tas₂, Science Advances 6, eaax9480 (2020), https://www.science.org/doi/pdf/10.1126/sciadv.aax9480.
- [30] E. Persky, A. V. Bjørlig, I. Feldman, A. Almoalem, E. Altman, E. Berg, I. Kimchi, J. Ruhman, A. Kanigel, and B. Kalisky, Magnetic memory and spontaneous vortices in a van der Waals superconductor, Nature 607, 692 (2022).
- [31] Z. Wan, G. Qiu, H. Ren, Q. Qian, Y. Li, D. Xu, J. Zhou, J. Zhou, B. Zhou, L. Wang, T.-H. Yang, Z. Sofer, Y. Huang, K. L. Wang, and X. Duan, Unconventional superconductivity in chiral molecule—TaS2 hybrid superlattices, Nature 632, 69 (2024).
- [32] A. Almoalem, I. Feldman, I. Mangel, M. Shlafman, Y. E. Yaish, M. H. Fischer, M. Moshe, J. Ruhman, and A. Kanigel, The observation of π -shifts in the Little-Parks effect in 4Hb-TaS2, Nature Communications 15, 4623 (2024).
- [33] S. Meyer, R. Howard, G. Stewart, J. V. Acrivos, and T. Geballe, Properties of intercalated 2h-nbse2, 4hb-tas2, and 1t-tas2, The Journal of Chemical Physics 62, 4411 (1975).
- [34] B. Liu, H. Li, Z. Wu, W. Han, M. Gao, Y. Wang, T. Qiu, J. Wang, and Z. Shi, Crystal growth, characterization, and transport properties of 4hb-tas2 single crystals, Journal of Alloys and Compounds, 183768 (2025).
- [35] Y. Huang, H. Li, X. Yang, W. Zhou, D. Jia, J. Feng, H. Zhang, G. Niu, B. Yan, F. Liu, et al., Pressure-induced evolution of superconductivity and structural stability in a bulk 4hb-tases heterostructure, Physical Review B 111, 144103 (2025).
- [36] H. Wang, Y. Jiao, F. Meng, X. Zhang, D. Dai, C. Tu, C. Zhao, L. Xin, S. Huang, H. Lei, et al., Evidence for multiband gapless superconductivity in the topological superconductor candidate 4 hb-tas 2, Physical Review Letters 135, 126002 (2025).
- [37] Y. Liu, L. Li, W. Lu, R. Ang, X. Liu, and Y. Sun, Coexistence of superconductivity and commensurate charge density wave in 4hb-tas2- xsex single crystals, Journal of Applied Physics 115 (2014).
- [38] D. Dentelski, E. Day-Roberts, T. Birol, R. M. Fernandes, and J. Ruhman, Robust gapless superconductivity in 4 h b-tas 2, Physical Review B 103, 224522 (2021).
- [39] Y. Zhou, F. Meng, Y. Huang, J. Zhang, J. Zhan, Y. Chen, Y. Liu, H. Lei, M. Smidman, and H. Yuan, Nodeless superconductivity in 4 h b-tas 2 with broken time-reversal symmetry, Physical Review B 112, 014507 (2025).

- [40] I. Silber, S. Mathimalar, I. Mangel, A. K. Nayak, O. Green, N. Avraham, H. Beidenkopf, I. Feldman, A. Kanigel, A. Klein, M. Goldstein, A. Banerjee, E. Sela, and Y. Dagan, Two-component nematic superconductivity in 4Hb-TaS2, Nature Communications 15, 824 (2024).
- [41] F. Meng, Y. Fu, S. Pan, S. Tian, S. Yan, Z. Li, S. Wang, J. Zhang, and H. Lei, Extreme orbital abplane upper critical fields far beyond the pauli limit in 4H_b-Ta(S,Se)₂ bulk crystals, Phys. Rev. B 109, 134510 (2024).
- [42] J. J. Gao, J. G. Si, X. Luo, J. Yan, Z. Z. Jiang, W. Wang, Y. Y. Han, P. Tong, W. H. Song, X. B. Zhu, Q. J. Li, W. J. Lu, and Y. P. Sun, Origin of the large magnetoresistance in the candidate chiral superconductor 4H_b-Tas₂, Phys. Rev. B **102**, 075138 (2020).
- [43] P. Wu, Z. Wang, Y. Zhang, Z. Chen, S. Yu, W. Ma, M. Shan, Z. Liang, X. Wei, J. Wang, et al., Unveiling the landscape of mottness and its proximity to superconductivity in 4hb-tas _2, arXiv preprint arXiv:2508.17861 (2025).
- [44] A. Kumar Nayak, A. Steinbok, Y. Roet, J. Koo, I. Feldman, A. Almoalem, A. Kanigel, B. Yan, A. Rosch, N. Avraham, et al., First-order quantum phase transition in the hybrid metal—mott insulator transition metal dichalcogenide 4hb-tas2, Proceedings of the National Academy of Sciences 120, e2304274120 (2023).
- [45] A. Ramires, From pure to mixed: Altermagnets as intrinsic symmetry-breaking indicators (2025), arXiv:2502.19162 [cond-mat.supr-con].
- [46] S. C. de la Barrera, M. R. Sinko, D. P. Gopalan, N. Sivadas, K. L. Seyler, K. Watanabe, T. Taniguchi, A. W. Tsen, X. Xu, D. Xiao, and B. M. Hunt, Tuning Ising superconductivity with layer and spin-orbit coupling in two-dimensional transition-metal dichalcogenides, Nature Communications 9, 1427 (2018).
- [47] Y. Kvashnin, D. VanGennep, M. Mito, S. A. Medvedev, R. Thiyagarajan, O. Karis, A. N. Vasiliev, O. Eriksson, and M. Abdel-Hafiez, Coexistence of Superconductivity and Charge Density Waves in Tantalum Disulfide: Experiment and Theory, Physical Review Letters 125, 186401 (2020).
- [48] L. Li, X. Deng, Z. Wang, Y. Liu, M. Abeykoon, E. Dooryhee, A. Tomic, Y. Huang, J. B. Warren, E. S. Bozin, S. J. L. Billinge, Y. Sun, Y. Zhu, G. Kotliar, and C. Petrovic, Superconducting order from disorder in 2H-TaSe 2-x S x, npj Quantum Materials 2, 11 (2017).
- [49] Y. Saito, Y. Nakamura, M. S. Bahramy, Y. Kohama, J. Ye, Y. Kasahara, Y. Nakagawa, M. Onga, M. Tokunaga, T. Nojima, Y. Yanase, and Y. Iwasa, Superconductivity protected by spin-valley locking in ion-gated MoS2, Nature Physics 12, 144 (2016).
- [50] X. Xi, Z. Wang, W. Zhao, J.-H. Park, K. T. Law, H. Berger, L. Forró, J. Shan, and K. F. Mak, Ising pairing in superconducting NbSe2 atomic layers, Nature Physics 12, 139 (2016).
- [51] J. Lu, O. Zheliuk, I. Leermakers, N. F. Yuan, U. Zeitler, K. T. Law, and J. Ye, Evidence for two-dimensional ising superconductivity in gated mos2, Science 350, 1353 (2015).
- [52] E. Navarro-Moratalla, J. O. Island, S. Mañas-Valero, E. Pinilla-Cienfuegos, A. Castellanos-Gomez, J. Quereda, G. Rubio-Bollinger, L. Chirolli, J. A. Silva-Guillén, N. Agraït, G. A. Steele, F. Guinea, H. S. J. van der Zant, and E. Coronado, Enhanced superconductiv-

- ity in atomically thin TaS2, Nature Communications 7, 11043 (2016).
- [53] Y. Yang, S. Fang, V. Fatemi, J. Ruhman, E. Navarro-Moratalla, K. Watanabe, T. Taniguchi, E. Kaxiras, and P. Jarillo-Herrero, Enhanced superconductivity upon weakening of charge density wave transport in 2h-tas₂ in the two-dimensional limit, Phys. Rev. B 98, 035203 (2018).
- [54] Y. Zhao, Z. Nie, H. Hong, X. Qiu, S. Han, Y. Yu, M. Liu, X. Qiu, K. Liu, S. Meng, L. Tong, and J. Zhang, Spectroscopic visualization and phase manipulation of chiral charge density waves in 1T-TaS2, Nature Communications 14, 2223 (2023).
- [55] F. Z. Yang, H. D. Zhang, S. Mandal, F. Y. Meng, G. Fabbris, A. Said, P. Mercado Lozano, A. Rajapitamahuni, E. Vescovo, C. Nelson, et al., Signature of magneto-electric coupling driven finite momentum pairing in 3d ising superconductor, Nature Communications 16, 6626 (2025).
- [56] M. Sigrist and K. Ueda, Phenomenological theory of unconventional superconductivity, Reviews of Modern Physics 63, 239 (1991).
- [57] L. P. Gor'kov and E. I. Rashba, Superconducting 2d system with lifted spin degeneracy: mixed singlet-triplet state, Physical Review Letters 87, 037004 (2001).
- [58] T. Yoshida, M. Sigrist, and Y. Yanase, Parity-mixed superconductivity in locally non-centrosymmetric system, Journal of the Physical Society of Japan 83, 013703 (2014).
- [59] E. Bauer and M. Sigrist, Non-centrosymmetric superconductors: introduction and overview, Vol. 847 (Springer Science & Business Media, 2012).
- [60] D. Shaffer, F. Burnell, and R. M. Fernandes, Weak-coupling theory of pair density wave instabilities in transition metal dichalcogenides, Physical Review B 107, 224516 (2023).
- [61] D. Möckli and M. Khodas, Magnetic-field induced s+if pairing in ising superconductors, Phys. Rev. B **99**, 180505 (2019).
- [62] D. Shaffer, J. Kang, F. J. Burnell, and R. M. Fernandes, Crystalline nodal topological superconductivity and bogolyubov fermi surfaces in monolayer nbse₂, Phys. Rev. B 101, 224503 (2020).
- [63] A. Hamill, B. Heischmidt, E. Sohn, D. Shaffer, K.-T. Tsai, X. Zhang, X. Xi, A. Suslov, H. Berger, L. Forró, et al., Two-fold symmetric superconductivity in few-layer nbse2, Nature physics 17, 949 (2021).
- [64] M. Haim, A. Levchenko, and M. Khodas, Mechanisms of in-plane magnetic anisotropy in superconducting nbse₂, Phys. Rev. B 105, 024515 (2022).
- [65] M. I. Aroyo, J. M. Perez-Mato, D. Orobengoa, E. Tasci, G. de la Flor, and A. Kirov, Crystallography online: Bilbao crystallographic server, Bulg. Chem. Commun 43, 183 (2011).
- [66] M. I. Aroyo, J. M. Perez-Mato, C. Capillas, E. Kroumova, S. Ivantchev, G. Madariaga, A. Kirov, and H. Wondratschek, Bilbao crystallographic server: I. databases and crystallographic computing programs, Zeitschrift für Kristallographie - Crystalline Materials 221, 15 (2006).
- [67] M. I. Aroyo, A. Kirov, C. Capillas, J. M. Perez-Mato, and H. Wondratschek, Bilbao Crystallographic Server. II. Representations of crystallographic point groups and space groups, Acta Crystallographica Section A 62, 115 (2006).

- [68] M. Sigrist, Time-Reversal Symmetry Breaking States in High-Temperature Superconductors, Progress of Theoretical Physics 99, 899 (1998).
- [69] M. Sigrist, Introduction to unconventional superconductivity in non-centrosymmetric metals, AIP Conference Proceedings 1162, 55 (2009).
- [70] D. Shaffer, D. V. Chichinadze, and A. Levchenko, Superconducting diode effect in multiphase superconductors, Physical Review B 110, 184509 (2024).
- [71] See supplemental material [url] for [brief description], which includes refs. (2025).
- [72] D. F. Agterberg and H. Tsunetsugu, Dislocations and vortices in pair-density-wave superconductors, Nature Physics 4, 639 (2008).
- [73] D. F. Agterberg, M. Geracie, and H. Tsunetsugu, Conventional and charge-six superfluids from melting hexagonal fulde-ferrell-larkin-ovchinnikov phases in two dimensions, Phys. Rev. B 84, 014513 (2011).
- [74] F. Gaggioli, D. Guerci, and L. Fu, Spontaneous vortexantivortex lattice and majorana fermions in rhombohedral graphene (2025).
- [75] A. Furusaki, M. Matsumoto, and M. Sigrist, Spontaneous Hall effect in a chiral p -wave superconductor, Physical Review B 64, 054514 (2001).
- [76] V. P. Mineev and K. V. Samokhin, Introduction to Unconventional Superconductivity (Gordon and Breach, Amsterdam, 1999).
- [77] J. W. F. Venderbos, V. Kozii, and L. Fu, Odd-parity superconductors with two-component order parameters: Nematic and chiral, full gap, and majorana node, Phys. Rev. B 94, 180504 (2016).
- [78] S. Hoshino, R. Wakatsuki, K. Hamamoto, and N. Nagaosa, Nonreciprocal charge transport in twodimensional noncentrosymmetric superconductors, Phys. Rev. B 98, 054510 (2018).
- [79] H. Narita, J. Ishizuka, D. Kan, Y. Shimakawa, Y. Yanase, and T. Ono, Magnetization control of zero-field intrinsic superconducting diode effect, Advanced Materials 35, 2304083 (2023).
- [80] J.-X. Lin, P. Siriviboon, H. D. Scammell, S. Liu, D. Rhodes, K. Watanabe, T. Taniguchi, J. Hone, M. S. Scheurer, and J. Li, Zero-field superconducting diode effect in small-twist-angle trilayer graphene, Nature Physics 18, 1221 (2022).
- [81] J. Ma, R. Zhan, and X. Lin, Superconducting diode effects: Mechanisms, materials and applications, Advanced Physics Research 4, 2400180 (2025).
- [82] V. V. Ryazanov, V. A. Oboznov, A. S. Prokofiev, V. V. Bolginov, and A. K. Feofanov, Superconductor— Ferromagnet—Superconductor π-junctions, Journal of Low Temperature Physics 136, 385 (2004).
- [83] S. M. Frolov, D. J. Van Harlingen, V. A. Oboznov, V. V. Bolginov, and V. V. Ryazanov, Measurement of the current-phase relation of superconductor/ferromagnet/superconductor π josephson junctions, Phys. Rev. B 70, 144505 (2004).
- [84] A. I. Buzdin, Proximity effects in superconductorferromagnet heterostructures, Reviews of modern physics 77, 935 (2005).
- [85] T. Han, Z. Lu, Z. Hadjri, L. Shi, Z. Wu, W. Xu, Y. Yao, A. A. Cotten, O. Sharifi Sedeh, H. Weldeyesus, et al., Signatures of chiral superconductivity in rhombohedral graphene, Nature 643, 654 (2025).
- [86] D. F. Agterberg, M. Sigrist, and H. Tsunetsugu, Order

- Parameter and Vortices in the Superconducting Q Phase of CeCoIn 5, Physical Review Letters **102**, 207004 ().
- [87] D. F. Agterberg, J. C. S. Davis, S. D. Edkins, E. Fradkin, D. J. V. Harlingen, S. A. Kivelson, P. A. Lee, L. Radzihovsky, J. M. Tranquada, and Y. Wang, The Physics of Pair Density Waves, Annual Review of Condensed Matter Physics 11, 231 (), 1904.09687.
- [88] V. Barzykin and L. P. Gor'kov, Inhomogeneous Stripe Phase Revisited for Surface Superconductivity, Physical Review Letters 89, 227002 (2002).
- [89] Y. Wang, S. D. Edkins, M. H. Hamidian, J. C. S. Davis, E. Fradkin, and S. A. Kivelson, Pair density waves in superconducting vortex halos, Physical Review B 97, 174510 (2018).
- [90] P. Fulde and R. A. Ferrell, Superconductivity in a strong spin-exchange field, Phys. Rev. 135, A550 (1964).

- [91] A. I. Larkin and Y. N. Ovchinnikov, Nonuniform state of superconductors, Zh. Eksp. Teor. Fiz. 47, 1136 (1964).
- [92] F. Gaggioli, D. Guerci, and L. Fu, Spontaneous vortexantivortex lattice and majorana fermions in rhombohedral graphene, Phys. Rev. Lett. 135, 116001 (2025).
- [93] Y. Wang, Y. Feng, Y. Zhu, Y. Tang, L. Yang, M. Zou, W. Geng, M. Han, X. Guo, B. Wu, et al., Polar meron lattice in strained oxide ferroelectrics, Nature Materials 19, 881 (2020).
- [94] M. Tinkham, Introduction to Superconductivity, Dover Books on Physics Series (Dover Publications, 2004).
- [95] N. F. Q. Yuan and L. Fu, Supercurrent diode effect and finite-momentum superconductors, Proceedings of the National Academy of Sciences 119, e2119548119 (2022).

Appendix A: Quadratic terms in Ginzburg-Landau free energy

In this section, we will discuss the pair-mixing terms between the A and E pairing due to non-zero momentum up to the quadratic terms of the order parameters in the Ginzburg-Landau (GL) theory. To consider the pair-mixing, we consider the form of the gap function in the momentum space as [56]

$$\Delta(\mathbf{k}, \mathbf{p}) = \sum_{\Gamma, m} \eta_{\Gamma, m}(\mathbf{k}) \hat{\Delta}_{\Gamma, m}(\mathbf{p}), \tag{A1}$$

where **k** represents the total momentum of the Cooper pair, which describes the modulation of the gap function in the real space, while **p** represents the relative momentum of the Cooper pair, which represents the orbital part of the Cooper pair wavefunction [69]. In Eq.(A1), $\hat{\Delta}_{\Gamma,m}(\mathbf{p})$ represents the basis function of the gap function expansion for the pairing channel belonging to the irreducible representation (irrep) Γ of the crystal symmetry group [86–89], denoted as \mathcal{G} , at certain high-symmetry momentum with m denoting different components of the basis function. The expansion coefficient $\eta_{\Gamma,m}(\mathbf{k})$ in Eq.(A1) can be viewed as the order parameter corresponding to the pairing channel of the basis function $\hat{\Delta}_{\Gamma,m}(\mathbf{p})$. One should note that $\hat{\Delta}_{\Gamma,m}(\mathbf{p})$ has a matrix form in the spin space of Cooper pairs, while $\eta_{\Gamma,m}(\mathbf{k})$ for $\Gamma = A, E$ is component of the order parameter vector

$$\Psi(\mathbf{k}) = \begin{pmatrix} \eta_{E+}(\mathbf{k}) \\ \eta_{A}(\mathbf{k}) \\ \eta_{E-}(\mathbf{k}) \end{pmatrix}. \tag{A2}$$

where we explicitly considered η_A as the order parameter for the dominant s-wave pairing and $\eta_{E\pm}$ as the order parameter for the chiral p-wave pairing. As the basis wavefunction $\hat{\Delta}_{\Gamma,m}(\mathbf{p})$ belongs to the irrep Γ of the crystal symmetry group \mathcal{G} , it transforms as

$$D_{\mathcal{S}}\hat{\Delta}_{\Gamma,m}(\mathcal{S}^{-1}\mathbf{p})D_{\mathcal{S}}^{T} = \sum_{n}\hat{\Delta}_{\Gamma,n}(\mathbf{p})(\mathcal{D}_{\mathcal{S}}^{\Gamma})_{nm}$$
(A3)

where $D_{\mathcal{S}}$ is the transformation matrix of electron wavefunction basis for the symmetry operator $\mathcal{S} \in \mathcal{G}$, while $\mathcal{D}_{\mathcal{S}}^{\Gamma}$ represents the representation matrix of the symmetry \mathcal{S} for the irrep Γ . The basis function $\hat{\Delta}_{\Gamma,m}(\mathbf{p})$ is composed of the orbital wavefunction, which is written as a polynomial of the relative momentum \mathbf{p} (e.g. s-wave, p-wave, ...), and spin wavefunction, which can be represented by Pauli matrices s (e.g. spin-singlet and spin-triplet). Table II lists the possible basis function $\hat{\Delta}_{\Gamma,m}(\mathbf{p})$ for the irrep Γ and its transformation matrices.

We consider two magnetic point groups (MPGs), $\bar{6}m2.1'$ and 31', which describe for a pure 1H-TaS₂ layer and the sandwich hetero-structure discussed in Fig.1(a) of the main text, respectively. The MPG 31' can be generated by three-fold rotation C_{3z} and time reversal (TR) \mathcal{T} , while the MPG $\bar{6}m21'$ can be generated by \mathcal{T} , x-directional mirror symmetry M_x and improper six-fold rotation $\mathcal{I}C_{6z}$ that combines inversion \mathcal{I} and six-fold rotation C_{6z} . For these symmetry operations, the transformation matrices are given by

$$D_{C_{3z}} = e^{-i\frac{\pi}{3}s_z}; \quad D_{\mathcal{T}} = -is_y \mathcal{K}$$
(A4)

$\boxed{\operatorname{Irrep}(\Gamma)}$	Basis functions $\hat{\Delta}_{\Gamma,m}(\mathbf{p})$	\mathcal{D}_E^{Γ}	$\mathcal{D}_{C_{3z}}^{\Gamma}$	$\mathcal{D}^{\Gamma}_{\mathcal{M}_x}$	$\mathcal{D}^{\Gamma}_{\mathcal{I}C_{6z}}$	$\mathcal{D}^{\Gamma}_{\mathcal{T}}$
A_1'	is_y	1	1	1	1	1
$A_1^{\prime\prime}$	is_x	1	1	-1	1	1
A_2'	$p_{+}(s_{0}-s_{z})-p_{-}(s_{0}+s_{z})$	1	1	-1	-1	1
$A_2^{\prime\prime}$	$ip_{+}(s_{0}-s_{z})+ip_{-}(s_{0}+s_{z})$	1	1	1	-1	1
E'	$i\{k_{+}^{3n+1},k_{-}^{3n+1}\},\{k_{-}^{3n+2},k_{+}^{3n+2}\}\\ \{p_{-}^{3l+2},p_{+}^{3l+2}\}is_{y}$	$ au_0 $	$e^{i2\pi\tau_z/3}$	$- au_x$	$e^{-i2\pi\tau_z/3}$	$ au_x$
E''	$\{p_+^{3l+1}(s_z+s_0), p^{3l+1}(s_z-s_0)\}$	$ au_0 $	$e^{i2\pi\tau_z/3}$	$- au_x$	$e^{i\pi\tau_z/3}$	$ au_x $

TABLE II. Possible basis functions for irreps (Γ) of MPG $\bar{6}m21'$ of the 1H-TaS₂ monolayers without chiral layer induced mirror symemtry breaking. s, τ labels the spin of Cooper pairs and the basis of the 2D E irreps respectively. $p_{\pm} = p_x \pm ip_y$ is for the relative momenta of each Cooper pair, whereas $k_{\pm} = k_x \pm ik_y$ is the center-of-mass momenta. The third to last columns give the representation matrix ($\mathcal{D}_{\Sigma}^{\Gamma}$) for a typical symmetry element (\mathcal{S}) from each conjugacy class of the local symmetry group.

$MPG\bar{6}m21'$	MPG31'
A_1'	
A_1''	A
A_2'	A
A_2''	
E'	$^{1}E^{2}E$
$E^{\prime\prime}$	

TABLE III. Compatibility relations between the MPG $\bar{6}m21'$ and its subgroup 31'.

for MPG 31'. There are additional symmetry generators

$$D_{\mathcal{I}C_{6z}} = e^{-i\frac{\pi}{6}s_z}; \quad D_{M_x} = is_x,$$
 (A5)

for MPG $\bar{6}m2.1'$. Here K is complex conjugation for the anti-unitary time reversal operations and s are the Pauli matrices acting on individual spin 1/2 basis. The transformation of the momentum \mathbf{k} is define as

$$\hat{C}_{3z}k_{\pm} = e^{\pm i\frac{2\pi}{3}}k_{\pm}; \quad \hat{\mathcal{I}}\hat{C}_{6z}k_{\pm} = -e^{\pm i\frac{\pi}{3}}k_{\pm}; \quad \hat{\mathcal{T}}k_{\pm} = -k_{\mp}; \quad \hat{M}_x k_{\pm} = -k_{\mp}.$$
(A6)

With the above transformation rules, we can construct the representation matrix $\mathcal{D}_{\mathcal{S}}^{\Gamma}$ for the basis wavefunction $\hat{\Delta}_{\Gamma,m}(\mathbf{p})$ using Eq.(A3), which is presented in TableII for MPG $\bar{6}m21'$. For the MPG 31', the representation matrix can be constructed from the compatibility relation in TableIII using the MPG $\bar{6}m21'$, shown in Table I of main text. With these transformation matrices, we can classify all the basis functions for the gap functions according to the irreps of $\mathcal{G} = \bar{6}m2.1'$ or 31' in TableII and III. The gap function can be expanded on the basis functions in Eq.(A1), from which we can derive the representation matrices for the order parameters $\eta_{\Gamma,m}(\mathbf{k})$ that belongs to the irrep Γ . For the unitary symmetry transformation \mathcal{S} acting on the expansion (A1) for the general form of gap function $\Delta(\mathbf{k}, \mathbf{p})$, we obtain

$$D_{\mathcal{S}}\Delta(\mathbf{k}, \mathbf{p})D_{\mathcal{S}}^{T} = \sum_{\Gamma, m} \eta_{\Gamma, m}(\mathbf{k})D_{\mathcal{S}}\hat{\Delta}_{\Gamma, m}(\mathbf{p})D_{\mathcal{S}}^{T}$$

$$= \sum_{\Gamma, n} \left\{ \sum_{m} (\mathcal{D}_{\mathcal{S}}^{\Gamma})_{nm} \eta_{\Gamma, m}(\mathbf{k}) \right\} \hat{\Delta}_{\Gamma, n}(\mathcal{S}\mathbf{p}). \tag{A7}$$

After the symmetry transformation, we can expand the gap function $\tilde{\Delta}(\mathcal{S}\mathbf{k},\mathcal{S}\mathbf{p}) = D_{\mathcal{S}}\Delta(\mathbf{k},\mathbf{p})D_{\mathcal{S}}^{T}$ with the basis function $\hat{\Delta}_{\Gamma,n}(\mathcal{S}\mathbf{p})$ at the total momentum $\mathcal{S}\mathbf{k}$ and the expansion coefficient, denoted as $\tilde{\eta}_{\Gamma,n}(\mathcal{S}\mathbf{k})$, should be defined

as

$$\tilde{\Delta}(\mathcal{S}\mathbf{k}, \mathcal{S}\mathbf{p}) = \sum_{\Gamma, n} \tilde{\eta}_{\Gamma, n}(\mathcal{S}\mathbf{k}) \hat{\Delta}_{\Gamma, n}(\mathcal{S}\mathbf{p}), \tag{A8}$$

leading to the transformation form of $\tilde{\eta}_{\Gamma,n}$ as

$$\tilde{\eta}_{\Gamma,n}(\mathcal{S}\mathbf{k}) = \sum_{m} (\mathcal{D}_{\mathcal{S}}^{\Gamma})_{nm} \eta_{\Gamma,m}(\mathbf{k}) \quad \to \quad \tilde{\eta}_{\Gamma,n}(\mathbf{k}) = \sum_{m} (\mathcal{D}_{\mathcal{S}}^{\Gamma})_{nm} \eta_{\Gamma,m}(\mathcal{S}^{-1}\mathbf{k})$$
(A9)

The representation matrices $\mathcal{D}_{\mathcal{S}}^{\Gamma}$ for all the generators in the MPG 31' are shown in Table I of the main text, and those for the MPG $\bar{6}m2.1'$ are shown in Table II.

For any anti-unitary symmetry transformation, we can rewrite it as a conjugation followed by a unitary operation, leading to

$$D_{\mathcal{S}}\eta_{\Gamma,m}(\mathbf{k})D_{\mathcal{S}}^{-1} = \eta_{\Gamma,m}^{*}(\mathbf{k}),\tag{A10}$$

from which we have

$$D_{\mathcal{S}}\Delta(\mathbf{k}, \mathbf{p})D_{\mathcal{S}}^{T} = \sum_{\Gamma, m} \eta_{\Gamma, m}^{*}(\mathbf{k})D_{\mathcal{S}}\hat{\Delta}_{\Gamma, m}(\mathbf{p})D_{\mathcal{S}}^{T}$$

$$= \sum_{\Gamma, n} \left\{ \sum_{m} (\mathcal{D}_{\mathcal{S}}^{\Gamma})_{nm} \eta_{\Gamma, m}^{*}(\mathbf{k}) \right\} \hat{\Delta}_{\Gamma, n}(\mathcal{S}\mathbf{p})$$
(A11)

and

$$\tilde{\eta}_{\Gamma,n}(\mathcal{S}\mathbf{k}) = \sum_{m} (\mathcal{D}_{\mathcal{S}}^{\Gamma})_{nm} \eta_{\Gamma,m}^{*}(\mathbf{k}) \quad \to \quad \tilde{\eta}_{\Gamma,n}(\mathbf{k}) = \sum_{m} (\mathcal{D}_{\mathcal{S}}^{\Gamma})_{nm} \eta_{\Gamma,m}^{*}(\mathcal{S}^{-1}\mathbf{k}). \tag{A12}$$

From the transformations of the order parameter under symmetry S in Eqs.(A9) and (A12), we will construct the Ginzburg-Landau free energy for the E and A pairing channels of the MPG 31'. The transformation of the order parameters in Eq.(A9) can be rewritten in a matrix form as

$$\tilde{\Psi}_{\alpha}(\mathcal{S}\mathbf{k}) = \sum_{\beta} \mathcal{R}_{\alpha\beta}^{\mathcal{S}} \Psi_{\beta}(\mathbf{k})$$

$$\mathcal{R}^{\mathcal{S}} = \mathcal{J} \begin{pmatrix} \mathcal{D}_{\mathcal{S}}^{A} & \mathbf{0}_{1\times 2} \\ \mathbf{0}_{2\times 1} & \mathcal{D}_{\mathcal{S}}^{E} \end{pmatrix} \mathcal{J}^{T}, \quad \mathcal{J} = \begin{pmatrix} 0 & 1 & 0 \\ 1 & 0 & 0 \\ 0 & 0 & 1 \end{pmatrix} \tag{A13}$$

where $\mathcal{R}^{\mathcal{S}}$ is the representation matrix of the symmetry transformation \mathcal{S} on the vector space of $\Psi(\mathbf{k})$ and $\mathbf{0}_{a\times b}$ is a zero matrix with dimensions (a,b). The permutation matrix \mathcal{J} re-arranges the order parameters from different channels in the form of $\Psi(\mathbf{k})$ as

$$\Psi(\mathbf{k}) = \begin{pmatrix} \eta_{E+}(\mathbf{k}) \\ \eta_{A}(\mathbf{k}) \\ \eta_{E-}(\mathbf{k}) \end{pmatrix} = \mathcal{J} \begin{pmatrix} \eta_{A}(\mathbf{k}) \\ \eta_{E+}(\mathbf{k}) \\ \eta_{E-}(\mathbf{k}) \end{pmatrix}. \tag{A14}$$

For anti-unitary transformations such as \mathcal{T} symmetry, the extra conjugation operation leads to

$$\tilde{\Psi}_{\alpha}(\mathcal{S}\mathbf{k}) = \sum_{\beta} \mathcal{R}_{\alpha\beta}^{\mathcal{S}} \Psi_{\beta}^{*}(\mathbf{k}). \tag{A15}$$

The representation matrices for MPG 31' are given by

$$\mathcal{R}^{C_{3z}} = \begin{pmatrix} e^{i\frac{2\pi}{3}} & 0 & 0\\ 0 & 1 & 0\\ 0 & 0 & e^{-i\frac{2\pi}{3}} \end{pmatrix}; \quad \mathcal{R}^{\mathcal{T}} = \begin{pmatrix} 0 & 0 & 1\\ 0 & 1 & 0\\ 1 & 0 & 0 \end{pmatrix}$$
(A16)

for C_{3z} and \mathcal{T} symmetry, respectively. The representation matrices for the remaining generators of MPG $\bar{6}m21'$ are defined as

$$\mathcal{R}^{M_x} = \begin{pmatrix} 0 & 0 & -1 \\ 0 & 1 & 0 \\ -1 & 0 & 0 \end{pmatrix}; \quad \mathcal{R}^{\mathcal{I}C_{6z}} = \begin{pmatrix} e^{i\frac{\pi}{3}} & 0 & 0 \\ 0 & 1 & 0 \\ 0 & 0 & e^{-i\frac{\pi}{3}} \end{pmatrix}$$
(A17)

for M_x and $\mathcal{I}C_{6z}$ symmetry, respectively. We note that the out-of-plane \mathcal{M}_z symmetry can be generated from $\mathcal{I}C_{6z}$ by

$$\mathcal{M}_z = (\mathcal{I}C_{6z})^3,\tag{A18}$$

and the corresponding representation matrix of \mathcal{M}_z is

$$\mathcal{R}^{M_z} = (\mathcal{R}^{\mathcal{I}C_{6z}})^3 = \begin{pmatrix} -1 & 0 & 0\\ 0 & 1 & 0\\ 0 & 0 & -1 \end{pmatrix}. \tag{A19}$$

From the symmetry property of the order parameter $\Psi(\mathbf{k})$, we next construct the phenomenological Ginzburg-Landau (GL) free energy given by

$$\mathcal{F} = \mathcal{F}^{(2)} + \mathcal{F}^{(4)}.\tag{A20}$$

where $\mathcal{F}^{(2)}$ is the term in the second order of order parameters $\eta_{\Gamma,m}(\mathbf{k})$ and $\mathcal{F}^{(4)}$ is the fourth-order term. We first consider the second-order term, written as

$$\mathcal{F}^{(2)} = \sum_{\mathbf{k},\alpha,\beta} \Psi_{\alpha}^{*}(\mathbf{k}) \mathcal{H}_{\alpha\beta}(\mathbf{k}) \Psi_{\beta}(\mathbf{k}), \tag{A21}$$

where α, β labels the different components of the order parameter $\Psi(\mathbf{k})$ in Eq.(A2), T is temperature, \mathbb{I} is a 3-by-3 identity matrix, \mathcal{H} is the momentum dependent matrix of the generalized Hamiltonian. To derive the form of $\mathcal{H}_{\alpha\beta}(\mathbf{k})$, we first consider the unitary symmetry transformation \mathcal{S} , under which the free energy that should be invariant. We may consider the free energy after the transformation of the basis $\Psi(\mathbf{k})$ in Eq.(A13), given by

$$\mathcal{F}^{(2)} = \sum_{\mathbf{k},\alpha,\beta} \tilde{\Psi}_{\alpha}^{*}(\mathbf{k}) \mathcal{H}_{\alpha\beta}(\mathbf{k}) \tilde{\Psi}_{\beta}(\mathbf{k})$$

$$= \sum_{\substack{\mathbf{k},\alpha,\beta\\\alpha',\beta'}} \Psi_{\alpha'}^{*}(\mathcal{S}^{-1}\mathbf{k}) (\mathcal{R}_{\alpha\alpha'}^{\mathcal{S}})^{*} \mathcal{H}_{\alpha\beta}(\mathbf{k}) \mathcal{R}_{\beta\beta'}^{\mathcal{S}} \Psi_{\beta}(\mathcal{S}^{-1}\mathbf{k})$$

$$= \sum_{\substack{\mathbf{k},\alpha,\beta\\\alpha',\beta'}} \Psi_{\alpha'}^{*}(\mathbf{k}) (\mathcal{R}^{\mathcal{S}})_{\alpha'\alpha}^{\dagger} \mathcal{H}_{\alpha\beta}(\mathcal{S}\mathbf{k}) \mathcal{R}_{\beta\beta'}^{\mathcal{S}} \Psi_{\beta}(\mathbf{k}), \tag{A22}$$

where we have used Eq.(A13) in the second step. The invariance of the free energy under symmetry transformation requires

$$\mathcal{H}_{\alpha'\beta'}(\mathbf{k}) = \sum_{\alpha,\beta} (\mathcal{R}^{\mathcal{S}})^{\dagger}_{\alpha'\alpha} \mathcal{H}_{\alpha\beta}(\mathcal{S}\mathbf{k}) \mathcal{R}^{\mathcal{S}}_{\beta\beta'}, \tag{A23}$$

which provides the symmetry constraint on the form of the matrix $\mathcal{H}(\mathbf{k})$. Similarly, for anti-unitary TR symmetry,

we have

$$\mathcal{F}^{(2)} = \sum_{k,\alpha,\beta} \tilde{\Psi}_{\alpha}^{*}(\mathbf{k}) \mathcal{H}_{\alpha\beta}(\mathbf{k}) \tilde{\Psi}_{\beta}(\mathbf{k})$$

$$= \sum_{\substack{k,\alpha,\beta\\\alpha',\beta'}} \Psi_{\alpha'}(-\mathbf{k}) (\mathcal{R}_{\alpha\alpha'}^{\mathcal{T}})^{*} \mathcal{H}_{\alpha\beta}(\mathbf{k}) \mathcal{R}_{\beta\beta'}^{\mathcal{T}} \Psi_{\beta'}^{*}(-\mathbf{k})$$

$$= \sum_{\substack{k,\alpha,\beta\\\alpha',\beta'}} \Psi_{\beta'}^{*}(\mathbf{k}) (\mathcal{R}^{\mathcal{T}})_{\alpha'\alpha}^{\dagger} \mathcal{H}_{\alpha\beta}(-\mathbf{k}) \mathcal{R}_{\beta\beta'}^{\mathcal{T}} \Psi_{\alpha'}(\mathbf{k}), \tag{A24}$$

which leads to

$$\mathcal{H}_{\beta'\alpha'}(\mathbf{k}) = \sum_{\alpha,\beta} (\mathcal{R}^{\mathcal{T}})^{\dagger}_{\alpha'\alpha} \mathcal{H}_{\alpha\beta}(-\mathbf{k}) \mathcal{R}^{\mathcal{T}}_{\beta\beta'}. \tag{A25}$$

In addition to the symmetry constraints in Eqs. (A23) and (A25), the matrix $\mathcal{H}(\mathbf{k})$ also demands hermicity,

$$\mathcal{H}(\mathbf{k}) = \mathcal{H}^{\dagger}(\mathbf{k}),\tag{A26}$$

as the free energy \mathcal{F} is real. Based on the above symmetry constraints from MPG 31', the GL free energy up to the second-order terms in order parameter is given by

$$\mathcal{F}^{(2)} = \mathcal{F}_{A}^{(2)} + \mathcal{F}_{E}^{(2)} + \mathcal{F}_{A-E}$$

$$\mathcal{F}_{A}^{(2)} = \sum_{k} (\alpha_{A} + \gamma_{A}k^{2}) |\eta_{A}(\mathbf{k})|^{2}$$

$$\mathcal{F}_{E}^{(2)} = \sum_{k} (\alpha_{E} + \gamma_{E}k^{2}) (|\eta_{E,+}(\mathbf{k})|^{2} + |\eta_{E,-}(\mathbf{k})|^{2})$$

$$\mathcal{F}_{A-E} = \sum_{k} \eta_{A}^{*} (i\zeta_{1}^{*}k_{-} + \zeta_{2}^{*}k_{+}^{2} + \zeta_{4}^{*}k_{+}^{4}) \eta_{E,+} + \eta_{A}^{*} (i\zeta_{1}k_{+} + \zeta_{2}k_{-}^{2} + \zeta_{4}k_{-}^{4}) \eta_{E,-} + h.c.$$
(A27)

where $T_{c,\Gamma}$ are the critical temperature of the $\Gamma = A, E$ irrep channels without any pair-mixing. The GL coefficients

$$\alpha_{\Gamma} = \tilde{\alpha}_{\Gamma} (T - T_{c \, \Gamma}) \tag{A28}$$

and γ_{Γ} represent constant and quadratic in center of mass momentum $\mathcal{O}(k^2)$ terms, respectively $(\Gamma = A, E)$. The parameters ζ_n represent the strength of the pair mixing between A and E irrep channels, coupled with n^{th} power of the center of mass momentum \mathbf{k} . All these parameters are material dependent. To rewrite the free energy $\mathcal{F}^{(2)}$ in a compact form, we rescale the coefficients as $\gamma'_{\Gamma} = \gamma_{\Gamma}/\tilde{\alpha}_{\Gamma}$, $\zeta'_{1,2,4} = \zeta_{1,2,4}/\sqrt{\tilde{\alpha}_A\tilde{\alpha}_E}$, where $\Gamma = A, E$ are the different irrep channels. Furthermore, we rescale the order parameter vector components as $\eta'_{\Gamma}(\mathbf{k}) = \frac{\eta_{\Gamma}(\mathbf{k})}{\sqrt{\tilde{\alpha}_{\Gamma}}}$. After the regularization, we rewrite the free energy in Eq.(A21) as

$$\mathcal{F}^{(2)} = \sum_{\mathbf{k},\alpha,\beta} \Psi_{\alpha}^{'*}(\mathbf{k}) \{ T\mathbb{I} - M_{\alpha\beta}(\mathbf{k}) \} \Psi_{\beta}^{\prime}(\mathbf{k})$$
(A29)

with

$$M(\mathbf{k}) = \begin{pmatrix} T_{c,E} - \gamma_E' k^2 & i\zeta_1' k_+ - \zeta_2' k_-^2 - \zeta_4' k_+^4 & 0\\ -i\zeta_1'^* k_- - \zeta_2'^* k_+^2 - \zeta_4'^* k_-^4 & T_{c,A} - \gamma_A' k^2 & -i\zeta_1' k_+ - \zeta_2' k_-^2 - \zeta_4' k_+^4\\ 0 & i\zeta_1'^* k_- - \zeta_2'^* k_+^2 - \zeta_4'^* k_-^4 & T_{c,E} - \gamma_E' k^2 \end{pmatrix}.$$
(A30)

Below we always renamed the rescaled order parameter vector $\Psi'(\mathbf{k})$ in (A29) as $\Psi(\mathbf{k})$. The matrix $M(\mathbf{k})$ also respects all the symmetry constraints of MPG 31' in Eqs.(A23), (A25) and (A26). For the MPG $\bar{6}m21'$ with extra symmetry operations, including x-directional mirror symmetry \mathcal{M}_x and the combined symmetry $\mathcal{I}C_{6z}$ symmetry with \mathcal{I} to be inversion and C_{6z} to be six-fold rotation and z-directional mirror symmetry \mathcal{M}_z , we can implement a similar symmetry

construction of the GL free energy as

$$\mathcal{F}_{\bar{6}m21'}^{(2)} = \sum_{\mathbf{k},\alpha,\beta} \Psi_{\alpha}^{*}(\mathbf{k}) \{ T\mathbb{I} - M_{\alpha\beta}^{\bar{6}m21'}(\mathbf{k}) \} \Psi_{\beta}(\mathbf{k}). \tag{A31}$$

Since we focus on pair mixing between s-wave (A'_1) and p-wave (E''), the order parameter basis $\Psi(\mathbf{k})$ is written as

$$\Psi(\mathbf{k}) = \begin{pmatrix} \eta_{E''+}(\mathbf{k}) \\ \eta_{A_1}(\mathbf{k}) \\ \eta_{E''-}(\mathbf{k}) \end{pmatrix}. \tag{A32}$$

In this basis, with all the regularization as before, we find the $M^{\bar{6}m21'}(\mathbf{k})$ matrix that respects all the symmetry constraints Eq. (A23) and (A25) for MPG $\bar{6}$ m21' is given by

$$M^{\bar{6}m21'}(\mathbf{k}) = \begin{pmatrix} T_{c,E} - \gamma_E' k^2 & 0 & 0\\ 0 & T_{c,A} - \gamma_A' k^2 & 0\\ 0 & 0 & T_{c,E} - \gamma_E' k^2 \end{pmatrix}.$$
 (A33)

Comparing Eq.(A30) with (A33), we find that the off-diagonal pair mixing terms disappear in MPG $\bar{6}$ m21'. Therefore the s-wave and p-wave pair mixing terms are limited to the MPG 31'.

For the derivation below, we will only focus on the GL free energy (A30) and (A27) for the MPG 31'. We next consider the linearized GL equation and thus drop the fourth-order term $\mathcal{F}^{(4)}$ in this section. The linearized GL equation can be derived as

$$\frac{\partial \mathcal{F}^{(2)}}{\partial \Psi^{\dagger}(\mathbf{k})} = 0 \Rightarrow M(\mathbf{k})\Psi(\mathbf{k}) = T\Psi(\mathbf{k}), \tag{A34}$$

where $M(\mathbf{k})$ is given in Eq.(A30). We can numerically solve this eigen-equation problem of $M(\mathbf{k})$ matrix and obtain three eigen-values, denoted as $T_{\lambda}(\mathbf{k})$ with $\lambda = 1, 2, 3$. We may arrange these eigen-values in descending orders, $T_1(\mathbf{k}) > T_2(\mathbf{k}) > T_3(\mathbf{k})$, and the critical temperature can be obtained by maximizing the function $T_1(\mathbf{k})$ with respect to \mathbf{k} , i.e.

$$T_c = \max_{\mathbf{k}}(T_1(\mathbf{k})). \tag{A35}$$

To gain more analytical understanding, we can consider solving the eigen-equation problem perturbatively. We separate the $M(\mathbf{k})$ matrix into two parts,

$$M(\mathbf{k}) = M^{(0)}(\mathbf{k}) + M^{(1)}(\mathbf{k})$$
 (A36)

where $M^{(0)}(\mathbf{k})$ has the full-rotation symmetry and is given by

$$M^{(0)}(\mathbf{k}) = \begin{pmatrix} T_{c,E} - \gamma_E' k^2 & i\zeta_1' k_+ & 0\\ -i\zeta_1'^* k_- & T_{c,A} - \gamma_A' k^2 & -i\zeta_1' k_+\\ 0 & i\zeta_1'^* k_- & T_{c,E} - \gamma_E' k^2 \end{pmatrix}$$
(A37)

while $M^{(1)}(\mathbf{k})$ is the anisotropic term,

$$M^{(1)}(\mathbf{k}) = \begin{pmatrix} 0 & -\zeta_2' k_-^2 - \zeta_4' k_+^4 & 0 \\ -\zeta_2'^* k_+^2 - \zeta_4'^* k_-^4 & 0 & -\zeta_2' k_-^2 - \zeta_4' k_+^4 \\ 0 & -\zeta_2'^* k_+^2 - \zeta_4'^* k_-^4 & 0 \end{pmatrix}. \tag{A38}$$

We first consider the eigen-equation problem for $M^{(0)}(\mathbf{k})$,

$$M^{(0)}(\mathbf{k})\Psi^{(0)}(\mathbf{k}) = T^{(0)}(\mathbf{k})\Psi^{(0)}(\mathbf{k}),\tag{A39}$$

which can be solved analytically. It has three eigenvalues,

$$T_{\nu=\pm 1}^{(0)}(\mathbf{k}) = \frac{1}{2} \left[T_{c,A} + T_{c,E} - k^2 (\gamma_A' + \gamma_E') + \nu \sqrt{\left\{ (T_{c,A} - T_{c,E}) + (\gamma_E' - \gamma_A') k^2 \right\}^2 + 8k^2 |\zeta_1'|^2} \right]$$

$$T_{\nu=0}^{(0)}(\mathbf{k}) = T_{c,E} - \gamma_E' k^2. \tag{A40}$$

The corresponding wavefunctions are given by

$$\Psi_{\nu=0,\pm1}^{(0)}(\mathbf{k}) = \frac{1}{\sqrt{N_{i=0,\pm1}(\mathbf{k})}} \begin{pmatrix} i\zeta_1' k_+ \\ T_{\nu=0,\pm1}^{(0)}(k) - T_{c,E} + \gamma_E k^2 \\ i\zeta_1'^* k_- \end{pmatrix},$$
(A41)

where $N_{\nu=0,\pm 1}$ are the normalization coefficient for the eigenstates. We assume $T_{c,\Gamma}, \gamma'_{\Gamma}$ for $\Gamma=A, E$ to be positive numbers and $T_{c,A}-T_{c,E}>(\gamma'_A-\gamma'_E)k^2$ for all relevant and smaller scales of magnitude of momenta, i.e.—when $k\in[0,1]$.

From these three eigen-values in Eq.(A40), we pick the largest one $(\lambda = +1)$, denoted as $T_c^{(0)}(k)$.

$$T_c^{(0)}(k) = T_1^{(0)}(\mathbf{k})$$
 (A42)

and the corresponding eigen-state wavefunction is denoted as

$$\Psi_c^{(0)}(\mathbf{k}) = \Psi_1^{(0)}(\mathbf{k}) \tag{A43}$$

It should be noted that $T_c^{(0)}(k)$ only depend on $k = |\mathbf{k}|$ since $M^{(0)}(\mathbf{k})$ is isotropic. Consequently, the maximum of $T_c^{(0)}(k)$ only depend on the momentum amplitude k, but not momentum angle θ ($\mathbf{k} = k(\cos\theta, \sin\theta)$), due to the full rotation symmetry.

To break the full rotation symmetry, we consider $M^{(1)}(\mathbf{k})$ in Eq.(A38) perturbatively, and the first order correction to the eigen-value is given by

$$\Delta T_c^{(1)}(\mathbf{k}) = \{\Psi_c^{(0)}(\mathbf{k})\}^{\dagger} M^{(1)}(\mathbf{k}) \Psi_c^{(0)}(\mathbf{k})$$
(A44)

with the eigen-state $\Psi_c^{(0)}(\mathbf{k})$ for the largest eigen-value $T_c^{(0)}(k)$ of $M^{(0)}(\mathbf{k})$. With the expression of $\Psi_c^{(0)}(\mathbf{k})$ in Eq. (4) in main text or Eq.(A43), we obtain the correction to be

$$\Delta T_c^{(1)}(\mathbf{k}) = 0. \tag{A45}$$

Thus, we calculate the second order correction,

$$\Delta T_c^{(2)}(\mathbf{k}) = \frac{|(\Psi_0^{(0)})^{\dagger}(\mathbf{k})M^{(1)}(\mathbf{k})\Psi_c^{(0)}(\mathbf{k})|^2}{T_c^{(0)}(\mathbf{k}) - T_0^{(0)}(\mathbf{k})} + \frac{|(\Psi_{-1}^{(0)})^{\dagger}(\mathbf{k})M^{(1)}(\mathbf{k})\Psi_c^{(0)}(\mathbf{k})|^2}{T_c^{(0)}(\mathbf{k}) - T_{-1}^{(0)}(\mathbf{k})}.$$
(A46)

Using the eigenstates in (A41), we find this perturbation to be

$$\Delta T_c^{(2)}(\mathbf{k}) \approx \frac{2k^4 \left\{ |\zeta_2'|^2 + k^4 |\zeta_4'|^2 + 2k^2 \Re(e^{-i6\theta} \zeta_2' \zeta_4'^*) \right\}}{\sqrt{\left\{ T_{c,A} - T_{c,E} + k^2 (\gamma_E' - \gamma_A') \right\}^2 + 8k^2 |\zeta_1'|^2}}.$$
(A47)

With the results in Eqs.(A42), (A45) and (A47), the critical temperature is given by

$$T_c = \max(T_c(\mathbf{k})); \quad T_c(\mathbf{k}) = T_c^{(0)}(k) + \Delta T_c^{(1)}(\mathbf{k}) + \Delta T_c^{(2)}(\mathbf{k}).$$
 (A48)

The numerical and analytical solutions of $T_c(\mathbf{k})$ are discussed in Fig. 1(b) and 1(c) of the main text. To get T_c , we need to maximize $T_c(\mathbf{k})$ with respect to \mathbf{k} , which can be achieved in two steps. First, we maximize the isotropic part of $T_c(\mathbf{k})$, i.e. $T_c^{(0)}(\mathbf{k})$, with respect to magnitude of momenta $|\mathbf{k}| = k_0$. As $T_c^{(0)}(\mathbf{k})$ is isotropic, we obtain a degenerate

subspace of momenta space with full rotational symmetry, characterized by the angle θ of the momentum, for the highest T_c . Second, the non-zero second order correction $\Delta T_c^{(2)}(\mathbf{k})$ remove this degeneracy and pick six values of the angle θ for the maximal T_c . Thus, the symmetry of the degenerate subspace is reduced from continuous rotational symmetry down to six momenta that are related by three fold-rotation and time reversal symmetry.

The direction of these momenta will depend on the values of the pair-mixing coupling parameters $\zeta'_{2,4}$. For example, if we assume $\zeta'_{2,4}$ are real or pure imaginary while $\zeta'_2\zeta'^*_4 > 0$, these momenta can be denoted by the set

$$Q_6 = \{ \mathbf{Q}_j = k_0 \cos(\theta_{\mathbf{Q}_j}) \hat{e}_x + k_0 \sin(\theta_{\mathbf{Q}_j}) \hat{e}_y; \theta_{\mathbf{Q}_j} = \frac{j\pi}{3}; \quad \forall j \in \mathbb{Z}_6 \},$$
(A49)

as depicted in Fig.1(c) in main text, and the corresponding critical temperature is denoted as

$$T_{c,0} = T_c(\mathbf{k} = \mathbf{Q}_j); \quad \mathbf{Q}_j \in \mathcal{Q}_6$$
 (A50)

where $T_c(\mathbf{k})$ is given in Eq.(A48) and we can choose any j value for the same $T_{c,0}$.

Appendix B: Fourth Order terms and Time reversal breaking Phase

1. Symmetry construction of the fourth-order terms

The GL free energy with the quadratic terms of order parameters can be solved by the eigen-problem of the linearized GL equation (A39) and the relevant eigenvalue for the maximal value of $T(\mathbf{k})$ and the corresponding eigenstates are given in Eq.(3)(expanded in Eq.(A42) and Eq.(A45)) and Eq.(4) in main text, respectively. We note that when the parameter ζ' is smaller than a critical value ζ'_{1c} ($\zeta'_{1} < \zeta'_{1c}$), the largest value of $T(\mathbf{k})$ occurs at $\mathbf{k} = 0$, corresponding to the zero-momentum pairing in the A irrep channel. However, when $\zeta' > \zeta'_{1c}$, the highest $T(\mathbf{k})$ occurs at non-zero \mathbf{k} , given by the momenta set in Eq.(A49). These six momenta \mathbf{Q}_j are related to each other by C_{3z} and TR symmetry, so the eigen-states $\Psi_c^{(0)}(\mathbf{Q}_j)$ at these six momenta are degenerate and form a U(6) subspace. The general form of the ground state should be a linear superposition of all $\Psi_c^{(0)}(\mathbf{Q}_j)$ in Eq.(5) of the main text. At the quadratic order, any linear superposition should share the same energy, but this degeneracy is expected to be split by the fourth-order terms of the order parameters. Thus, we will construct all the fourth-order terms of the GL free energy within the U(6) subspace in this section.

We consider the order parameter Ψ in the real space, which is related to $\Psi(\mathbf{k})$ by the Fourier transform

$$\Psi_{\alpha}(\mathbf{r}) = \frac{1}{V} \sum_{\mathbf{k}} \Psi_{\alpha}(\mathbf{k}) e^{i\mathbf{k} \cdot \mathbf{r}}, \tag{B1}$$

where α labels the order parameter components, i.e.– $\Psi_1(\mathbf{k}) = \eta_{E+}(\mathbf{k}), \Psi_2(\mathbf{k}) = \eta_A(\mathbf{k}), \Psi_3(\mathbf{k}) = \eta_{E-}(\mathbf{k})$. Under the unitary symmetry transformation \mathcal{S} , the real space order parameter $\Psi_{\alpha}(\mathbf{r})$ is transformed as

$$\tilde{\Psi}_{\alpha}(\mathbf{r}) = \frac{1}{V} \sum_{\mathbf{k}} \tilde{\Psi}_{\alpha}(\mathbf{k}) e^{i\mathbf{k}\cdot\mathbf{r}} = \frac{1}{V} \sum_{\mathbf{k},\beta} \mathcal{R}_{\alpha\beta}^{\mathcal{S}} \Psi_{\beta}(\mathcal{S}^{-1}\mathbf{k}) e^{i\mathbf{k}\cdot\mathbf{r}}$$

$$= \frac{1}{V} \sum_{\mathbf{k}',\beta} \mathcal{R}_{\alpha\beta}^{\mathcal{S}} \Psi_{\beta}(\mathbf{k}') e^{i\mathcal{S}\mathbf{k}'\cdot\mathbf{r}} = \frac{1}{V} \sum_{\mathbf{k}',\beta} \mathcal{R}_{\alpha\beta}^{\mathcal{S}} \Psi_{\beta}(\mathbf{k}') e^{i\mathbf{k}'\cdot\mathcal{S}^{-1}\mathbf{r}}$$

$$= \sum_{\beta} \mathcal{R}_{\alpha\beta}^{\mathcal{S}} \Psi_{\beta}(\mathcal{S}^{-1}\mathbf{r}) \tag{B2}$$

where V is the volumn of the system and we have used Eq.(A13) in the second step, $\mathbf{k}' = \mathcal{S}^{-1}\mathbf{k}$ in the third step, and the definition of Fourier transform in the last step. For anti-unitary symmetry \mathcal{T} , this becomes

$$\tilde{\Psi}_{\alpha}(\mathbf{r}) = \frac{1}{V} \sum_{\mathbf{k}} \tilde{\Psi}_{\alpha}(\mathbf{k}) e^{i\mathbf{k}\cdot\mathbf{r}} = \frac{1}{V} \sum_{\mathbf{k},\beta} \mathcal{R}_{\alpha\beta}^{\mathcal{T}} \Psi_{\beta}^{*}(-\mathbf{k}) e^{i\mathbf{k}\cdot\mathbf{r}}$$

$$= \frac{1}{V} \sum_{\mathbf{k}',\beta} \mathcal{R}_{\alpha\beta}^{\mathcal{T}} \Psi_{\beta}^{*}(\mathbf{k}') e^{i(-\mathbf{k}')\cdot\mathbf{r}} = \frac{1}{V} \sum_{\mathbf{k}',\beta} \mathcal{R}_{\alpha\beta}^{\mathcal{T}} \Psi_{\beta}^{*}(\mathbf{k}') e^{-i\mathbf{k}'\cdot\mathbf{r}}$$

$$= \sum_{\beta} \mathcal{R}_{\alpha\beta}^{\mathcal{T}} \Psi_{\beta}^{*}(\mathbf{r}) \tag{B3}$$

where $\mathbf{k}' = -\mathbf{k}$ in the third equality. As we have described above, the quadratic terms in the GL free energy will give the maximal T_c for degenerate eigen-states $\Psi_c^{(0)}(\mathbf{Q}_j)$ located at these six momenta $(\mathbf{Q}_j \in \mathcal{Q}_6)$ and we hope to consider the solution within this U(6) subspace, so we consider the wavefunction ansatz

$$\Psi_{\alpha}(\mathbf{k}) = \sum_{\mathbf{Q}_j \in \mathcal{Q}_6} \delta(\mathbf{k} - \mathbf{Q}_j) P_{\mathbf{Q}_j} \Psi_{c,\alpha}^{(0)}(\mathbf{Q}_j)$$
(B4)

where $P_{\mathbf{Q}_j}$ is a superposition coefficient that accounts for the contribution from $\Psi_{c,\alpha}^{(0)}(\mathbf{Q}_j)$, given in Eq.(A43), at different momenta \mathbf{Q}_j in the ground state. Substituting Eq.(B4) into the Fourier transform in Eq.(B1) leads to

$$\Psi_{\alpha}(\mathbf{r}) = \frac{1}{V} \sum_{\mathbf{Q}_j \in \mathcal{Q}_6} P_{\mathbf{Q}_j} \Psi_{c,\alpha}^{(0)}(\mathbf{Q}_j) e^{i\mathbf{Q}_j \cdot \mathbf{r}}.$$
 (B5)

Eq.(B5) can be viewed as the mode expansion of $\Psi(\mathbf{r})$ on the eigen-state $\Psi^{(0)}(\mathbf{Q}_j)$ with the expansion parameter $P_{\mathbf{Q}_j}$. We can introduce a vector

$$\mathcal{P} = (P_{\mathbf{Q}_0}, \cdots, P_{\mathbf{Q}_5})^T, \tag{B6}$$

to describe the order parameter in this U(6) space, and hope to figure out the transformation form of the vector \mathcal{P} under the symmetry operations in the MPG 31' that is generated by C_{3z} and \mathcal{T} , namely

$$\hat{\mathcal{C}}_{3z}\mathbf{Q}_j = \mathbf{Q}_{j+2}; \quad \hat{\mathcal{T}}\mathbf{Q}_j = -\mathbf{Q}_j = \mathbf{Q}_{j+3}$$
(B7)

where $\mathbf{Q}_j = \mathbf{Q}_{j+6}$ from Eq.(A49). We consider the symmetry transformation of $\Psi_{\alpha}(\mathbf{r})$ in Eq.(B2) and apply the expansion ansatz in Eq.(B5) to derive

$$\tilde{\Psi}_{\alpha}(\mathbf{r}) = \sum_{\beta} \mathcal{R}_{\alpha\beta}^{\mathcal{S}} \Psi_{\beta}(\mathcal{S}^{-1}\mathbf{r})$$

$$= \frac{1}{V} \sum_{\mathbf{Q}_{j} \in \mathcal{Q}_{6}, \beta} \mathcal{R}_{\alpha\beta}^{\mathcal{S}} P_{\mathbf{Q}_{j}} \Psi_{c, \beta}^{(0)}(\mathbf{Q}_{j}) e^{i\mathbf{Q}_{j} \cdot \mathcal{S}^{-1}\mathbf{r}}$$

$$= \frac{1}{V} \sum_{\mathbf{Q}_{j} \in \mathcal{Q}_{6}} P_{\mathbf{Q}_{j}} \tilde{\Psi}_{c, \alpha}^{(0)}(\mathcal{S}\mathbf{Q}_{j}) e^{i\mathbf{Q}_{j} \cdot \mathcal{S}^{-1}\mathbf{r}}$$

$$= \frac{1}{V} \sum_{\tilde{\mathbf{Q}}_{j} = \mathcal{S}\mathbf{Q}_{j}} P_{\mathcal{S}^{-1}\tilde{\mathbf{Q}}_{j}} \tilde{\Psi}_{c, \alpha}^{(0)}(\tilde{\mathbf{Q}}_{j}) e^{i(\mathcal{S}^{-1}\tilde{\mathbf{Q}}_{j}) \cdot (\mathcal{S}^{-1}\mathbf{r})}$$

$$= \frac{1}{V} \sum_{\tilde{\mathbf{Q}}_{j} \in \mathcal{Q}_{6}} P_{\mathcal{S}^{-1}\tilde{\mathbf{Q}}_{j}} \tilde{\Psi}_{c, \alpha}^{(0)}(\tilde{\mathbf{Q}}_{j}) e^{i\tilde{\mathbf{Q}}_{j} \cdot \mathbf{r}}, \tag{B8}$$

where we have used Eq.(A13) at the third equality. By definition, we should have

$$\tilde{\Psi}(\mathbf{r}) = \frac{1}{V} \sum_{\mathbf{Q}_j \in \mathcal{Q}_6} \tilde{P}_{\mathbf{Q}_j} \tilde{\Psi}_c^{(0)}(\mathbf{Q}_j) e^{i\mathbf{Q}_j \cdot \mathbf{r}}$$
(B9)

after symmetry transformation. Thus, we find

$$\tilde{P}_{\mathbf{Q}_i} = P_{\mathcal{S}^{-1}\mathbf{Q}_i} \tag{B10}$$

for the unitary symmetry transformation \mathcal{S} . For the anti-unitary time-reversal transformation

$$\tilde{\Psi}_{\alpha}(\mathbf{r}) = \sum_{\beta} \mathcal{R}_{\alpha\beta}^{\mathcal{T}} \Psi_{\beta}^{*}(\mathbf{r})$$

$$= \frac{1}{V} \sum_{\mathbf{Q}_{j} \in \mathcal{Q}_{6}, \beta} \mathcal{R}_{\alpha\beta}^{\mathcal{T}} P_{\mathbf{Q}_{j}}^{*} \Psi_{c, \beta}^{(0)*}(\mathbf{Q}_{j}) e^{-i\mathbf{Q}_{j} \cdot \mathbf{r}}$$

$$= \frac{1}{V} \sum_{\mathbf{Q}_{j} \in \mathcal{Q}_{6}} P_{\mathbf{Q}_{j}}^{*} \tilde{\Psi}_{c, \alpha}^{(0)}(-\mathbf{Q}_{j}) e^{-i\mathbf{Q}_{j} \cdot \mathbf{r}}$$

$$= \frac{1}{V} \sum_{\tilde{\mathbf{Q}}_{j} = -\mathbf{Q}_{j}} P_{-\tilde{\mathbf{Q}}_{j}}^{*} \tilde{\Psi}_{c, \alpha}^{(0)}(\tilde{\mathbf{Q}}_{j}) e^{i\tilde{\mathbf{Q}}_{j} \cdot \mathbf{r}}$$
(B11)

where the second equality comes from anti-unitary symmetry transformation in Eq. (A13). By comparing with the transformed form in Eq. (B9) and we find

$$\tilde{P}_{\mathbf{Q}_i} = P_{-\mathbf{Q}_i}^* \tag{B12}$$

for TR symmetry. Based on Eq.(B10) and Eq.(B12), the symmetry operations in MPG 31' should transform the order parameter vector \mathcal{P} in the following way:

$$C_{3z}: \tilde{P}_{\mathbf{Q}_i} = P_{\mathbf{Q}_{i-2}} \Rightarrow \tilde{\mathcal{P}} = U_{C_{3z}} \mathcal{P}$$
 (B13)

$$\mathcal{T}: \tilde{P}_{\mathbf{Q}_j} = P_{-\mathbf{Q}_j}^* = P_{\mathbf{Q}_{j+3}}^* \Rightarrow \tilde{\mathcal{P}} = U_{\mathcal{T}} \mathcal{K} \mathcal{P} \quad \forall \mathbf{Q}_j \in \mathcal{Q}_6$$
(B14)

$$U_{C_{3z}} = \begin{pmatrix} 0 & 0 & 0 & 0 & 1 & 0 \\ 0 & 0 & 0 & 0 & 0 & 1 \\ 1 & 0 & 0 & 0 & 0 & 0 \\ 0 & 1 & 0 & 0 & 0 & 0 \\ 0 & 0 & 1 & 0 & 0 & 0 \\ 0 & 0 & 0 & 1 & 0 & 0 \end{pmatrix}; \quad U_{\mathcal{T}} = \begin{pmatrix} 0 & 0 & 0 & 1 & 0 & 0 \\ 0 & 0 & 0 & 1 & 0 & 0 \\ 0 & 0 & 0 & 0 & 0 & 1 \\ 1 & 0 & 0 & 0 & 0 & 0 \\ 0 & 1 & 0 & 0 & 0 & 0 \\ 0 & 0 & 1 & 0 & 0 & 0 \end{pmatrix}.$$
(B15)

Before the symmetry construction of the $\mathcal{F}^{(4)}$ term in Eq.(A20), we first project the $\mathcal{F}^{(2)}$ term in Eq.(A30) into the U(6) subspace of the order parameter vector \mathcal{P} . We substitute the order parameter ansatz in Eq.(B4) into Eq.(A21) and obtain

$$\mathcal{F}^{(2)} \approx \sum_{\mathbf{k}, \mathbf{Q}_j, \mathbf{Q}_k \in \mathcal{Q}_6, \alpha\beta} |P_{\mathbf{k}}|^2 \delta(\mathbf{k} - \mathbf{Q}_j) \delta(\mathbf{k} - \mathbf{Q}_k) (\Psi_{c, \alpha}^{(0)}(\mathbf{k}))^{\dagger} (T - M_{\alpha\beta}(\mathbf{k})) \Psi_{c, \beta}^{(0)}(\mathbf{k}). \tag{B16}$$

Since $\Psi^{(0)}$ can be viewed as an approximated eigen-state of $M(\mathbf{Q}_j)$ matrix with its eigen-value to be $T_{c,0}$ given in Eq.(A50), the $\mathcal{F}^{(2)}$ term can be simplified as

$$\mathcal{F}^{(2)} = (T - T_{c,0}) \sum_{\mathbf{Q}_i \in \mathcal{Q}_6} |P_{\mathbf{Q}_j}|^2.$$
 (B17)

We next aim to construct the fourth-order term $\mathcal{F}^{(4)}$ from the symmetry consideration. The generic fourth-order

terms in the GL free energy for the A and E irrep pairing channels take the form

$$\mathcal{F}^{(4)} = \mathcal{F}_A^{(4)} + \mathcal{F}_E^{(4)}$$

$$\mathcal{F}_A^{(4)} = \frac{1}{V} \int d^2 \mathbf{r} b_A |\eta_A(\mathbf{r})|^2 |\eta_A(\mathbf{r})|^2$$

$$\mathcal{F}_E^{(4)} = \frac{1}{V} \int d^2 \mathbf{r} \sum_{m,n=\pm} b_{E,mn} |\eta_{E,m}(\mathbf{r})|^2 |\eta_{E,n}(\mathbf{r})|^2$$
(B18)

where b_A and $b_{E,mn}$ are the fourth-order coefficients and $\eta_A, \eta_{E,\pm}$ are the order parameter components of $\Psi(\mathbf{r})$ in Eq.(A14). Here we only consider the local terms for the fourth-order GL free energy. Next, we substitute Eq.(B5) into $\mathcal{F}^{(4)}$ to project Ψ_{α} into the U(6) subspace and find

$$\mathcal{F}^{(4)} = \sum_{i,j,k,l \in \mathbb{Z}_6} \delta_{\mathbf{Q}_j + \mathbf{Q}_k, \mathbf{Q}_l + \mathbf{Q}_l} c(\mathbf{Q}_j, \mathbf{Q}_k, \mathbf{Q}_l, \mathbf{Q}_l) P_{\mathbf{Q}_j} P_{\mathbf{Q}_k} P_{\mathbf{Q}_l}^* P_{\mathbf{Q}_l}^* P_{\mathbf{Q}_l}^*$$
(B19)

$$c(\mathbf{Q}_{j}, \mathbf{Q}_{k}, \mathbf{Q}_{l}, \mathbf{Q}_{l}) = b_{A} \eta_{c,A}^{(0)}(\mathbf{Q}_{j}) \eta_{c,A}^{(0)}(\mathbf{Q}_{k}) \eta_{c,A}^{(0)*}(\mathbf{Q}_{l}) \eta_{c,A}^{(0)*}(\mathbf{Q}_{l}) + \sum_{mn} b_{E,mn} \eta_{c,E,m}^{(0)}(\mathbf{Q}_{j}) \eta_{c,E,n}^{(0)}(\mathbf{Q}_{k}) \eta_{c,E,m}^{(0)*}(\mathbf{Q}_{l}) \eta_{c,E,n}^{(0)*}(\mathbf{Q}_{l}),$$
(B20)

where $\eta_{c,A}^{(0)}(\mathbf{k}), \eta_{c,E,\pm}^{(0)}(\mathbf{k})$ are the order parameter components of the eigen-state $\Psi_c^{(0)}(\mathbf{k})$. Since six \mathbf{Q}_j points have same magnitude $|\mathbf{Q}_j| = k_0$ for any j = 0, 1, ..., 5, the momentum conservation in $\delta_{\mathbf{Q}_j + \mathbf{Q}_k, \mathbf{Q}_l + \mathbf{Q}_l}$ appears in only three ways, resulting in

$$\mathcal{F}^{(4)} = \sum_{\mathbf{Q}_j, j,k \in \mathcal{Q}_6} \left(\mathcal{F}^{(4,1)}(\mathbf{Q}_j, \mathbf{Q}_k) + \mathcal{F}^{(4,2)}(\mathbf{Q}_j, \mathbf{Q}_k) + \mathcal{F}^{(4,3)}(\mathbf{Q}_j, \mathbf{Q}_l) \right)$$
(B21)

$$\mathcal{F}^{(4,1)}(\mathbf{Q}_i, \mathbf{Q}_k) = c(\mathbf{Q}_i, \mathbf{Q}_k, \mathbf{Q}_i, \mathbf{Q}_k) |P_{\mathbf{Q}_i}|^2 |P_{\mathbf{Q}_k}|^2 \quad \text{if} \quad \mathbf{Q}_i = \mathbf{Q}_l \cap \mathbf{Q}_k = \mathbf{Q}_l$$
(B22)

$$\mathcal{F}^{(4,2)}(\mathbf{Q}_j, \mathbf{Q}_k) = c(\mathbf{Q}_j, \mathbf{Q}_k, \mathbf{Q}_k, \mathbf{Q}_j) |P_{\mathbf{Q}_j}|^2 |P_{\mathbf{Q}_k}|^2 \quad \text{if} \quad \mathbf{Q}_j = \mathbf{Q}_l \cap \mathbf{Q}_k = \mathbf{Q}_l$$
 (B23)

$$\mathcal{F}^{(4,3)}(\mathbf{Q}_j, \mathbf{Q}_l) = c(\mathbf{Q}_j, -\mathbf{Q}_j, \mathbf{Q}_l, -\mathbf{Q}_l) P_{\mathbf{Q}_j} P_{-\mathbf{Q}_l} (P_{\mathbf{Q}_l} P_{-\mathbf{Q}_l})^* \quad \text{if} \quad \mathbf{Q}_j = -\mathbf{Q}_k \cap \mathbf{Q}_l = -\mathbf{Q}_l. \tag{B24}$$

Using the definitions of order parameters in Eq. (A41), we can compute the coefficients as

$$c(\mathbf{Q}_j, \mathbf{Q}_k, \mathbf{Q}_j, \mathbf{Q}_k) = \frac{b_A}{N_1^2(k_0)} (T_c^{(0)}(k_0) - T_{c,E} + \gamma_E' k_0^2)^4 + \sum_{mn} \frac{b_{E,mn}}{N_1^2(k_0)} |\zeta_1'|^4 k_0^4$$
(B25)

$$c(\mathbf{Q}_{j}, \mathbf{Q}_{k}, \mathbf{Q}_{k}, \mathbf{Q}_{j}) = \frac{b_{A}}{N_{1}^{2}(k_{0})} (T_{c}^{(0)}(k_{0}) - T_{c,E} + \gamma_{E}' k_{0}^{2})^{4}$$

$$+ \sum_{m} \left[\frac{b_{E,mm}}{N_{1}^{2}(k_{0})} |\zeta_{1}'|^{4} k_{0}^{4} + \frac{b_{E,m,-m}}{N_{1}^{2}(k_{0})} |\zeta_{1}'|^{4} k_{0}^{4} \cos \left\{ 2m(\theta_{\mathbf{Q}_{j}} - \theta_{\mathbf{Q}_{l}}) \right\} \right]$$
(B26)

$$c(\mathbf{Q}_{j}, -\mathbf{Q}_{j}, \mathbf{Q}_{l}, -\mathbf{Q}_{l}) = \frac{b_{A}}{N_{1}^{2}(k_{0})} (T_{c}^{(0)}(k_{0}) - T_{c,E} + \gamma_{E}' k_{0}^{2})^{4}$$

$$+ \sum_{m} \left[\frac{b_{E,m,-m}}{N_{1}^{2}(k_{0})} |\zeta_{1}'|^{4} k_{0}^{4} + \frac{b_{E,mm}}{N_{1}^{2}(k_{0})} |\zeta_{1}'|^{4} k_{0}^{4} \cos \left\{ 2m(\theta_{\mathbf{Q}_{j}} - \theta_{\mathbf{Q}_{l}}) \right\} \right].$$
(B27)

where $\theta_{\mathbf{Q}_j} = \frac{j\pi}{3}$ is defined in Eq.(A49). The derivation of Eq.(B27) has used the fact that $c_{mn}(...) = c_{nm}(...)$, since $b_{E,nm} = b_{E,mn}$ in Eq. (B18). We first consider the first two terms in Eq.(B21), $\mathcal{F}^{(4,1)}(\mathbf{Q}_j, \mathbf{Q}_k)$ and $\mathcal{F}^{(4,2)}(\mathbf{Q}_j, \mathbf{Q}_k)$. From Eq.(B25), the coefficients $c(\mathbf{Q}_j, \mathbf{Q}_k, \mathbf{Q}_j, \mathbf{Q}_k)$ is independent of $\mathbf{Q}_j, \mathbf{Q}_k$. From Eq. (B26), $c(\mathbf{Q}_j, \mathbf{Q}_k, \mathbf{Q}_j, \mathbf{Q}_k)$ depends on the momentum angle $\theta_{\mathbf{Q}_j} - \theta_{\mathbf{Q}_l}$ and can take two different values, one for $\theta_{\mathbf{Q}_j} - \theta_{\mathbf{Q}_l} = \{0, \pi\}$, namely,

$$c(\mathbf{Q}_j, \mathbf{Q}_k, \mathbf{Q}_k, \mathbf{Q}_j) = \frac{b_A}{N_1^2(k_0)} (T_c^{(0)}(k_0) - T_{c,E} + \gamma_E' k_0^2)^4 + \sum_{m,n} \left[\frac{b_{E,mn}}{N_1^2(k_0)} |\zeta_1'|^4 k_0^4 \right],$$
(B28)

and the other for $\theta_{\mathbf{Q}_j} - \theta_{\mathbf{Q}_l} = \{\frac{\pi}{3}, \frac{2\pi}{3}, \frac{4\pi}{3}, \frac{5\pi}{3}\}$, namely,

$$c(\mathbf{Q}_j, \mathbf{Q}_k, \mathbf{Q}_k, \mathbf{Q}_j) = \frac{b_A}{N_1^2(k_0)} (T_c^{(0)}(k_0) - T_{c,E} + \gamma_E' k_0^2)^4 + \sum_m \frac{|\zeta_1'|^4 k_0^4}{N_1^2(k_0)} \left[b_{E,mm} - \frac{b_{E,m,-m}}{2} \right].$$
(B29)

These values are fixed for any $\mathbf{Q}_{j,k,l}$. Combining these results, the first two terms in Eq.(B21) give rise to

$$\sum_{\mathbf{Q}_{i,j} \in \mathcal{Q}_{6}} \mathcal{F}^{(4,1)}(\mathbf{Q}_{j}, \mathbf{Q}_{k}) + \mathcal{F}^{(4,2)}(\mathbf{Q}_{j}, \mathbf{Q}_{k}) = \sum_{\mathbf{Q}_{i} \in \mathcal{Q}_{6} \\ q = \{0,1,2,3\}} \mathcal{F}^{(4,1)}(\mathbf{Q}_{j}, \mathbf{Q}_{j+q}) + \mathcal{F}^{(4,2)}(\mathbf{Q}_{j}, \mathbf{Q}_{j+q})$$

$$= \tilde{c}_{0} \left[\sum_{\mathbf{Q}_{j} \in \mathcal{Q}_{6}} |P_{\mathbf{Q}_{j}}|^{4} \right] + \tilde{c}_{1} \left[\sum_{\mathbf{Q}_{j} \in \mathcal{Q}_{6}} |P_{\mathbf{Q}_{j}}|^{2} |P_{\mathbf{Q}_{j+1}}|^{2} \right] + \tilde{c}_{2} \left[\sum_{\mathbf{Q}_{j} \in \mathcal{Q}_{6}} |P_{\mathbf{Q}_{j}}|^{2} |P_{\mathbf{Q}_{j+2}}|^{2} \right]$$

$$+ \tilde{c}_{3,1} \left[\sum_{\mathbf{Q}_{j} \in \mathcal{Q}_{6}} |P_{\mathbf{Q}_{j}}|^{2} |P_{-\mathbf{Q}_{j}}|^{2} \right] \tag{B30}$$

where

$$\tilde{c}_p = c(\mathbf{Q}_i, \mathbf{Q}_{i+p}, \mathbf{Q}_i, \mathbf{Q}_{i+p}) + c(\mathbf{Q}_i, \mathbf{Q}_{i+p}, \mathbf{Q}_{i+p}, \mathbf{Q}_i)$$
(B31)

for p = 0, 1, 2 and

$$\tilde{c}_{3,1} = c(\mathbf{Q}_j, -\mathbf{Q}_i, \mathbf{Q}_i, -\mathbf{Q}_j) + c(\mathbf{Q}_j, -\mathbf{Q}_i, -\mathbf{Q}_i, \mathbf{Q}_j) = 2c(\mathbf{Q}_j, -\mathbf{Q}_i, \mathbf{Q}_i, -\mathbf{Q}_j). \tag{B32}$$

It should be noted that the values of the parameters \tilde{c}_p and $\tilde{c}_{3,1}$ are independent of \mathbf{Q}_j .

For the last term in Eq.(B21), $c(\mathbf{Q}_j, -\mathbf{Q}_j, \mathbf{Q}_l, -\mathbf{Q}_l)$ also depends on the momentum angle $\theta_{\mathbf{Q}_j} - \theta_{\mathbf{Q}_l}$ and is given

$$c(\mathbf{Q}_j, -\mathbf{Q}_j, \pm \mathbf{Q}_j, \mp \mathbf{Q}_j) = \frac{b_A}{N_1^2(k_0)} (T_c^{(0)}(k_0) - T_{c,E} + \gamma_E' k_0^2)^4 + \sum_{m,n} \left[\frac{b_{E,mn}}{N_1^2(k_0)} |\zeta_1'|^4 k_0^4 \right],$$
(B33)

for $\theta_{\mathbf{Q}_j} - \theta_{\mathbf{Q}_l} \in \{0, \pi\}$, and

$$c(\mathbf{Q}_{j}, -\mathbf{Q}_{j}, \mathbf{Q}_{l}, -\mathbf{Q}_{l}) = \frac{b_{A}}{N_{1}^{2}(k_{0})} \left(T_{c}^{(0)}(k_{0}) - T_{c,E} + \gamma_{E}' k_{0}^{2}\right)^{4} + \sum_{m} \frac{|\zeta_{1}'|^{4} k_{0}^{4}}{N_{1}^{2}(k_{0})} \left[b_{E,m,-m} - \frac{b_{E,mm}}{2}\right]$$
(B34)

for $\theta_{\mathbf{Q}_j} - \theta_{\mathbf{Q}_l} = \{\frac{\pi}{3}, \frac{2\pi}{3}, \frac{4\pi}{3}, \frac{5\pi}{3}\}.$ With the expression Eq.(B27), the last term in Eq.(B21) becomes

$$\sum_{\mathbf{Q}_{i,k} \in \mathcal{Q}_{6}} \mathcal{F}^{(4,3)}(\mathbf{Q}_{j}, \mathbf{Q}_{l}) = \sum_{\mathbf{Q}_{i} \in \mathcal{Q}_{6} \atop q = \{0,1,2,3\}} \mathcal{F}^{(4,3)}(\mathbf{Q}_{j}, \mathbf{Q}_{j+q})$$

$$= \tilde{c}_{3,2} \left[\sum_{\mathbf{Q}_{j} \in \mathcal{Q}_{6}} |P_{\mathbf{Q}_{j}}|^{2} |P_{-\mathbf{Q}_{j}}|^{2} \right] + \tilde{c}_{4} \sum_{\mathbf{Q}_{j} \in \mathcal{Q}_{6}} \left[P_{\mathbf{Q}_{j}} P_{-\mathbf{Q}_{j}} (P_{\mathbf{Q}_{j+1}}^{*} P_{-\mathbf{Q}_{j+1}}^{*} + P_{\mathbf{Q}_{j+2}}^{*} P_{-\mathbf{Q}_{j+2}}^{*}) \right]$$
(B35)

where

$$\tilde{c}_{3,2} = c(\mathbf{Q}_j, -\mathbf{Q}_j, \mathbf{Q}_j, -\mathbf{Q}_j) + c(\mathbf{Q}_j, -\mathbf{Q}_j, -\mathbf{Q}_j, \mathbf{Q}_j) = 2c(\mathbf{Q}_j, -\mathbf{Q}_j, \mathbf{Q}_j, -\mathbf{Q}_j)
\tilde{c}_4 = c(\mathbf{Q}_i, -\mathbf{Q}_i, \mathbf{Q}_{i+1}, -\mathbf{Q}_{i+1}) = c(\mathbf{Q}_i, -\mathbf{Q}_i, \mathbf{Q}_{i+2}, -\mathbf{Q}_{i+2}).$$
(B36)

One should note that the values of the above equations for both $\tilde{c}_{3,2}$ and \tilde{c}_4 are independent of \mathbf{Q}_j and thus we treat $\tilde{c}_{3,2}$ and \tilde{c}_4 as constant parameters.

Combining all the terms in Eqs.(B30) and (B35) leads to

$$\mathcal{F}^{(4)} = \tilde{c}_{0} \left[\sum_{\mathbf{Q}_{j} \in \mathcal{Q}_{6}} |P_{\mathbf{Q}_{j}}|^{4} \right] + \tilde{c}_{1} \left[\sum_{\mathbf{Q}_{j} \in \mathcal{Q}_{6}} |P_{\mathbf{Q}_{j}}|^{2} |P_{\mathbf{Q}_{j+1}}|^{2} \right] + \tilde{c}_{2} \left[\sum_{\mathbf{Q}_{j} \in \mathcal{Q}_{6}} |P_{\mathbf{Q}_{j}}|^{2} |P_{\mathbf{Q}_{j+2}}|^{2} \right]$$

$$+ \tilde{c}_{3} \left[\sum_{\mathbf{Q}_{j} \in \mathcal{Q}_{6}} |P_{\mathbf{Q}_{j}}|^{2} |P_{-\mathbf{Q}_{j}}|^{2} \right] + \tilde{c}_{4} \sum_{\mathbf{Q}_{j} \in \mathcal{Q}_{6}} \left[P_{\mathbf{Q}_{j}} P_{-\mathbf{Q}_{j}} (P_{\mathbf{Q}_{j+1}}^{*} P_{-\mathbf{Q}_{j+1}}^{*} + P_{\mathbf{Q}_{j+2}}^{*} P_{-\mathbf{Q}_{j+2}}^{*}) \right], \quad (B38)$$

where $\tilde{c}_3 = \tilde{c}_{3,1} + \tilde{c}_{3,2}$. Eq.(B38) is equivalent to Eq.(6) in main text with their coefficients related by $c_{0,4} = \tilde{c}_{0,4}$, $c_p = \tilde{c}_p - 2\tilde{c}_0$ with p = 1, 2 and $c_3 = \tilde{c}_3 - \tilde{c}_0$.

Next, we show that Eq.(B38) is invariant under the MPG 31' symmetry group that is generated by C_{3z} and \mathcal{T} symmetries.

(i) \tilde{c}_0 term: Using the symmetry transformation in Eq.(B13) for MPG 31', the \tilde{c}_0 term transforms as

$$C_{3z} : \sum_{\mathbf{Q}_{j} \in \mathcal{Q}_{6}} |\tilde{P}_{\mathbf{Q}_{j}}|^{4} = \sum_{\mathbf{Q}_{j} \in \mathcal{Q}_{6}} |P_{\mathbf{Q}_{j-2}}|^{4} = \sum_{\mathbf{Q}_{j} \in \mathcal{Q}_{6}} |P_{\mathbf{Q}_{i}}|^{4}$$

$$\mathcal{T} : \sum_{\mathbf{Q}_{j} \in \mathcal{Q}_{6}} |\tilde{P}_{\mathbf{Q}_{j}}|^{4} = \sum_{\mathbf{Q}_{j} \in \mathcal{Q}_{6}} |P_{\mathbf{Q}_{j+3}}|^{4} = \sum_{\mathbf{Q}_{j} \in \mathcal{Q}_{6}} |P_{\mathbf{Q}_{j+3}}|^{4} = \sum_{\mathbf{Q}_{j} \in \mathcal{Q}_{6}} |P_{\mathbf{Q}_{i}}|^{4},$$
(B39)

which is invariant under both C_{3z} and \mathcal{T} .

(ii) $\tilde{c}_{1,2,3}$ terms: Using the symmetry transformation in Eq.(B13) for MPG 31', the \tilde{c}_p terms with p=1,2,3 transform as

$$C_{3z}: \sum_{\mathbf{Q}_{j} \in \mathcal{Q}_{6}} |\tilde{P}_{\mathbf{Q}_{j}}|^{2} |\tilde{P}_{\mathbf{Q}_{j+p}}|^{2} = \sum_{\mathbf{Q}_{j} \in \mathcal{Q}_{6}} |P_{\mathbf{Q}_{j-2}}|^{2} P_{\mathbf{Q}_{j+p-2}}|^{2} = \sum_{\mathbf{Q}_{j} \in \mathcal{Q}_{6}} |P_{\mathbf{Q}_{i}}|^{2} P_{\mathbf{Q}_{j+p}}|^{2}$$
(B40)

$$\mathcal{T}: \sum_{\mathbf{Q}_{j} \in \mathcal{Q}_{6}} |\tilde{P}_{\mathbf{Q}_{j}}|^{2} |\tilde{P}_{\mathbf{Q}_{j+p}}|^{2} = \sum_{\mathbf{Q}_{j} \in \mathcal{Q}_{6}} |P_{\mathbf{Q}_{j+3}}|^{2} P_{\mathbf{Q}_{j+p+3}}|^{2} = \sum_{\mathbf{Q}_{j} \in \mathcal{Q}_{6}} |P_{\mathbf{Q}_{i}}|^{2} P_{\mathbf{Q}_{j+p}}|^{2}, \tag{B41}$$

which is invariant under both C_{3z} and \mathcal{T} .

(iii) \tilde{c}_4 term: Using the symmetry transformation in Eq.(B13) for MPG 31', the \tilde{c}_4 term transforms as

$$C_{3z} : \sum_{\mathbf{Q}_{j} \in \mathcal{Q}_{6}} \tilde{P}_{\mathbf{Q}_{j}} \tilde{P}_{\mathbf{Q}_{j+3}} (\tilde{P}_{\mathbf{Q}_{j+p}} \tilde{P}_{\mathbf{Q}_{j+p+3}})^{*}$$

$$= \sum_{\mathbf{Q}_{j} \in \mathcal{Q}_{6}} P_{\mathbf{Q}_{j-2}} P_{\mathbf{Q}_{j+1}} (P_{\mathbf{Q}_{j+p-2}} P_{\mathbf{Q}_{j+p+1}})^{*} = \sum_{\mathbf{Q}_{j} \in \mathcal{Q}_{6}} P_{\mathbf{Q}_{i}} P_{\mathbf{Q}_{j+3}} (P_{\mathbf{Q}_{j+p}} P_{\mathbf{Q}_{j+p+3}})^{*}$$

$$\mathcal{T} : \sum_{\mathbf{Q}_{j} \in \mathcal{Q}_{6}} \tilde{P}_{\mathbf{Q}_{j}} \tilde{P}_{\mathbf{Q}_{j+3}} (\tilde{P}_{\mathbf{Q}_{j+p}} \tilde{P}_{\mathbf{Q}_{j+p+3}})^{*}$$

$$= \sum_{\mathbf{Q}_{j} \in \mathcal{Q}_{6}} (P_{\mathbf{Q}_{i}} P_{\mathbf{Q}_{j+3}})^{*} P_{\mathbf{Q}_{j+p}} P_{\mathbf{Q}_{j+p+3}} = \sum_{\mathbf{Q}_{j} \in \mathcal{Q}_{6}} P_{\mathbf{Q}_{i}} P_{\mathbf{Q}_{j+3}} (P_{\mathbf{Q}_{j+p}} P_{\mathbf{Q}_{j+p+3}})^{*}$$
(B43)

for both p=1,2, from which one can see $\sum_{\mathbf{Q}_j \in \mathcal{Q}_6} P_{\mathbf{Q}_j} P_{-\mathbf{Q}_j} (P_{\mathbf{Q}_{j+p-2}}^* P_{-\mathbf{Q}_{j+p+1}}^*)$ is invariant under the symmetry operations in the MPG 31', so that the entire \tilde{c}_4 term is also invariant under the symmetry operations in the MPG 31'.

2. SC Ground states in the U(6) subspace

In this section, we will first describe our strategy to minimize the fourth-order term $\mathcal{F}^{(4)}$ within the U(6) subspace and then describe our main results of the superconducting ground states. Our strategy to solve the problem includes two steps. In the first step, we will derive the GL equations from the free energy \mathcal{F} in Eq.(B18) and solve the GL equations within a certain solution ansatz subspace, which are expected to give us possible minima of \mathcal{F} . In the second step, we will compare the minimal free energies of different solution ansätze to identify the ground states \mathcal{F} by combining analytical and numerical approaches.

We first define $P_{\mathbf{Q}_j} = \alpha_j e^{i\phi_i}$ $(j \in \mathbb{Z}_6)$, and rewrite the vector \mathcal{P} in Eq. (B6) as

$$\mathcal{P} = (\alpha_0 e^{i\phi_0}, \alpha_1 e^{i\phi_1}, \alpha_2 e^{i\phi_2}, \alpha_3 e^{i\phi_3}, \alpha_4 e^{i\phi_4}, \alpha_5 e^{i\phi_5})^T$$
(B44)

where α_j is the magnitude of the component $P_{\mathbf{Q}_j}$ which is chosen to be positive and $\phi_i \in [0, 2\pi)$ is the phase of $P_{\mathbf{Q}_j}$. With this form of $P_{\mathbf{Q}_j}$, we can rewrite the total free energy $\mathcal{F} = \mathcal{F}^{(2)} + \mathcal{F}^{(4)}$, with $\mathcal{F}^{(2)}$ in Eq.(B17) and $\mathcal{F}^{(4)}$ in Eq.(B38) as

$$\mathcal{F}[\{\alpha,\phi\};\{c\}] = \sum_{j\in\mathbb{Z}_{6}} \Delta T \alpha_{j}^{2} + c_{0} \left(\sum_{j\in\mathbb{Z}_{6}} \alpha_{j}^{2}\right)^{2} + c_{1} \sum_{j\in\mathbb{Z}_{6}} \alpha_{j}^{2} \alpha_{j+1}^{2} + c_{2} \sum_{j\in\mathbb{Z}_{6}} \alpha_{j}^{2} \alpha_{j+2}^{2} + c_{3} \sum_{j\in\mathbb{Z}_{6}} \alpha_{j}^{2} \alpha_{j+3}^{2} + 4c_{4} \left\{\alpha_{0}\alpha_{3}\alpha_{1}\alpha_{4}\cos(\phi_{0} + \phi_{3} - \phi_{1} - \phi_{4}) + \alpha_{1}\alpha_{4}\alpha_{2}\alpha_{5}\cos(\phi_{1} + \phi_{4} - \phi_{2} - \phi_{5}) + \alpha_{2}\alpha_{5}\alpha_{0}\alpha_{3}\cos(\phi_{2} + \phi_{5} - \phi_{0} - \phi_{3})\right\},$$
(B45)

where $\Delta T = T - T_{c,0}$, $\{\alpha, \phi\}$ labels the variables of the order parameters and $\{c\}$ labels the parameter space. The ground state will be the configuration of $\{\alpha_j, \phi_j | j \in \mathbb{Z}_6\}$ that minimizes the free energy Eq. (B45). To identify all the minima of the free energy, we first consider the GL equation,

$$\frac{\partial \mathcal{F}}{\partial \alpha_j} = 0, \quad \frac{\partial \mathcal{F}}{\partial \phi_j} = 0; \quad \forall j \in \mathbb{Z}_6.$$
 (B46)

Using the free energy \mathcal{F} in Eq.(B45), we find a set of GL equations, given by

$$\alpha_{0}\Delta T + \alpha_{0} \left\{ 2c_{0}\Delta_{0}^{2} + c_{1}(\alpha_{1}^{2} + \alpha_{5}^{2}) + c_{2}(\alpha_{2}^{2} + \alpha_{4}^{2}) + 2c_{3}\alpha_{3}^{2} \right\} + 4c_{4} \left\{ \alpha_{3}\alpha_{1}\alpha_{4}\cos(\theta_{1}) + \alpha_{2}\alpha_{5}\alpha_{3}\cos(\theta_{3}) \right\} = 0 \text{ (B47)}$$

$$\alpha_{1}\Delta T + \alpha_{1} \left\{ 2c_{0}\Delta_{0}^{2} + c_{1}(\alpha_{2}^{2} + \alpha_{0}^{2}) + c_{2}(\alpha_{3}^{2} + \alpha_{5}^{2}) + 2c_{3}\alpha_{4}^{2} \right\} + 4c_{4} \left\{ \alpha_{4}\alpha_{2}\alpha_{5}\cos(\theta_{2}) + \alpha_{3}\alpha_{0}\alpha_{4}\cos(\theta_{1}) \right\} = 0 \text{ (B48)}$$

$$\alpha_{2}\Delta T + \alpha_{2} \left\{ 2c_{0}\Delta_{0}^{2} + c_{1}(\alpha_{3}^{2} + \alpha_{1}^{2}) + c_{2}(\alpha_{4}^{2} + \alpha_{0}^{2}) + 2c_{3}\alpha_{5}^{2} \right\} + 4c_{4} \left\{ \alpha_{5}\alpha_{3}\alpha_{0}\cos(\theta_{3}) + \alpha_{4}\alpha_{1}\alpha_{5}\cos(\theta_{2}) \right\} = 0 \text{ (B49)}$$

$$\alpha_{3}\Delta T + \alpha_{3} \left\{ 2c_{0}\Delta_{0}^{2} + c_{1}(\alpha_{4}^{2} + \alpha_{2}^{2}) + c_{2}(\alpha_{5}^{2} + \alpha_{1}^{2}) + 2c_{3}\alpha_{0}^{2} \right\} + 4c_{4} \left\{ \alpha_{0}\alpha_{4}\alpha_{1}\cos(\theta_{1}) + \alpha_{5}\alpha_{2}\alpha_{0}\cos(\theta_{3}) \right\} = 0 \text{ (B50)}$$

$$\alpha_{4}\Delta T + \alpha_{4} \left\{ 2c_{0}\Delta_{0}^{2} + c_{1}(\alpha_{5}^{2} + \alpha_{3}^{2}) + c_{2}(\alpha_{0}^{2} + \alpha_{2}^{2}) + 2c_{3}\alpha_{1}^{2} \right\} + 4c_{4} \left\{ \alpha_{1}\alpha_{5}\alpha_{2}\cos(\theta_{2}) + \alpha_{0}\alpha_{3}\alpha_{1}\cos(\theta_{1}) \right\} = 0 \text{ (B51)}$$

$$\alpha_{5}\Delta T + \alpha_{5} \left\{ 2c_{0}\Delta_{0}^{2} + c_{1}(\alpha_{0}^{2} + \alpha_{4}^{2}) + c_{2}(\alpha_{1}^{2} + \alpha_{3}^{2}) + 2c_{3}\alpha_{2}^{2} \right\} + 4c_{4} \left\{ \alpha_{2}\alpha_{0}\alpha_{3}\cos(\theta_{3}) + \alpha_{1}\alpha_{4}\alpha_{2}\cos(\theta_{2}) \right\} = 0 \text{ (B52)}$$

$$c_{4}\alpha_{0} \left\{ \alpha_{3}\alpha_{1}\alpha_{4}\sin(\theta_{1}) + \alpha_{3}\alpha_{2}\alpha_{5}\sin(\theta_{3}) \right\} = 0 \text{ (B53)}$$

$$c_4\alpha_1 \Big\{ \alpha_4\alpha_2\alpha_5 \sin(\theta_2) + \alpha_4\alpha_3\alpha_0 \sin(\theta_1) \Big\} = 0$$
(B54)

$$c_4\alpha_2 \Big\{ \alpha_5\alpha_3\alpha_0 \sin(\theta_3) + \alpha_5\alpha_4\alpha_1 \sin(\theta_2) \Big\} = 0$$
(B55)

$$c_4\alpha_3 \left\{ \alpha_0\alpha_4\alpha_1 \sin(\theta_1) + \alpha_0\alpha_5\alpha_2 \sin(\theta_3) \right\} = 0$$
 (B56)

$$c_4 \alpha_4 \Big\{ \alpha_1 \alpha_5 \alpha_2 \sin(\theta_2) + \alpha_1 \alpha_0 \alpha_3 \sin(\theta_1) \Big\} = 0$$
(B57)

$$c_4 \alpha_5 \Big\{ \alpha_2 \alpha_0 \alpha_3 \sin(\theta_3) + \alpha_2 \alpha_1 \alpha_4 \sin(\theta_2) \Big\} = 0$$
(B58)

where

$$\Delta_0^2 = \sum_{j \in \mathbb{Z}_6} \alpha_j^2 \tag{B59}$$

gives the amplitude of the order parameter vector \mathcal{P} and the θ angles are defined by

$$\theta_1 = \phi_0 + \phi_3 - \phi_1 - \phi_4; \quad \theta_2 = \phi_1 + \phi_4 - \phi_2 - \phi_5; \quad \theta_3 = -\theta_1 - \theta_2.$$
 (B60)

Among this set of nonlinear GL equations, Eqs.(B47)-(B52) describe the extremes of free energy with respect to the amplitude of each component α_j , while Eqs.(B53)-(B58) describe the extremes with respect to the phase ϕ_i . Since only the c_4 term in the free energy (B45) depends on the phase ϕ , this phase dependence is only relevant for non-zero c_4 . In the discussion below, we will only focus on the $c_4 = 0$ situations, so the phase ϕ dependence is removed from the free energy \mathcal{F} in Eq.(B45). Correspondingly, the GL equations are simplified as

$$\alpha_0 \Delta T + \alpha_0 \left\{ 2c_0 \Delta_0^2 + c_1(\alpha_1^2 + \alpha_5^2) + c_2(\alpha_2^2 + \alpha_4^2) + 2c_3 \alpha_3^2 \right\} = 0$$
 (B61)

$$\alpha_1 \Delta T + \alpha_1 \left\{ 2c_0 \Delta_0^2 + c_1(\alpha_2^2 + \alpha_0^2) + c_2(\alpha_3^2 + \alpha_5^2) + 2c_3 \alpha_4^2 \right\} = 0$$
 (B62)

$$\alpha_2 \Delta T + \alpha_2 \left\{ 2c_0 \Delta_0^2 + c_1(\alpha_3^2 + \alpha_1^2) + c_2(\alpha_4^2 + \alpha_0^2) + 2c_3 \alpha_5^2 \right\} = 0$$
 (B63)

$$\alpha_3 \Delta T + \alpha_3 \left\{ 2c_0 \Delta_0^2 + c_1(\alpha_4^2 + \alpha_2^2) + c_2(\alpha_5^2 + \alpha_1^2) + 2c_3 \alpha_0^2 \right\} = 0$$
 (B64)

$$\alpha_4 \Delta T + \alpha_4 \left\{ 2c_0 \Delta_0^2 + c_1(\alpha_5^2 + \alpha_3^2) + c_2(\alpha_0^2 + \alpha_2^2) + 2c_3 \alpha_1^2 \right\} = 0$$
 (B65)

$$\alpha_5 \Delta T + \alpha_5 \left\{ 2c_0 \Delta_0^2 + c_1(\alpha_0^2 + \alpha_4^2) + c_2(\alpha_1^2 + \alpha_3^2) + 2c_3 \alpha_2^2 \right\} = 0.$$
 (B66)

This set of GL equations can be solved and all the extremes (including minima, maxima and saddle points) of the free energy \mathcal{F} can be obtained. We further substitute the extreme solutions back into Eq.(B45) to find the minimal free energy \mathcal{F} of different solutions and identify the superconducting ground state, by comparing these minimal free energies.

It is instructive to rewrite the order parameter components α_i 's as

$$\alpha_i = \Delta_0 a_i, \tag{B67}$$

where Δ_0 is the amplitude given in Eq.(B59) while a_i describes the direction of the vector \mathcal{P} and satisfies

$$\sum_{j \in \mathbb{Z}_6} a_j^2 = \sum_{j \in \mathbb{Z}_6} \left(\frac{\alpha_j}{\Delta_0}\right)^2 = 1.$$
 (B68)

Consequently, the vector \mathcal{P} in Eq. (B44) can be written as

$$\mathcal{P} = \Delta_0(a_0 e^{i\phi_0}, a_1 e^{i\phi_1}, a_2 e^{i\phi_2}, a_3 e^{i\phi_3}, a_4 e^{i\phi_4}, a_5 e^{i\phi_5}). \tag{B69}$$

Substituting Eq.(B69) into the free energy \mathcal{F} in Eq.(B45) leads to

$$\mathcal{F} = \Delta T \Delta_0^2 + f(\{a, \phi\}; \{c\}) \Delta_0^4 \tag{B70}$$

where

$$f(\lbrace a, \phi \rbrace; \lbrace c \rbrace) = c_0 + c_1 \sum_{j \in \mathbb{Z}_6} a_j^2 a_{j+1}^2 + c_2 \sum_{j \in \mathbb{Z}_6} a_j^2 a_{j+2}^2 + c_3 \sum_{j \in \mathbb{Z}_6} a_j^2 a_{j+3}^2$$
 (B71)

with $c_4 = 0$.

If we treat Δ_0 in Eq.(B70) as a variable, this free energy includes the Δ_0^2 and Δ_0^4 terms and can be minimized with respect to Δ_0^2 as

$$\mathcal{F}_{min} = -\frac{\Delta T^2}{4f(\lbrace a, \phi \rbrace; \lbrace c \rbrace)} \tag{B72}$$

at

$$\Delta_0 = \sqrt{-\frac{\Delta T}{2f(\{a,\phi\};\{c\})}},$$
(B73)

when $f(\{a,\phi\};\{c\})$ is positive and $\Delta T < 0$ is required for a non-zero order parameter. The smallest value of $f(\{a,\phi\};\{c\})$ under the constraint (B68) will minimize the free energy \mathcal{F}_{min} . Of course, this is equivalent to solving the GL equations (B61)-(B66), so we substitute all the extreme solutions from Eq.(B61)-(B66) into the free energy (B72) to search for the superconducting ground state. Finally, we also perform the numerical minimization of the free energy \mathcal{F} in Eq.(B45) to verify the stability of these superconducting ground states. In this work, we only focus on the case with $c_4 = 0$. More general cases for non-zero c_4 and even higher order terms have been previously studied in Ref. [73].

Before proceeding further, we want to comment on symmetry property of the state vector \mathcal{P} to keep the free energy \mathcal{F} invariant. Since the free energy is real, the action of conjugation (\mathcal{K}) on $P_{\mathbf{Q}_i}$, namely

$$\mathcal{K}: \tilde{P}_{\mathbf{Q}_{i}} = P_{\mathbf{Q}_{i}}^{*}, \tag{B74}$$

keeps the free energy in Eq.(B38) invariant. Combining the conjugation K with the C_{3z} and T symmetries in the MPG 31', we find the symmetry

$$C_1 = \mathcal{K}TC_{3z} : \tilde{P}_{\mathbf{Q}_i} = P_{-\mathbf{Q}_{i-2}} = P_{\mathbf{Q}_{i+1}}$$
(B75)

for the free energy Eq.(B38). We can repeat the symmetry transformation of \mathcal{KTC}_{3z} , so that all the cyclic permutations of \mathcal{P} in Eq.(B44)

$$C_k: P_{\mathbf{Q}_j} \to \tilde{P}_{\mathbf{Q}_j} = P_{\mathbf{Q}_{j+k}} \to \alpha_j \to \tilde{\alpha}_j = \alpha_{j+k} \quad \phi_j \to \tilde{\phi}_j = \phi_{j+k}, \quad \forall \quad j, k \in \mathbb{Z}_6,$$
(B76)

are the symmetry operators for the free energy in Eq.(B38). Any two states that are related by the C_j symmetry operator are degenerate, and this degeneracy can be removed for the superconducting ground state due to spontaneous symmetry breaking. This cyclic permutation (C_1) is schematically depicted in Fig.3.

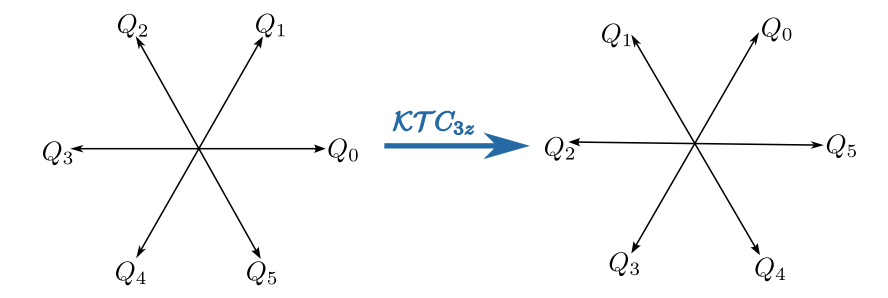


FIG. 3. The transformation $\mathcal{KT}C_{3z}$ that leads to cyclic permutations \mathcal{C}_1 , the emergent symmetry of the free energy.

Our aim below is to solve the set of GL equations (B61)-(B66) and identify the superconducting ground state described by the order parameter vector \mathcal{P} that minimizes the free energy in Eq.(B70). We assume $c_0 \gg |c_{1,2,3,4}|$ and $c_0 > 0$, so that the function f in Eq.(B70) is always positive, which is required for the existence of minima of \mathcal{F} .

Below we will consider different ansätze for the order parameter vector \mathcal{P} , labeled by \mathcal{P}_{λ} , where λ denotes different ansätze. We notice that Eqs.(B61)-(B66) contain the common factor α_{j} with j=0,1,...,5, so if any $\alpha_{j}=0$, the corresponding GL equation will be naturally satisfied. This motivates us to enumerate the solution ansätze with different numbers of non-zero components α_{j} . Below, the **phase 1** has only one non-zero component with the ansatz form $\mathcal{P}_{1}=\Delta_{0}(a_{0}e^{i\phi_{0}},0,0,0,0,0)^{T}$. Due to the symmetry of cyclic permutation, we would expect all other ansätze with one non-zero component are equivalent to \mathcal{P}_{1} . For the phases with two non-zero components, there are three inequivalent ansätze, namely $\mathcal{P}_{2a}=e^{i\theta}\Delta_{0}(a_{0}e^{i\phi_{1}},a_{1}e^{-i\phi_{1}},0,0,0,0)^{T}$ for **phase 2a**, $\mathcal{P}_{2b}=e^{i\theta}\Delta_{0}(a_{0}e^{i\phi_{1}},0,a_{2}e^{-i\phi_{2}},0,0,0)^{T}$ for **phase 2b** and $\mathcal{P}_{2c}=e^{i\theta}\Delta_{0}(a_{0}e^{i\phi_{1}},0,a_{3}e^{-i\phi_{1}},0,0)^{T}$ for **phase 2c**. There are four inequivalent ansätze for the phases with three non-zero components of \mathcal{P} , which can be listed as $\mathcal{P}_{3a}=e^{i\theta}\Delta_{0}(a_{0}e^{i\phi_{1}},a_{1}e^{-i(\phi_{1}+\phi_{2})},a_{2}e^{-i\phi_{2}},0,0,0)^{T}$ for phase **phase 3a**, $\mathcal{P}_{3b}=e^{i\theta}\Delta_{0}(a_{0}e^{i\phi_{1}},a_{1}e^{-i(\phi_{1}+\phi_{2})},0,a_{3}e^{-i\phi_{2}},0)^{T}$ for phase **phase 3b**, $\mathcal{P}_{3c}=e^{i\theta}\Delta_{0}(a_{0}e^{i\phi_{1}},a_{1}e^{-i(\phi_{1}+\phi_{2})},0,a_{4}e^{-i\phi_{2}},0)^{T}$ for phase **phase 3c** and $\mathcal{P}_{3d}=e^{i\theta}\Delta_{0}(a_{0}e^{i\phi_{1}},0,a_{2}e^{-i(\phi_{1}+\phi_{2})},0,a_{4}e^{-i\phi_{2}},0)^{T}$ for phase **phase 3c** and $\mathcal{P}_{3d}=e^{i\theta}\Delta_{0}(a_{0}e^{i\phi_{1}},0,a_{2}e^{-i(\phi_{1}+\phi_{2})},0,a_{4}e^{-i\phi_{2}},0)^{T}$ for phase **phase 3d**. For four non-

zero component ansätze, we have three candidates, namely, $\mathcal{P}_{4a} = e^{i\theta}\Delta_0(a_0e^{i\phi_1}, a_1e^{-i(\phi_1+\phi_2)}, a_2e^{-i\phi_2}, a_3e^{-i\phi_3}, 0, 0)^T$ for **phase 4a**, $\mathcal{P}_{4b} = e^{i\theta}\Delta_0(a_0e^{i\phi_1}, a_1e^{-i(\phi_1+\phi_2)}, a_2e^{-i\phi_2}, 0, a_4e^{-i\phi_3}, 0)^T$ for **phase 4b** and $\mathcal{P}_{4c} = e^{i\theta}\Delta_0(a_0e^{i\phi_1}, a_1e^{-i(\phi_1+\phi_2)}, 0, a_3e^{-i\phi_2}, a_4e^{-i\phi_3}, 0)^T$ for **phase 4c**. For five-component phase, we have one possible ansatz $\mathcal{P}_5 = e^{i\theta}\Delta_0(a_0e^{i\phi_1}, a_1e^{-i(\phi_1+\phi_2)}, a_2e^{-i\phi_2}, a_3e^{-i\phi_3}, a_4e^{-i\phi_4}, 0)^T$ called **phase 5**. For six-component, the general **phase 6** ansatz will be $\mathcal{P}_6 = e^{i\theta}\Delta_0(a_0e^{i\phi_1}, a_1e^{-i(\phi_1+\phi_2)}, a_2e^{-i\phi_2}, a_3e^{-i\phi_3}, a_4e^{-i\phi_4}, a_5e^{-i\phi_5})^T$.

Below we will calculate the minimal free energy for each phase and then compare them to determine the superconducting ground states in the $\{c\}$ parameter space.

Phase 1: The order parameter vector of the ground state ansatz for this phase is written as

$$\mathcal{P}_1 = \Delta_0 (a_0 e^{i\phi_0}, 0, 0, 0, 0, 0)^T \tag{B77}$$

with $a_0, \Delta_0 \neq 0$. Thus, the GL equations in Eqs.(B62)-(B66) are all naturally satisfied, and Eq.(B61) reads

$$\Delta T + 2c_0 \Delta_0^2 = 0,\tag{B78}$$

in which the common factors a_0 and Δ_0 have been dropped since they are non-zero. The normalization condition in Eq.(B68) requires $a_0 = 1$, and when $\Delta T < 0$ (the temperature T is below $T_{c,0}$), we have

$$\Delta_0 = \sqrt{-\Delta T/2c_0}. ag{B79}$$

Thus, we find the solution $\{\Delta_0, a_0\} = \{\sqrt{-\Delta T/c_0}, 1\}$ within the order parameter vector described by \mathcal{P}_1 . For this solution, the function f in Eq.(B71) is given by

$$f_1[\{c\}] = c_0,$$
 (B80)

and is larger than 0, so the solution indeed gives a free energy minimum,

$$\mathcal{F}_{min,1} = -\frac{\Delta T^2}{4c_0}.\tag{B81}$$

Phase 2a: The ground state ansatz is given by

$$\mathcal{P}_{2a} = e^{i\theta} \Delta_0 (a_0 e^{i\phi_1}, a_1 e^{-i\phi_1}, 0, 0, 0, 0)^T,$$
(B82)

with $\Delta_0, a_0, a_1 \neq 0$. For this ansatz, the GL equations (B63)-(B66) are all naturally satisfied, and Eqs.(B61) and (B62) read

$$\Delta T + \Delta_0^2 \left[2c_0 + c_1 a_1^2 \right] = 0 \tag{B83}$$

$$\Delta T + \Delta_0^2 \left[2c_0 + c_1 a_0^2 \right] = 0. {(B84)}$$

Together with the normalization condition in Eq.(B68), Eqs.(B83) and (B84) yield the solution $\{\Delta_0, a_0, a_1\}$ given by

$$a_0 = a_1 = 1/\sqrt{2}; \quad \Delta_0 = \sqrt{-\frac{\Delta T}{2c_0 + c_1/2}}.$$
 (B85)

The corresponding function f in Eq.(B71) is given by

$$f_{2a}[\{c\}] = c_0 + c_1/4,$$
 (B86)

and the minimal free energy is given by

$$\mathcal{F}_{min,2a} = -\frac{\Delta T^2}{4c_0 + c_1}.\tag{B87}$$

Phase 2b: The ground state ansatz is given by

$$\mathcal{P}_{2b} = e^{i\theta} \Delta_0 (a_0 e^{i\phi_1}, 0, a_2 e^{-i\phi_1}, 0, 0, 0)^T, \tag{B88}$$

with $\Delta_0, a_0, a_2 \neq 0$. For this ansatz, the GL equations (B61)-(B66) are all naturally satisfied, and Eqs.(B61) and (B63) read

$$\Delta T + \Delta_0^2 \left[2c_0 + c_2 a_2^2 \right] = 0 \tag{B89}$$

$$\Delta T + \Delta_0^2 \left[2c_0 + c_2 a_0^2 \right] = 0. {(B90)}$$

Together with the normalization condition in Eq.(B68), Eqs.(B89) and (B90) yield the solution $\{\Delta_0, a_0, a_2\}$ given by

$$a_0 = a_2 = 1/\sqrt{2}; \quad \Delta_0 = \sqrt{-\frac{\Delta T}{2c_0 + c_2/2}}.$$
 (B91)

The corresponding function f in Eq.(B71) is given by

$$f_{2b}[\{c\}] = c_0 + c_2/4, (B92)$$

and the minimal free energy is given by

$$\mathcal{F}_{min,2b} = -\frac{\Delta T^2}{4c_0 + c_2}. ag{B93}$$

Phase 2c: The ground state ansatz is given by

$$\mathcal{P}_{2c} = e^{i\theta} \Delta_0(a_0 e^{i\phi_1}, 0, 0, a_3 e^{-i\phi_1}, 0, 0)^T, \tag{B94}$$

with $\Delta_0, a_0, a_3 \neq 0$. For this ansatz, the GL equations (B61)-(B66) are all naturally satisfied, and Eqs.(B61) and (B64) read

$$\Delta T + \Delta_0^2 \left[2c_0 + 2c_3 a_3^2 \right] = 0 \tag{B95}$$

$$\Delta T + \Delta_0^2 \left[2c_0 + 2c_3 a_0^2 \right] = 0. {(B96)}$$

Together with the normalization condition in Eq.(B68), Eqs.(B95) and (B96) yield the solution $\{\Delta_0, a_0, a_3\}$ given by

$$a_0 = a_3 = 1/\sqrt{2}; \quad \Delta_0 = \sqrt{-\frac{\Delta T}{2c_0 + c_3}}.$$
 (B97)

The corresponding function f in Eq.(B71) is given by

$$f_{2c}[\{c\}] = c_0 + c_3/2,$$
 (B98)

and the minimal free energy is given by

$$\mathcal{F}_{min,2c} = \frac{\Delta T^2}{4c_0 + 2c_3}. (B99)$$

Phase 3a: The ground state ansatz is given by

$$\mathcal{P}_{3a} = e^{i\theta} \Delta_0 (a_0 e^{i\phi_1}, a_1 e^{-i(\phi_1 + \phi_2)}, a_2 e^{i\phi_2}, 0, 0, 0)^T,$$
(B100)

with Δ_0 , a_0 , a_1 , $a_2 \neq 0$. For this ansatz, the GL equations (B61)-(B66) are all naturally satisfied, and Eqs.(B61)-(B63) read

$$\Delta T + \Delta_0^2 \left[2c_0 + c_1 a_1^2 + c_2 a_2^2 \right] = 0$$
 (B101)

$$\Delta T + \Delta_0^2 \left[2c_0 + c_1(a_0^2 + a_2^2) \right] = 0$$
(B102)

$$\Delta T + \Delta_0^2 \left[2c_0 + c_1 a_1^2 + c_2 a_0^2 \right] = 0.$$
 (B103)

Together with the normalization condition in Eq.(B68), Eqs.(B101)-(B103) yield the solution $\{\Delta_0, a_0, a_1, a_2\}$ given by

$$a_0 = a_2 = \frac{a_1}{\sqrt{2 - c_2/c_1}} = \sqrt{\frac{c_1}{4c_1 - c_2}}; \quad \Delta_0 = \sqrt{-\frac{\Delta T}{2c_0 + \frac{2c_1^2}{4c_1 - c_2}}}.$$
 (B104)

The corresponding function f in Eq.(B71) is given by

$$f_{3a}[\{c\}] = c_0 + \frac{c_1^2}{4c_1 - c_2},\tag{B105}$$

and the minimal free energy is given by

$$\mathcal{F}_{min,3a} = -\frac{\Delta T^2}{4c_0 + \frac{4c_1^2}{4c_1 - c_2}}.$$
 (B106)

Phase 3b: The ground state ansatz is given by

$$\mathcal{P}_{3b} = e^{i\theta} \Delta_0(a_0 e^{i\phi_1}, a_1 e^{-i(\phi_1 + \phi_2)}, 0, a_3 e^{i\phi_2}, 0, 0)^T,$$
(B107)

with $\Delta_0, a_0, a_1, a_3 \neq 0$. For this ansatz, the GL equations (B61)-(B66) are all naturally satisfied, and Eqs.(B61),(B62) and (B64) read

$$\Delta T + \Delta_0^2 \left[2c_0 + c_1 a_1^2 + 2c_3 a_3^2 \right] = 0$$
 (B108)

$$\Delta T + \Delta_0^2 \left[2c_0 + c_1 a_0^2 + c_2 a_3^2 \right] = 0$$
(B109)

$$\Delta T + \Delta_0^2 \left[2c_0 + c_2 a_1^2 + 2c_3 a_0^2 \right] = 0.$$
 (B110)

Together with the normalization condition in Eq.(B68), Eqs.(B108), (B109) and (B110) yield the solution $\{\Delta_0, a_0, a_3\}$ given by

$$\frac{a_0}{\sqrt{c_2(c_2 - c_1 - 2c_3)}} = \frac{a_1}{\sqrt{-2c_3(c_1 + c_2 - 2c_3)}} = \frac{a_3}{\sqrt{c_1(c_1 - c_2 - 2c_3)}} = \frac{1}{\sqrt{c_1^2 + (c_2 - 2c_3)^2 - 2c_1(c_2 + 2c_3)}};$$

$$\Delta_0 = \sqrt{-\frac{\Delta T}{2c_0 - \frac{4c_1c_2c_3}{c_1^2 + (c_2 - 2c_3)^2 - 2c_1(c_2 + 2c_3)}}}.$$
(B111)

The corresponding function f in Eq.(B71) is given by

$$f_{3b}[\{c\}] = c_0 - \frac{2c_1c_2c_3}{c_1^2 + (c_2 - 2c_3)^2 - 2c_1(c_2 + 2c_3)},$$
(B112)

and the minimal free energy is given by

$$\mathcal{F}_{min,3b} = \frac{\Delta T^2}{4c_0 - \frac{8c_1c_2c_3}{c_1^2 + (c_2 - 2c_3)^2 - 2c_1(c_2 + 2c_3)}}.$$
(B113)

Phase 3c: The ground state ansatz is given by

$$\mathcal{P}_{3c} = e^{i\theta} \Delta_0(a_0 e^{i\phi_1}, a_1 e^{-i(\phi_1 + \phi_2)}, 0, 0, a_4 e^{i\phi_2}, 0)^T,$$
(B114)

with $\Delta_0, a_0, a_1, a_4 \neq 0$. For this ansatz, the GL equations (B61)-(B66) are all naturally satisfied, and Eqs.(B61),

(B63) read

$$\Delta T + \Delta_0^2 \left[2c_0 + c_1 a_1^2 + c_2 a_4^2 \right] = 0$$
(B115)

$$\Delta T + \Delta_0^2 \left[2c_0 + c_1 a_0^2 + 2c_3 a_4^2 \right] = 0$$
(B116)

$$\Delta T + \Delta_0^2 \left[2c_0 + c_2 a_0^2 + 2c_3 a_1^2 \right] = 0.$$
(B117)

Together with the normalization condition in Eq.(B68), Eqs.(B115)- (B117) yield the solution $\{\Delta_0, a_0, a_1, a_4\}$ given by

$$\frac{a_0}{\sqrt{-2c_3(c_2+c_1-2c_3)}} = \frac{a_1}{\sqrt{c_2(c_1-c_2+2c_3)}} = \frac{a_4}{\sqrt{c_1(c_1-c_2-2c_3)}} = \frac{1}{\sqrt{c_1^2+(c_2-2c_3)^2-2c_1(c_2+2c_3)}};$$

$$\Delta_0 = \sqrt{-\frac{\Delta T}{2c_0 - \frac{4c_1c_2c_3}{c_1^2+(c_2-2c_3)^2-2c_1(c_2+2c_3)}}}.$$
(B118)

The corresponding function f in Eq.(B71) is given by

$$f_{3c}[\{c\}] = c_0 - \frac{2c_1c_2c_3}{c_1^2 + (c_2 - 2c_3)^2 - 2c_1(c_2 + 2c_3)},$$
(B119)

and the minimal free energy is given by

$$\mathcal{F}_{min,3c} = -\frac{\Delta T^2}{4c_0 - \frac{8c_1c_2c_3}{c_1^2 + (c_2 - 2c_3)^2 - 2c_1(c_2 + 2c_3)}}.$$
(B120)

Phase 3d: The ground state ansatz is given by

$$\mathcal{P}_{3d} = e^{i\theta} \Delta_0(a_0 e^{i\phi_1}, 0, a_2 e^{-i(\phi_1 + \phi_2)}, 0, a_4 e^{i\phi_2}, 0)^T, \tag{B121}$$

with $\Delta_0, a_0, a_2, a_4 \neq 0$. For this ansatz, the GL equations (B61)-(B66) are all naturally satisfied, and Eqs.(B61), (B63) and (B65) read

$$\Delta T + \Delta_0^2 \left[2c_0 + c_2(a_2^2 + a_4^2) \right] = 0$$
(B122)

$$\Delta T + \Delta_0^2 \left[2c_0 + c_2(a_4^2 + a_0^2) \right] = 0$$
(B123)

$$\Delta T + \Delta_0^2 \left[2c_0 + c_2(a_0^2 + a_2^2) \right] = 0.$$
 (B124)

Together with the normalization condition in Eq.(B68), Eqs.(B122)- (B124) yield the solution $\{\Delta_0, a_0, a_2, a_4\}$ given by

$$a_0 = a_2 = a_4 = \frac{1}{\sqrt{3}}; \quad \Delta_0 = \sqrt{-\frac{\Delta T}{2c_0 + \frac{2c_2}{3}}}.$$
 (B125)

The corresponding function f in Eq.(B71) is given by

$$f_{3d}[\{c\}] = c_0 + \frac{c_2}{3},$$
 (B126)

and the minimal free energy is given by

$$\mathcal{F}_{min,3d} = -\frac{\Delta T^2}{4c_0 + \frac{4c_2}{3}}. (B127)$$

Phase 4a: The ground state ansatz is given by

$$\mathcal{P}_{4a} = e^{i\theta} \Delta_0(a_0 e^{i\phi_1}, a_1 e^{-i(\phi_1 + \phi_2)}, a_2 e^{i\phi_2}, a_3 e^{-i\phi_3}, 0, 0)^T,$$
(B128)

with $\Delta_0, a_0, a_1, a_4 \neq 0$. For this ansatz, the GL equations (B61)-(B66) are all naturally satisfied, and Eqs.(B61)-(B64) read

$$\Delta T + \Delta_0^2 \left[2c_0 + c_1 a_1^2 + c_2 a_2^2 + 2c_3 a_3^2 \right] = 0$$
(B129)

$$\Delta T + \Delta_0^2 \left[2c_0 + c_1(a_0^2 + a_1^2) + c_2 a_3^2 \right] = 0$$
(B130)

$$\Delta T + \Delta_0^2 \left[2c_0 + c_1(a_1^2 + a_3^2) + c_2 a_0^2 \right] = 0$$
(B131)

$$\Delta T + \Delta_0^2 \left[2c_0 + c_2 a_1^2 + c_1 a_2^2 + 2c_3 a_0^2 \right] = 0.$$
 (B132)

Together with the normalization condition in Eq.(B68), Eqs.(B129)-(B132) yield the solution $\{\Delta_0, a_0, a_1, a_2, a_3\}$ given by

$$\frac{a_0}{\sqrt{c_2}} = \frac{a_1}{\sqrt{c_1 + c_2 - 2c_3}} = \frac{a_2}{\sqrt{c_1 + c_2 - 2c_3}} = \frac{a_3}{\sqrt{c_2}} = \frac{1}{\sqrt{2c_1 + 4c_2 - 4c_3}};$$

$$\Delta_0 = \sqrt{-\frac{\Delta T}{2c_0 + \frac{1}{2}\left(c_1 + \frac{c_2^2}{c_1 + 2c_2 - 2c_3}\right)}}.$$
(B133)

The corresponding function f in Eq.(B71) is given by

$$f_{4a}[\{c\}] = c_0 + \frac{1}{4} \left(c_1 + \frac{c_2^2}{c_1 + 2c_2 - 2c_3} \right),$$
 (B134)

and the minimal free energy is given by

$$\mathcal{F}_{min,4a} = -\frac{\Delta T^2}{4c_0 + \left(c_1 + \frac{c_2^2}{c_1 + 2c_2 - 2c_3}\right)}.$$
(B135)

Phase 4b: The ground state ansatz is given by

$$\mathcal{P}_{4b} = e^{i\theta} \Delta_0(a_0 e^{i\phi_1}, a_1 e^{-i(\phi_1 + \phi_2)}, a_2 e^{-i\phi_2}, 0, a_4 e^{-i\phi_3}, 0)^T,$$
(B136)

with $\Delta_0, a_0, a_1, a_2, a_4 \neq 0$. For this ansatz, the GL equations (B61)-(B66) are all naturally satisfied, and Eqs.(B61),(B62),(B63) and (B65) read

$$\Delta T + \Delta_0^2 \left[2c_0 + c_1 a_1^2 + c_2 (a_2^2 + a_4^2) \right] = 0$$
(B137)

$$\Delta T + \Delta_0^2 \left[2c_0 + c_1(a_0^2 + a_2^2) + 2c_3 a_4^2 \right] = 0$$
(B138)

$$\Delta T + \Delta_0^2 \left[2c_0 + c_1 a_1^2 + c_2 (a_0^2 + a_4^2) \right] = 0$$
(B139)

$$\Delta T + \Delta_0^2 \left[2c_0 + c_2(a_0^2 + a_2^2) + 2c_3 a_1^2 \right] = 0.$$
(B140)

Together with the normalization condition in Eq.(B68), Eqs.(B137)-(B140) yield the solution $\{\Delta_0, a_0, a_2, a_3\}$ given by

$$\frac{a_0}{\sqrt{-(c_1 + c_2 - 2c_3)c_3}} = \frac{a_1}{\sqrt{c_2(-c_1 + c_2 - c_3)}} = \frac{a_2}{\sqrt{-c_3(c_1 + c_2 - 2c_3)}} = \frac{a_4}{\sqrt{c_1(c_2 + 2c_3) - c_1^2 - c_2c_3}}$$

$$= \frac{1}{\sqrt{(c_1 - c_2)^2 - 2(2c_1 + c_2)c_3 + 4c_3^2}}; \quad \Delta_0 = \sqrt{-\frac{\Delta T}{2c_0 + 2\frac{c_2c_3(c_3 - 2c_1)}{(c_1 - c_2)^2 - 2(2c_1 + c_2)c_3 + 4c_3^2}}}.$$
(B141)

The corresponding function f in Eq.(B71) is given by

$$f_{4b}[\{c\}] = c_0 + \frac{c_2 c_3 (c_3 - 2c_1)}{(c_1 - c_2)^2 - 2(2c_1 + c_2)c_3 + 4c_3^2},$$
(B142)

and the minimal free energy is given by

$$\mathcal{F}_{min,4b} = -\frac{\Delta T^2}{4c_0 + \frac{4c_2c_3(c_3 - 2c_1)}{(c_1 - c_2)^2 - 2(2c_1 + c_2)c_3 + 4c_3^2}}.$$
(B143)

Phase 4c: The ground state ansatz is given by

$$\mathcal{P}_{4c} = e^{i\theta} \Delta_0(a_0 e^{i\phi_1}, a_1 e^{-i(\phi_1 + \phi_2)}, 0, a_3 e^{i\phi_2}, a_4 e^{-i\phi_3}, 0)^T,$$
(B144)

with $\Delta_0, a_0, a_1, a_3, a_4 \neq 0$. For this ansatz, the GL equations (B61)-(B66) are all naturally satisfied, and Eqs.(B61),(B62),(B64) and (B65) read

$$\Delta T + \Delta_0^2 \left[2c_0 + c_1 a_1^2 + 2c_3 a_3^2 + c_2 a_4^2 \right] = 0$$
(B145)

$$\Delta T + \Delta_0^2 \left[2c_0 + c_1 a_0^2 + 2c_3 a_4^2 + c_2 a_3^2 \right] = 0$$
(B146)

$$\Delta T + \Delta_0^2 \left[2c_0 + c_1 a_4^2 + 2c_3 a_0^2 + c_2 a_1^2 \right] = 0$$
(B147)

$$\Delta T + \Delta_0^2 \left[2c_0 + c_1 a_3^2 + 2c_3 a_1^2 + c_2 a_0^2 \right] = 0.$$
(B148)

Together with the normalization condition in Eq.(B68), Eqs.(B145)- (B148) yield the solution $\{\Delta_0, a_0, a_2, a_3\}$ given by

$$a_0 = a_1 = a_3 = a_4 = \frac{1}{2};$$

$$\Delta_0 = \sqrt{-\frac{\Delta T}{2c_0 + \frac{c_1 + c_2 + 2c_3}{4}}}.$$
(B149)

The corresponding function f in Eq.(B71) is given by

$$f_{4c}[\{c\}] = c_0 + \frac{c_1 + c_2 + 2c_3}{8},$$
 (B150)

and the minimal free energy is given by

$$\mathcal{F}_{min,4c} = -\frac{\Delta T^2}{4c_0 + \frac{c_1 + c_2 + 2c_3}{2}}.$$
(B151)

Phase 5: The ground state ansatz is given by

$$\mathcal{P}_5 = e^{i\theta} \Delta_0(a_0 e^{i\phi_1}, a_1 e^{-i(\phi_1 + \phi_2)}, a_2 e^{-i\phi_2}, a_3 e^{-i\phi_3}, a_4 e^{-i\phi_4}, 0)^T,$$
(B152)

with $\Delta_0, a_0, a_1, a_2, a_3, a_4 \neq 0$. For this ansatz, the GL equations (B61)-(B66) are all naturally satisfied, and Eqs.(B61)-(B65) read

$$\Delta T + \Delta_0^2 \left[2c_0 + c_1 a_1^2 + 2c_3 a_3^2 + c_2 (a_2^2 + a_4^2) \right] = 0$$
(B153)

$$\Delta T + \Delta_0^2 \left[2c_0 + c_1(a_0^2 + a_2^2) + 2c_3a_4^2 + c_2a_3^2 \right] = 0$$
(B154)

$$\Delta T + \Delta_0^2 \left[2c_0 + c_1(a_1^2 + a_3^2) + c_2(a_0^2 + a_4^2) \right] = 0$$
(B155)

$$\Delta T + \Delta_0^2 \left[2c_0 + c_1(a_2^2 + a_4^2) + 2c_3a_0^2 + c_2a_1^2 \right] = 0$$
(B156)

$$\Delta T + \Delta_0^2 \left[2c_0 + c_1 a_3^2 + 2c_3 a_1^2 + c_2 (a_0^2 + a_2^2) \right] = 0.$$
 (B157)

Together with the normalization condition in Eq.(B68), Eqs.(B153)-(B157) yield the solution $\{\Delta_0, a_0, a_2, a_3\}$ given by

$$\frac{a_0}{\sqrt{c_1^2 + c_2^2 - 2c_1(c_2 + c_3)}} = \frac{a_1}{\sqrt{2c_2(-c_1 + c_2 - c_3)}} = \frac{a_2}{\sqrt{c_1^2 - (c_2 - 2c_3)^2}}$$

$$= \frac{a_3}{\sqrt{2c_2(-c_1 + c_2 - c_3)}} = \frac{a_4}{\sqrt{c_1^2 + c_2^2 - 2c_1(c_2 + c_3)}}$$

$$= \frac{1}{\sqrt{c_1^2 + 7c_2^2 - 8c_2c_3 + 4c_3^2 - 4c_1(2c_2 + c_3)}}; \quad \Delta_0 = \sqrt{-\frac{\Delta T}{2c_0 + 2\frac{c_2\{c_2^2 - c_1(c_1 + 4c_3)\}}{c_1^2 + 7c_2^2 - 8c_2c_3 + 4c_3^2 - 4c_1(2c_2 + c_3)}}. \quad (B158)$$

The corresponding function f in Eq.(B71) is given by

$$f_5[\{c\}] = c_0 + \frac{c_2\{c_2^2 - c_1(c_1 + 4c_3)\}}{c_1^2 + 7c_2^2 - 8c_2c_3 + 4c_3^2 - 4c_1(2c_2 + c_3)},$$
(B159)

and the minimal free energy is given by

$$\mathcal{F}_{min,5} = -\frac{\Delta T^2}{4c_0 + \frac{4c_2\{c_2^2 - c_1(c_1 + 4c_3)\}}{c_1^2 + 7c_2^2 - 8c_2c_3 + 4c_2^2 - 4c_1(2c_2 + c_3)}}.$$
(B160)

Phase 6: The ground state ansatz is given by

$$\mathcal{P}_6 = e^{i\theta} \Delta_0(a_0 e^{i\phi_1}, a_1 e^{-i(\phi_1 + \phi_2)}, a_2 e^{-i\phi_2}, a_3 e^{i\phi_3}, a_4 e^{i\phi_4}, a_5 e^{-i\phi_5})^T,$$
(B161)

with $\Delta_0, a_0, a_1, a_4 \neq 0$. For this ansatz, the GL equations (B61)-(B66) are all naturally satisfied,

$$\Delta T + \Delta_0^2 \left[2c_0 + c_1(a_1^2 + a_5^2) + 2c_3a_3^2 + c_2(a_2^2 + a_4^2) \right] = 0$$
(B162)

$$\Delta T + \Delta_0^2 \left[2c_0 + c_1(a_0^2 + a_2^2) + 2c_3a_4^2 + c_2(a_5^2 + a_3^2) \right] = 0$$
(B163)

$$\Delta T + \Delta_0^2 \left[2c_0 + c_1(a_1^2 + a_3^2) + c_2(a_0^2 + a_4^2) + 2c_3a_5^2 \right] = 0$$
(B164)

$$\Delta T + \Delta_0^2 \left[2c_0 + c_1(a_2^2 + a_4^2) + 2c_3a_0^2 + c_2(a_1^2 + a_5^2) \right] = 0$$
(B165)

$$\Delta T + \Delta_0^2 \left[2c_0 + c_1(a_3^2 + a_5^2) + 2c_3a_1^2 + c_2(a_0^2 + a_2^2) \right] = 0$$
(B166)

$$\Delta_0^2 \left[2c_0 + c_1(a_0^2 + a_4^2) + 2c_3a_2^2 + c_2(a_1^2 + a_3^2) \right] = 0.$$
(B167)

Together with the normalization condition in Eq.(B68), Eqs.(B162)-(B167) yield the solution $\{\Delta_0, a_0, a_2, a_3, a_4, a_5\}$ given by

$$a_0 = a_1 = a_2 = a_3 = a_4 = a_5 = \frac{1}{\sqrt{6}}; \quad \Delta_0 = \sqrt{-\frac{\Delta T}{2c_0 + \frac{c_1 + c_2 + c_3}{3}}}.$$
 (B168)

The corresponding function f in Eq.(B71) is given by

$$f_6[\{c\}] = c_0 + \frac{c_1 + c_2 + c_3}{6},\tag{B169}$$

and the minimal free energy is given by

$$\mathcal{F}_{min,6} = -\frac{\Delta T^2}{4c_0 + \frac{2(c_1 + c_2 + c_3)}{2}}.$$
(B170)

Table III summarized all phases possible as local minima of of the free energy. We have derived the minimal free energy \mathcal{F}_{min} for a certain ansatz of SC order parameter, which is a function of the second order and fourth order GL parameters, ΔT and $\{c\}$, respectively. To determine the ground state for a particular choice of ΔT and $\{c\}$, we need to compare the minimal free energy $\mathcal{F}_{min,\lambda}$ for different ansätze (we below label different ansätze by the index λ) and

Phase	Ground state vector \mathcal{P}	\mathcal{F}_{min}
1	$e^{i heta}lpha_0(1,0,0,0,0,0)^T$	$\frac{\Delta T^2}{4c_0}$
2a	$e^{i heta}lpha_0(e^{i\phi_1},e^{-i\phi_1},0,0,0,0)^T$	$-\frac{\Delta T^2}{4c_0+c_1}$
2b	$e^{i\theta}\alpha_0(e^{i\phi_1}, 0, e^{-i\phi_1}, 0, 0, 0)^T$	$-\frac{\Delta T^2}{4c_0+c_2}$
2c	$e^{i heta}lpha_0(e^{i\phi_1},0,0,e^{-i\phi_1},0,0)^T$	$\frac{\Delta T^2}{4c_0 + 2c_3}$
3a	$e^{i heta}lpha_0(rac{\cos\epsilon}{\sqrt{2}}e^{i\phi_1},e^{-i(\phi_1+\phi_2)}\sin\epsilon,rac{\cos\epsilon}{\sqrt{2}}e^{-i\phi_1},0,0,0)^T$	$-\frac{\Delta T^2}{4c_0+4c_1^2/(4c_1-c_2)}$
3b	$e^{i\theta}(\alpha_0 e^{i\phi_1}, \alpha_1 e^{-i(\phi_1 + \phi_2)}, 0, \alpha_3 e^{i\phi_2}, 0, 0)^T$	$\frac{\Delta T^2}{4c_0 - 8c_1c_2c_3/(c_1^2 + (c_2 - 2c_3)^2 - 2c_1(c_2 + 2c_3))}$
3c	$e^{i\theta}(\alpha_0 e^{i\phi_1}, \alpha_1 e^{-i(\phi_1 + \phi_2)}, 0, 0, \alpha_3 e^{i\phi_2}, 0)^T$	$-\frac{\Delta T^2}{4c_0 - 8c_1c_2c_3/(c_1^2 + (c_2 - 2c_3)^2 - 2c_1(c_2 + 2c_3))}$
3d	$e^{i heta}lpha_0(e^{i\phi_1},0,e^{i\phi_2},0,e^{-i(\phi_1+\phi_2)},0)^T$	$-rac{\Delta T^2}{4c_0+rac{4c_2}{4}}$
4a	$e^{i heta}(lpha_0e^{i\phi_1},lpha_1e^{-i(\phi_1+\phi_2)},lpha_1e^{i\phi_2},lpha_0e^{-i\phi_3},0,0)^T$	$-\frac{\Delta T^2}{4c_0+c_1+c_2^2/(c_1+2c_2-2c_3)}$
4b	$e^{i heta}(lpha_0e^{i\phi_1},lpha_1e^{-i(\phi_1+\phi_2)},lpha_0e^{i\phi_2},0,lpha_4ie^{-i\phi_3},0)^T$	$-\frac{\Delta T^2}{4c_0+4c_2c_3(c_3-2c_1)/\{(c_1-c_2)^2-2(2c_1+c_2)c_3+4c_3^2\}}$
4c	$e^{i\theta}\alpha_0(e^{i\phi_1}, e^{-i(\phi_1+\phi_2)}, 0, e^{i\phi_2}, e^{i\phi_4}, 0)^T$	$-\frac{\Delta T^2}{4c_0+\frac{c_1+c_2+2c_3}{2}}$
5	$e^{i\theta}(\alpha_0 e^{i\phi_1}, \alpha_1 e^{-i(\phi_1 + \phi_2)}, \alpha_2 e^{-i\phi_2}, \alpha_1 e^{-i\phi_3}, \alpha_0 e^{-i\phi_4}, 0)^T$	$-\frac{\Delta T^2}{4c_0 + \frac{4c_2\{c_2^2 - c_1(c_1 + 4c_3)\}}{c_1^2 + 7c_2^2 - 8c_2c_3 + 4c_3^2 - 4c_1(2c_2 + c_3)}}{\Delta T^2}$
6	$e^{i\theta}\alpha_0(e^{i\phi_1}, e^{-i(\phi_1+\phi_2)}, e^{-i\phi_2}, e^{i\phi_3}, e^{i\phi_4}, e^{-i\phi_5})^T$	$-\frac{\Delta T^2}{4c_0 + \frac{2(c_1 + c_2 + c_3)}{3}}$

TABLE IV. General form of the possible ground states from solving the total free energy for $c_4 = 0$. $\alpha_j = \Delta_0 a_j$, where Δ_0 is the global and a_j is the relative amplitude of the components in \mathcal{P} for each phase. Details on these magnitudes are discussed in Sec.B 2. Ground states highlighted are the ones that exist in some parameter regions of fourth order GL parameters $\{c\}$. The other states never form a global minima. The last column shows the minimal free energy \mathcal{F}_{min} for each possible ground state \mathcal{P} .

identify the ansatz with the lowest value of $\mathcal{F}_{min,\lambda}$. Note that ΔT is a constant in the U(6) subspace, the minimal free energy requires the conditions

$$\bigcap_{\substack{\lambda' \in \mathcal{Y} \\ \lambda' \neq \lambda}} \left\{ \mathcal{F}_{min,\lambda} < \mathcal{F}_{min,\lambda'} \right\} \Rightarrow \bigcap_{\substack{\lambda' \in \mathcal{Y} \\ \lambda' \neq \lambda}} \left\{ -\frac{(\Delta T)^2}{f_{\lambda}[\{c\}]} < -\frac{(\Delta T)^2}{f_{\lambda'}[\{c\}]} \right\} \Rightarrow \bigcap_{\substack{\lambda' \in \mathcal{Y} \\ \lambda' \neq \lambda}} \left\{ f_{\lambda}[\{c\}] < f_{\lambda'}[\{c\}] \right\}, \tag{B171}$$

where the \mathcal{Y} is the set of the all the ansatz labels,

$$\mathcal{Y} = \{1, 2a, 2b, 2c, 3a, 3b, 3c, 3d, 4a, 4b, 4c, 5, 6\}. \tag{B172}$$

These sets of inequalities in Eq.(B171) give the domains in $\{c\}$ parameter space for a particular ansatz to be the ground state with lower energy than other ansätze. We below always make the assumption $c_0 \gg |c_{1,2,3}|$, which is necessary to avoid the unphysical situation that the free energy is not lower bounded and negative infinite free energy appears in some regions of the GL parameter space due to zero $f[\{c\}]$ according to Eqs.(B71) and (B72). We numerically compare the free energy of different ansätze for the conditions in Eqs.(B171) and find that except $\{2b, 3b, 3c, 4c\}$, all the other ansätze can exist in some regions of GL parameter $\{c\}$.

These finite SC phases can spontaneously break crystal symmetry and time reversal. By examining the transformation property of these SC phases under the symmetry operator \mathcal{S} in MPG31' (See Eqs.(B13)), one can compare the order parameter after the symmetry transformation, denoted as $\tilde{\mathcal{P}}$, with \mathcal{P} before the symmetry transformation, and if one finds

$$\tilde{\mathcal{P}} \neq e^{i\alpha}\mathcal{P} \tag{B173}$$

for a certain $\alpha \in [0, 2\pi]$, the symmetry \mathcal{S} is spontaneously broken. The physical meaning and symmetry properties of the possible SC ground states are summarized as the following.

Phase 1 with the order parameter in Eqs.(B77),(B79) and the minimal free energy form in Eq.(B81) represents a single-**Q** Fulde-Ferrell(FF) state [90]. From the transformation in Eqs.(B13), we find

$$C_{3z}: \tilde{\mathcal{P}}_1 = U_{C_{3z}} \mathcal{P}_1 = \Delta_0(0, 0, a_0 e^{i\phi_0}, 0, 0, 0)^T,$$
 (B174)

$$\mathcal{T}: \tilde{\mathcal{P}}_1 = U_{\mathcal{T}} \mathcal{K} \mathcal{P}_1 = \Delta_0(0, 0, 0, a_0 e^{-i\phi_0}, 0, 0)^T$$
(B175)

for the C_{3z} and \mathcal{T} symmetries, respectively, both of which are different from \mathcal{P}_1 itself. Thus, we conclude that both the C_{3z} and \mathcal{T} symmetries are spontaneously broken.

Phase 2a with the order parameter in Eqs.(B82),(B85) and the minimal free energy in Eq.(B87) represents a double-Q FF state [86]. From the transformation form in Eqs.(B13), we find

$$C_{3z}: \tilde{\mathcal{P}}_{2a} = U_{C_{3z}} \mathcal{P}_{2a} = \Delta_0 a_0 e^{i\theta} (0, 0, 0, 0, e^{i\phi_1}, e^{-i\phi_1})^T,$$
(B176)

$$\mathcal{T}: \tilde{\mathcal{P}}_{2a} = U_{\mathcal{T}} \mathcal{K} \mathcal{P}_{2a} = \Delta_0 a_0 e^{-i\theta} (0, 0, e^{i\phi_1}, e^{-i\phi_1}, 0, 0)^T.$$
(B177)

As one can see, both symmetries are broken according to Eq.(B173), making the system breaking C_{3z} and \mathcal{T} spontaneously.

Phase 2c with the order parameter in Eqs.(B94),(B97) and minimum free energy (B99) represents a single-**Q** Larkin-Ovchinikov (LO) state [91] or a stripe phase [87]. From Eq.(B94), we see that it can break C_{3z} symmetry spontaneously, but not the TR symmetry, as

$$C_{3z}: \tilde{\mathcal{P}}_{2c} = U_{C_{3z}} \mathcal{P}_{2c} = \Delta_0 a_0 e^{i\theta} (0, 0, e^{-i\phi_1}, 0, 0, e^{i\phi_1})^T,$$
(B178)

$$\mathcal{T}: \tilde{\mathcal{P}}_{2c} = U_{\mathcal{T}} \mathcal{K} \mathcal{P}_{2c} = \Delta_0 a_0 e^{-i\theta} (e^{i\phi_1}, 0, 0, e^{-i\phi_1}, 0, 0)^T = e^{i2\theta} \mathcal{P}_{2c}.$$
 (B179)

Phase 3a with the order parameter in Eqs.(B100),(B104) and minimum free energy (B106) represents a three-**Q** FF state. From Eq.(B100), we see that it can break both \mathcal{T}, C_{3z} symmetries spontaneously,

$$C_{3z}: \tilde{\mathcal{P}}_{3a} = U_{C_{3z}} \mathcal{P}_{3a} = \Delta_0 e^{i\theta} (a_0 e^{i\phi_2}, 0, 0, 0, a_0 e^{i\phi_1}, a_1 e^{-i(\phi_1 + \phi_2)})^T,$$
(B180)

$$\mathcal{T}: \tilde{\mathcal{P}}_{3a} = U_{\mathcal{T}} \mathcal{K} \mathcal{P}_{3a} = \Delta_0 e^{-i\theta} (0, 0, 0, a_0 e^{-i\phi_1}, a_1 e^{i(\phi_1 + \phi_2)}, a_0 e^{-i\phi_2})^T.$$
(B181)

Phase 3d with the order parameter in Eqs.(B121),(B125) and minimum free energy (B127) represents the vortex-antivortex phase, which corresponds to formation of vortex-antivortex hexagonal lattice[73, 74]. From Eq.(B121), the transformation rules yield

$$C_{3z}: \tilde{\mathcal{P}}_{3d} = U_{C_{3z}} \mathcal{P}_{3d} = \Delta_0 a_0 (e^{-i(\phi_1 + \phi_2)}, 0, e^{i\phi_2}, 0, e^{i\phi_1}, 0)^T,$$
(B182)

$$\mathcal{T}: \tilde{\mathcal{P}}_{3d} = U_{\mathcal{T}} \mathcal{K} \mathcal{P}_{3d} = e^{-i\theta} \Delta_0 a_0 (0, e^{-i\phi_2}, 0, e^{-i\phi_1}, 0, e^{i(\phi_1 + \phi_2)})^T.$$
(B183)

From the above equations, one can see that the **phase 3d** breaks TR symmetry spontaneously. For the C_{3z} symmetry, it is more tricky. At the first sight, it seems the C_{3z} symmetry only exists when both the phase factors ϕ_1 and ϕ_2 are zero. We may define

$$\mathcal{P}_{3d,0} = e^{i\theta} \Delta_0(a_0, 0, a_0, 0, a_0, 0)$$
(B184)

with $\phi_1 = \phi_2 = 0$ so that $C_{3z} : \tilde{\mathcal{P}}_{3d,0} = \mathcal{P}_{3d,0}$. Next we will show that \mathcal{P}_{3d} with any values of ϕ_1 and ϕ_2 can be connected to $\mathcal{P}_{3d,0}$ with a lattice translation. To see that, we consider the real space wavefunction of the **phase 3d** in Eq.(B5) for \mathcal{P}_{3d} and $\mathcal{P}_{3d,0}$, which are given by

$$\Psi_{\alpha}^{(3d)}(\mathbf{r}) = \frac{1}{V} \sum_{\mathbf{Q}_j \in \mathcal{Q}_6} P_{\mathbf{Q}_j}^{(3d)} \Psi_{c,\alpha}^{(0)}(\mathbf{Q}_j) e^{i\mathbf{Q}_j \cdot \mathbf{r}}$$
(B185)

and

$$\Psi_{\alpha}^{(3d,0)}(\mathbf{r}) = \frac{1}{V} \sum_{\mathbf{Q}_j \in \mathcal{Q}_6} P_{\mathbf{Q}_j}^{(3d,0)} \Psi_{c,\alpha}^{(0)}(\mathbf{Q}_j) e^{i\mathbf{Q}_j \cdot \mathbf{r}}$$
(B186)

where $P_{\mathbf{Q}_{i}}^{(3d)}$ and $P_{\mathbf{Q}_{i}}^{(3d,0)}$ are the jth components of \mathcal{P}_{3d} and $\mathcal{P}_{3d,0}$, respectively. Explicitly, we have

$$\begin{split} \Psi_{\alpha}^{(3d)}(\mathbf{r}) &= \frac{\Delta_{0}a_{0}e^{i\theta}}{V} \Big[\Psi_{0,\alpha}(\mathbf{Q}_{0})e^{i(\mathbf{Q}_{0}\cdot\mathbf{r}+\phi_{1})} + \Psi_{0,\alpha}(\mathbf{Q}_{2})e^{i(\mathbf{Q}_{2}\cdot\mathbf{r}-\phi_{1}-\phi_{2})} + \Psi_{0,\alpha}(\mathbf{Q}_{4})e^{i(\mathbf{Q}_{4}\cdot\mathbf{r}+\phi_{2})} \Big] \\ &= \frac{\Delta_{0}a_{0}e^{i\theta}}{V} \Big[\Psi_{0,\alpha}(\mathbf{Q}_{0})e^{ik_{0}(x+\frac{\phi_{1}}{k_{0}})} + \Psi_{0,\alpha}(\mathbf{Q}_{2})e^{ik_{0}\{-\frac{1}{2}(x+\frac{\phi_{1}}{k_{0}})+\frac{\sqrt{3}}{2}(y-\frac{\phi_{1}}{\sqrt{3}k_{0}}-\frac{2\phi_{2}}{\sqrt{3}k_{0}})\}} \\ &+ \Psi_{0,\alpha}(\mathbf{Q}_{4})e^{ik_{0}\{-\frac{1}{2}(x+\frac{\phi_{1}}{k_{0}})-\frac{\sqrt{3}}{2}(y-\frac{\phi_{1}}{\sqrt{3}k_{0}}-\frac{2\phi_{2}}{\sqrt{3}k_{0}})\}} \Big] \\ &= \frac{\Delta_{0}a_{0}e^{i\theta}}{V} \Big[\Psi_{0,\alpha}(\mathbf{Q}_{0})e^{i(\mathbf{Q}_{0}\cdot(\mathbf{r}+\mathbf{d}(\phi_{1},\phi_{2})))} + \Psi_{0,\alpha}(\mathbf{Q}_{2})e^{i(\mathbf{Q}_{2}\cdot(\mathbf{r}+\mathbf{d}(\phi_{1},\phi_{2})))} + \Psi_{0,\alpha}(\mathbf{Q}_{4})e^{i(\mathbf{Q}_{4}\cdot(\mathbf{r}+\mathbf{d}(\phi_{1},\phi_{2})))} \Big] \\ &= \Psi_{\alpha}^{(3d,0)}(\mathbf{r}+\mathbf{d}(\phi_{1},\phi_{2})) \end{split}$$
(B187)

where \mathbf{Q}_j is given in Eq.(A49), $\alpha = 0, \pm 1$ labels three components of the order parameters and

$$\mathbf{d}(\phi_1, \phi_2) = \frac{\phi_1}{k_0} \hat{e}_x - \left(\frac{\phi_1}{2} + \phi_2\right) \hat{e}_y$$
 (B188)

is a vector representing the translation of the vortex-antivortex lattice. Thus, $\Psi_{\alpha}^{(3d)}(\mathbf{r})$ can be viewed as the Goldstone mode of $\Psi_{\alpha}^{(3d,0)}(\mathbf{r})$ with a translation of $\mathbf{d}(\phi_1,\phi_2)[92]$ characterized by two U(1) phases (ϕ_1,ϕ_2) between different components of \mathcal{P}_{3d} . Since $\Psi_{\alpha}^{(3d,0)}(\mathbf{r})$ has C_{3z} symmetry, we would expect $\Psi_{\alpha}^{(3d)}(\mathbf{r})$ is also C_{3z} invariant, but its rotation center is shifted by the vector $\mathbf{d}(\phi_1,\phi_2)$. Mathematically, we have

$$\Psi_{\alpha}^{(3d,0)}(\mathbf{r}) = \Psi_{\alpha}^{(3d)}(\mathbf{r} - \mathbf{d}(\phi_1, \phi_2)), \tag{B189}$$

which implies

$$t[-\mathbf{d}(\phi_1, \phi_2)]: \quad \tilde{\mathcal{P}}_{3d} = U_t[-\mathbf{d}(\phi_1, \phi_2)]\mathcal{P}_{3d} = \Delta_0 a_0 e^{i\theta}(1, 0, 1, 0, 1, 0) = \mathcal{P}_{3d,0}$$
(B190)

according to Eq.(B5). As $\mathcal{P}_{3d,0}$ is invariant under C_{3z} , we must have

$$t[\mathbf{d}(\phi_1, \phi_2)]C_{3z}t[-\mathbf{d}(\phi_1, \phi_2)]: \quad \tilde{\mathcal{P}}_{3d} = U_t[\mathbf{d}(\phi_1, \phi_2)]U_{C_{3z}}\mathcal{P}_{3d,0} = \Delta_0 a_0 e^{i\theta}(e^{i\phi_1}, 0, e^{-i(\phi_1 + \phi_2)}, 0, e^{i\phi_2}, 0), \quad (B191)$$

which indicates that \mathcal{P}_{3d} is invariant under the three-fold rotation symmetry with the rotation center at $\mathbf{d}(\phi_1, \phi_2)$, as described by $t[\mathbf{d}(\phi_1, \phi_2)]C_{3z}t[-\mathbf{d}(\phi_1, \phi_2)]$.

Phase 4a with the order parameter in Eqs.(B128),(B133) and minimum free energy (B135) represents a superposition state between the two-Q FF state and a single-Q LO/PDW state. From Eq.(B128), we find

$$C_{3z}: \tilde{\mathcal{P}}_{4a} = U_{C_{3z}} \mathcal{P}_{4a} = \Delta_0 e^{i\theta} (a_1 e^{i\phi_2}, a_0 e^{-i\phi_3}, 0, 0, a_0 e^{i\phi_1}, a_1 e^{-i(\phi_1 + \phi_2)})^T,$$
(B192)

$$\mathcal{T}: \tilde{\mathcal{P}}_{4a} = U_{\mathcal{T}} \mathcal{K} \mathcal{P}_{4a} = \Delta_0 e^{-i\theta} (a_0 e^{i\phi_3}, 0, 0, a_0^{-i\phi_1}, a_1 e^{i(\phi_1 + \phi_2)}, a_1^{-i\phi_2})^T,$$
(B193)

and thus **Phase 4a** spontaneously break both \mathcal{T} and C_{3z} symmetries,

Phase 4b with the order parameter in Eqs.(B128),(B141) and minimum free energy (B143), represent a four-**Q** FF state. From Eq.(B136), we find

$$C_{3z}: \tilde{\mathcal{P}}_{4b} = U_{C_{3z}} \mathcal{P}_{4b} = \Delta_0 e^{i\theta} (a_0 e^{-i\phi_2}, 0, a_4 e^{-i\phi_3}, 0, a_0 e^{i\phi_1}, a_1 e^{-i(\phi_1 + \phi_2)})^T,$$
(B194)

$$\mathcal{T}: \tilde{\mathcal{P}}_{4b} = U_{\mathcal{T}} \mathcal{K} \mathcal{P}_{4b} = \Delta_0 e^{-i\theta} (0, a_4 e^{i\phi_3}, 0, a_0 e^{-i\phi_1}, a_1 e^{i(\phi_1 + \phi_2)}, a_0 e^{i\phi_2})^T, \tag{B195}$$

so that **Phase 4b** spontaneously break both \mathcal{T} and C_{3z} symmetries.

Phase 5 with the order parameter in Eqs.(B152),(B158) and minimum free energy (B160), represent a superposition of the two-**Q** FF and the three-**Q** FF states. From Eq.(B152), we find

$$C_{3z}: \tilde{\mathcal{P}}_5 = U_{C_{2z}} \mathcal{P}_5 = e^{i\theta} \Delta_0(a_2 e^{-i\phi_2}, a_1 e^{-i\phi_3}, a_0 e^{-i\phi_4}, 0, a_0 e^{i\phi_1}, a_1 e^{-i(\phi_1 + \phi_2)})^T,$$
(B196)

$$\mathcal{T}: \tilde{\mathcal{P}}_5 = U_{\mathcal{T}} \mathcal{K} \mathcal{P}_5 = \Delta_0 e^{-i\theta} (a_1 e^{-i\phi_3}, a_0 e^{-i\phi_4}, 0, a_0 e^{-i\phi_1}, a_1 e^{i(\phi_1 + \phi_2)}, a_2 e^{i\phi_2})^T,$$
(B197)

so that **Phase 5** spontaneously break both \mathcal{T} and C_{3z} symmetries.

For **Phase 6**, we find all six components in \mathcal{P} are non-zero and equal, according to Eq.(B168). Consequently,

the presence and absence of \mathcal{T} and C_{3z} of **Phase 6** rely on the relative phases between different components, which requires to take into account the phase dependent terms, such as the c_4 term. This phase has been previously explored in Ref.[73].

From the above discussion, we find that a variety of superconducting ground states can spontaneously break either C_{3z} or \mathcal{T} symmetry. In particular, the **Phase 3d** (vortex-antivortex lattice phase) breaks time-reversal (\mathcal{T}) but preserves three-fold rotation $(t[\mathbf{d}(\phi_1,\phi_2)]C_{3z}t[-\mathbf{d}(\phi_1,\phi_2)])$, while the **Phase 2c** (stripe phase) breaks three-fold rotation but preserves time reversal. The **phases 1, 2a, 3a, 4a, 4b, 5** all break both three-fold rotation and time reversal.

The real space distribution of the order parameters, as well as their different components (A_{1g} or E components), are depicted in Fig.6 for **phases 2a**, **3a**, **4a and 4b**, in Fig. 5 for **phase 3d** and in Fig. 4 for **phase 2c**. The **phase 1** is the single- \mathbf{Q} FF phase with only phase modulation, while its amplitude is uniform, and thus we do not plot its amplitude. We find the **phase 2a**, **2c** and **4a** are stripe phases. **Phase 2a**, as shown in Fig.6(a-c), has a sinusoidal modulation in the direction of $\mathbf{Q}_0 - \mathbf{Q}_1$, where \mathbf{Q}_j is defined in Eq.(A49). Likewise, **phase 2c** has stripe modulation along $\mathbf{Q}_0 - \mathbf{Q}_3$, as seen in Fig.4(a-c). **Phase 4a** is a combination of two stripe modulations of different periodicity, both along the \mathbf{Q}_0 direction, as seen in Fig.6(g-i), which can be viewed as a mixture of two stripe phases **2a and 2c**. **Phase 3a** forms a planar oblique lattice with the longer diagonal oriented along \mathbf{Q}_1 , as seen in Fig.6(d-f). **Phase 4b and 3d** form hexagonal lattices, as seen in Fig.6(j-l) and Fig.5(a-c), respectively.

3. Example: phase transition between Phases 3d and 2c

As an example, we will focus on two representative phases, the **Phase 3d** and **Phase 2c**, in which the former breaks \mathcal{T} and the latter breaks C_{3z} . It turns out that these two phases can be controlled by a single tuning parameter in the phase diagram. Below we will first figure out the existence regions in the parameter space for these two phases.

For **Phase 2c**, the constraints in Eq.(B171) can be explicitly written down. When $c_1 \leq 0$, **Phase 2c** turns out to be the ground state in the following parameter regimes, $c_2 < 4c_1 \cap c_3 < \frac{1}{2}(c_1 + 2c_2)$ or $4c_1 < c_2 \leq \frac{43c_1}{14} - \frac{1}{14}\sqrt{57}\sqrt{c_1^2} \cap c_3 < \frac{2c_1^2}{4c_1-c_2}$ or $\frac{43c_1}{14} - \frac{1}{14}\sqrt{57}\sqrt{c_1^2} < c_2 \leq 0 \cap c_3 < \frac{1}{2}(c_1 + 2c_2) - \frac{1}{2}\sqrt{3}\sqrt{4c_1c_2-c_2^2}$ or $c_2 > 0 \cap c_3 < \frac{c_1}{2}$. When $c_1 > 0$, **Phase 2c** can also be the ground state in the following parameter regimes, $c_2 \leq -\frac{1}{2}(3c_1) \cap c_3 < \frac{1}{2}(c_1 + 2c_2)$ or $-\frac{1}{2}(3c_1) < c_2 \leq 0 \cap c_3 < \frac{2c_2}{3}$ or $0 < c_2 \leq \frac{c_1}{7} \cap c_3 < \frac{1}{4}(c_1 + 3c_2) - \frac{1}{4}\sqrt{c_1^2 + 22c_1c_2 - 7c_2^2}$ or $\frac{c_1}{7} < c_2 < c_1 \cap \left(c_3 < \frac{1}{4}(c_1 + 3c_2) - \frac{1}{4}\sqrt{c_1^2 + 22c_1c_2 - 7c_2^2} \cup \frac{1}{2}(c_1 + 2c_2) - \frac{1}{2}\sqrt{3}\sqrt{4c_1c_2 - c_2^2} < c_3 < 0\right)$ or $c_1 \leq c_2 < 4c_1 \cap c_3 < 0$ or $c_2 > 4c_1 \cap c_3 < \frac{2c_1^2}{4c_1-c_2}$.

 $c_2 > 4c_1 \cap c_3 < \frac{2c_1^2}{4c_1 - c_2}.$ Similarly, we can also explicitly simplify the constraints in Eq.(B171) for **Phase 3d**. For **phase 3d**, when $c_1 < 0$, this phase exists when $c_2 < \frac{69c_1}{2} - \frac{9}{2}\sqrt{57}\sqrt{c_1^2}$ and $\frac{3c_1^2 + 2c_1c_2 - 5c_2^2}{6c_1 - 8c_2} < c_3 < \frac{c_1 + c_2}{2} - \sqrt{c_1c_2}$ or $\frac{1}{4}(2c_2 - c_1) - \frac{1}{4}\sqrt{4c_1c_2 - 3c_1^2} < c_3 < \frac{1}{4}\sqrt{4c_1c_2 - 3c_1^2} + \frac{1}{4}(2c_2 - c_1)$ or $c_3 > \frac{c_1 + c_2}{2} + \sqrt{c_1c_2}$. It also expands through $\frac{69c_1}{2} - \frac{9}{2}\sqrt{57}\sqrt{c_1^2} \le c_2 < 4c_1$ and $\frac{1}{4}(2c_2 - c_1) - \frac{1}{4}\sqrt{4c_1c_2 - 3c_1^2} < c_3 < \frac{1}{4}\sqrt{4c_1c_2 - 3c_1^2} + \frac{1}{4}(2c_2 - c_1)$ or $c_3 > \frac{c_1 + c_2}{2} + \sqrt{c_1c_2}$. The last zone of parameters is $3c_1 < c_2 < c_1 \cap c_3 > \frac{c_1 + c_2}{2} + \sqrt{c_1c_2}$ for $c_1 < 0$. When $c_1 = 0$, we find the parameter regions are defined by $c_2 < 0$ with $\frac{5c_2}{8} < c_3 < \frac{c_2}{2}$ or $c_3 > \frac{c_2}{2}$. When $c_1 > 0$ we find two regions of parameters where the phase exists. The first one is $c_2 \le -\frac{1}{2}(3c_1) \cap c_3 > \frac{3c_1^2 + 2c_1c_2 - 5c_2^2}{6c_1 - 8c_2}$. The second one is $\frac{1}{2}(3c_1) < c_2 < 0$ when $\frac{2c_2}{3} < c_3 < \frac{1}{2}(c_1 + 2c_2)$ or $c_3 > \frac{3c_1^2 + 2c_1c_2 - 5c_2^2}{6c_1 - 8c_2}$. The second one is $\frac{1}{2}(3c_1) < c_2 < 0$ when $\frac{2c_2}{3} < c_3 < \frac{1}{2}(c_1 + 2c_2)$ or $c_3 > \frac{3c_1^2 + 2c_1c_2 - 5c_2^2}{6c_1 - 8c_2}$. The second one is $\frac{1}{2}(3c_1) < c_2 < 0$ when $\frac{2c_2}{3} < c_3 < \frac{1}{2}(c_1 + 2c_2)$ or $c_3 > \frac{3c_1^2 + 2c_1c_2 - 5c_2^2}{6c_1 - 8c_2}$. The second one is $\frac{1}{2}(3c_1) < c_2 < 0$ when $\frac{2c_2}{3} < c_3 < \frac{1}{2}(c_1 + 2c_2)$ or $c_3 > \frac{3c_1^2 + 2c_1c_2 - 5c_2^2}{6c_1 - 8c_2}$. The second one is $\frac{1}{2}(3c_1) < c_2 < 0$ when $\frac{2c_2}{3} < c_3 < \frac{1}{2}(c_1 + 2c_2)$ or $c_3 > \frac{3c_1^2 + 2c_1c_2 - 5c_2^2}{6c_1 - 8c_2}$. The general conditions for the above parameter regions are complicated. We find when $c_1 + c_2 = 0$ is satisfied, the above parameter regions can be greatly simplified. In this case, the **Phase 2c** exists in two parameter regions, (i) c_2

4. Vortex-antivortex lattice and effective angular momentum

The real space distribution of order parameter for **Phase 3d** has been shown in Fig.5(c) and discussed in Sec.B 2. Next we discuss the A and E components of the order parameter for **phase 3d** separately. The amplitude of A order parameter $|\eta_A(\mathbf{r})|$ in **phase 3d**, as shown in 5(a), is one order larger than the amplitude of E order parameter $|\eta_E(\mathbf{r})|$,

as shown in Fig.5b, which is defined as

$$|\eta_E(\mathbf{r})| = \sqrt{|\eta_{E+}(\mathbf{r})|^2 + |\eta_{E-}(\mathbf{r})|^2}.$$
 (B198)

In Fig.5c, the colors represent the overall amplitude,

$$|\Psi(\mathbf{r})| = \sqrt{\eta_A(\mathbf{r})^2 + |\eta_{E+}(\mathbf{r})|^2 + |\eta_{E-}(\mathbf{r})|^2},$$
(B199)

which primarily follows the spatial distribution of $\eta_A(\mathbf{r})$ in Fig.5a, further testifying the dominance of $\eta_A(\mathbf{r})$ over the $\eta_E(\mathbf{r})$ amplitude. This dominance is evident for all other phases as well, as shown in Figs.4 and 6.

We examine the supercurrent distribution of **Phase 3d** in Fig.5c, to extract its vortex-antivortex structure. The local supercurrent can be defined from total free energy in Eq.(A20), defined by

$$\mathbf{j}_s(\mathbf{r}) = -2e\nabla_{\mathbf{A}}\{\mathcal{F}^{(2)}(\mathbf{r}) + \mathcal{F}^{(4)}(\mathbf{r})\}|_{\mathbf{A}=\mathbf{0}},\tag{B200}$$

where $\mathcal{F}^{(2)}(\mathbf{r})$ is defined as the inverse Fourier transform of Eq.(A27) and $\mathcal{F}^{(4)}(\mathbf{r})$ is defined in Eq.(B18). The vector field **A** is gauge coupled to the momentum as as $\mathbf{k} \to \mathbf{k} - 2e\mathbf{A}$ in (A27), which gives rise to

$$\mathbf{j}_s(\mathbf{r}) = 2e(\gamma_A + \gamma_E)\Im\{\Psi^*(\mathbf{r})\nabla\Psi(\mathbf{r})\}.$$
(B201)

The supercurrent distribution is shown by the red arrows in Fig.5c for **phase 3d**. The unit cell of the finite momentum order parameter is shown by the black hexagon in Fig.5c, from which one can see that the winding of the supercurrent (red arrows) that forms vortex is around six corners of the hexagon. For the cyan and yellow small hexagons in Fig.5c, the supercurrent is winding in the opposite directions, clockwise and counter-clockwise, leading to the formations of vortices and antivortices, respectively. This alternating vortex-antivortex structure is known as the vortex-antivortex lattice [73, 74].

Since the s-wave A component with zero intrinsic angular momentum and the E components with chiral $p \pm ip$ structure has ± 1 intrinsic angular momenta, we can define the effective angular momentum as

$$\mathbf{L}(\mathbf{r}) = \Psi^{\dagger}(\mathbf{r})\mathbf{m}\Psi(\mathbf{r}),\tag{B202}$$

where **m** is the vector of angular momentum component matrices,

$$m_x = \frac{1}{\sqrt{2}} \begin{pmatrix} 0 & 1 & 0 \\ 1 & 0 & 1 \\ 0 & 1 & 0 \end{pmatrix}; m_y = \frac{1}{\sqrt{2}} \begin{pmatrix} 0 & -i & 0 \\ i & 0 & -i \\ 0 & i & 0 \end{pmatrix}; m_z = \begin{pmatrix} 1 & 0 & 0 \\ 0 & 0 & 0 \\ 0 & 0 & -1 \end{pmatrix}.$$
(B203)

Using the form of the order parameter $\Psi(\mathbf{r})$, we find

$$L_{x}(\mathbf{r}) = \sqrt{2}\Re\left[\eta_{A}^{*}(\mathbf{r})\{\eta_{E+}(\mathbf{r}) + \eta_{E-}(\mathbf{r})\}\right]$$

$$L_{y}(\mathbf{r}) = -\sqrt{2}\Im\left[\eta_{A}^{*}(\mathbf{r})\{\eta_{E+}(\mathbf{r}) - \eta_{E-}(\mathbf{r})\}\right]$$

$$L_{z}(\mathbf{r}) = |\eta_{E+}(\mathbf{r})|^{2} - |\eta_{E-}(\mathbf{r})|^{2}.$$
(B204)

The expression can be further expanded using the components of the order parameter in main text Eq. (B5)

$$\eta_{E,\pm}(\mathbf{r}) = \sum_{j \in \mathbb{Z}_6} P_{\mathbf{Q}_j} \eta_{E,\pm}^{(0)}(\mathbf{Q}_j) e^{i\mathbf{Q}_j \cdot \mathbf{r}}.$$
(B205)

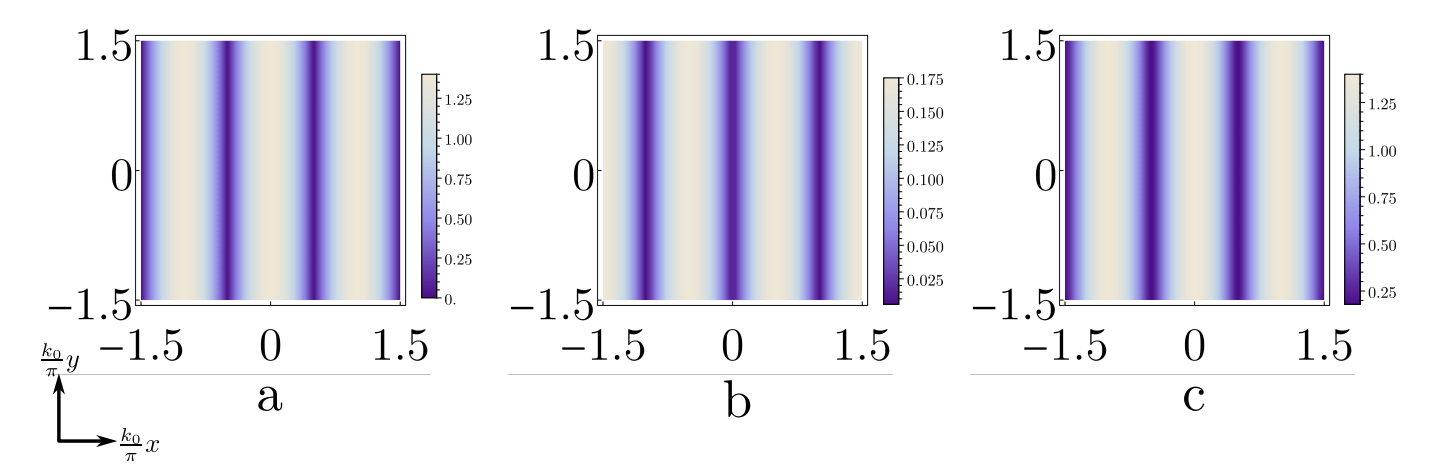


FIG. 4. Spatial distribution of different order parameter $\Psi(\mathbf{r})$ in striped **phase 2c**. All axes represent the x,y coordinates in scales of $\frac{\pi}{k_0}$. (a) Real-space distribution of the A-component $|\eta_A(\mathbf{r})|$ (b)Real-space distribution of the E components $|\eta_E(\mathbf{r})|$, defined in Eq.(B198)(c)The total amplitude of the order parameter, $|\Psi(\mathbf{r})|$, defined in Eq.(B199). All numerical parameters are same as Fig 1. in main-text.

With the eigenvector $\eta_{E,\pm}^{(0)}(\mathbf{Q}_j)$ in Eq. (A41), we find

$$L_{x}(\mathbf{r}) = \frac{2\sqrt{2}}{N(k_{0})} \left\{ T_{c}(k_{0}) - T_{c,E} - \gamma_{E} k_{0}^{2} \right\} \sum_{i,j \in \mathbb{Z}_{6}} \Re(\zeta_{1}' \mathbf{Q}_{j+}) \Re \left\{ P_{\mathbf{Q}_{j}} P_{\mathbf{Q}_{k}}^{*} e^{i(\mathbf{Q}_{j} - \mathbf{Q}_{k}) \cdot \mathbf{r}} \right\}$$

$$L_{y}(\mathbf{r}) = -\frac{2\sqrt{2}}{N(k_{0})} \left\{ T_{c}(k_{0}) - T_{c,E} - \gamma_{E} k_{0}^{2} \right\} \sum_{i,j \in \mathbb{Z}_{6}} \Im(\zeta_{1}' \mathbf{Q}_{j+}) \Im \left\{ P_{\mathbf{Q}_{j}} P_{\mathbf{Q}_{k}}^{*} e^{i(\mathbf{Q}_{j} - \mathbf{Q}_{k}) \cdot \mathbf{r}} \right\}$$

$$L_{z}(\mathbf{r}) = -\frac{2}{N(k_{0})} \sum_{i,j \in \mathbb{Z}_{6}} |\zeta_{1}'|^{2} \Im(\mathbf{Q}_{j+} \mathbf{Q}_{j-}) \Im\left(P_{\mathbf{Q}_{j}} P_{\mathbf{Q}_{k}}^{*} e^{i(\mathbf{Q}_{j} - \mathbf{Q}_{k}) \cdot \mathbf{r}} \right). \tag{B206}$$

We emphasize this angular momentum \mathbf{L} is an effective one since the order parameter is a combination of s-wave and p-wave pairing. A non-zero value of $L_z(\mathbf{r})$ can demonstrate spontaneous time reversal symmetry breaking. From Eq.(B204), one can see that $L_z(\mathbf{r})$ describes the difference between the amplitudes $|\eta_{E+}(\mathbf{r})|$ and $|\eta_{E-}(\mathbf{r})|$. From (B11), time reversal operation transforms $\eta_{E,\mp}(\mathbf{r})$ as

$$\mathcal{T}: \quad \tilde{\eta}_{E,\pm}(\mathbf{r}) = \eta_{E,\pm}^*(\mathbf{r}). \tag{B207}$$

Non-zero $L_z(\mathbf{r})$ means different amplitudes between the $\eta_{E,+}(\mathbf{r})$ and $\eta_{E,-}(\mathbf{r})$ components and thus \mathcal{T} must be broken. Fig.5(d) reveals the distribution of $\mathbf{L}(\mathbf{r})$ in the real space. The color represents the local $L_z(\mathbf{r})$ component, while the arrow length and direction represent the magnitude and direction of the in-plane components $(L_x(\mathbf{r}), L_y(\mathbf{r}))$, respectively. The distribution follows hexagonal lattices, as colored in black hexagon in Fig.5(d). Each adjacent corners of the unit cell has opposite $L_z(\mathbf{r})$ and in-plane component windings. We further normalize \mathbf{L} , defined by the unit-vector $\mathbf{n}(\mathbf{r}) = \frac{\mathbf{L}(\mathbf{r})}{|\mathbf{L}(\mathbf{r})|}$, which is shown in Fig.5e. The color shows $n_z(\mathbf{r})$ while the arrow represents the in-plane vector $(n_x(\mathbf{r}), n_y(\mathbf{r}))$ and the black hexagon denotes the unit cell. The winding structure of the $\mathbf{n}(\mathbf{r})$ field exhibits a hexagonal lattice of meron-antimeron pairs [93]. To quantify these features, we plot the local winding density $\mathcal{W}(\mathbf{r})$, defined as

$$W(\mathbf{r}) = \frac{1}{4\pi} \mathbf{n}(\mathbf{r}) \cdot \{\partial_x \mathbf{n}(\mathbf{r}) \times \partial_y \mathbf{n}(\mathbf{r})\},$$
(B208)

in Fig.5(f), which characterizes the meron-antimeron configuration. Non-zero values of $W(\mathbf{r})$ reveal a dipole structure at each corner of hexagon in Fig.5(f), suggesting that a hexagonal lattice of meron-antimeron dipoles is formed for the unit vector $\mathbf{n}(\mathbf{r})$ field. Thus, the spontaneous breaking of time-reversal symmetry in the vortex-antivortex phase can give rise to meron-antimeron-pair lattice of the normalized unit vector $\mathbf{n}(\mathbf{r})$ for the **phase 3d**.

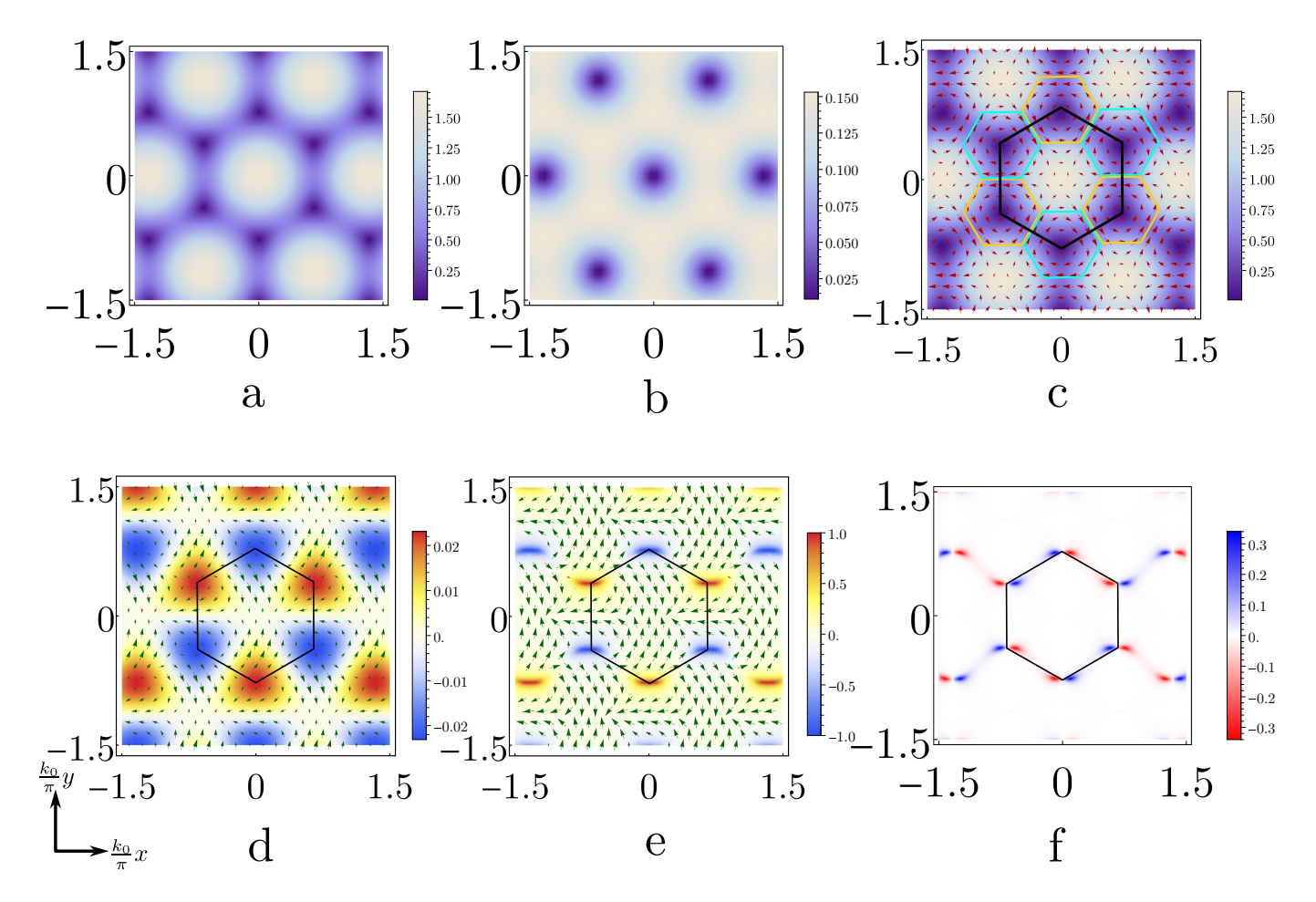


FIG. 5. The spatial distribution and angular momentum properties of the order parameter $\Psi(\mathbf{r})$ in vortex-antivortex **phase** 3d. All axes represent the x,y coordinates in scales of $\frac{\pi}{k_0}$. $\phi_1 = \phi_2 = 0$ for all settings, since these Goldstone modes only act in translation. All black hexagons represent the unit cells appearing in the corresponding quantity distributions. (a) Spatial distribution of $|\eta_A(\mathbf{r})|$ (b) Spatial distribution of $|\eta_E(\mathbf{r})|$ in Eq.(B198) (c)Spatial distribution of overall amplitude $|\Psi(\mathbf{r})|$. Arrows represent local current vector $\frac{1}{2e\gamma}\mathbf{j}_S(\mathbf{r})$ in Eq.(B201), it forms a hexagonal vortex-antivortex lattice. The bigger hexagon represents the unit cell and the yellow and cyan colored hexagonal plaquettes represent the domain of the vortices and antivortices, respectively. (d)Local distribution of intrinsic angular momenta $\mathbf{L}(\mathbf{r})$. Arrows represent the $L_x(\mathbf{r}), L_y(\mathbf{r})$ components and the color-bar represents $L_z(\mathbf{r})$ (e)Local distribution of normalized intrinsic angular momenta $\mathbf{n}(\mathbf{r})$. Arrows represent the $n_x(\mathbf{r}), n_y(\mathbf{r})$ components and the color-bar represents $n_z(\mathbf{r})$ (f) Distribution of the local winding number $\mathbf{n}(\mathbf{r}) \cdot (\partial_x \mathbf{n}(\mathbf{r}) \times \partial_\mathbf{n}(\mathbf{r}))$. For all plots, the same parameters as Fig. 1(c) in maintext is used.

Appendix C: Supercurrent and SC Diode Effect

In this section, we will calculate the supercurrent and study the SC diode effect for this pair-mixing system. We first apply the generic expression of supercurrent in Eq.(B200) to our particular ground states in the momentum space. We can characterize the motion of the Cooper pairs in the supercurrent with superfluid momentum [94] $\mathbf{q}_s = \frac{\hbar}{2(\gamma_A + \gamma_E)} \mathbf{v}_s$, where \mathbf{v}_s is the superfluid velocity and $\gamma_A + \gamma_E$ gives the effective mass of Cooper pairs. The superfluid velocity should be included in the kinetic energy terms of the GL free energy when a supercurrent is driven through a bulk superconductor, and thus we should change the free energy in Eq.(B45) to

$$\mathcal{F} \equiv \mathcal{F}(\{\mathbf{Q}_j\}, \{P_{\mathbf{Q}_j}\}) \to \mathcal{F}(\{\mathbf{Q}_j + \mathbf{q}_s\}, \{P_{\mathbf{Q}_j + \mathbf{q}_s}\}). \tag{C1}$$

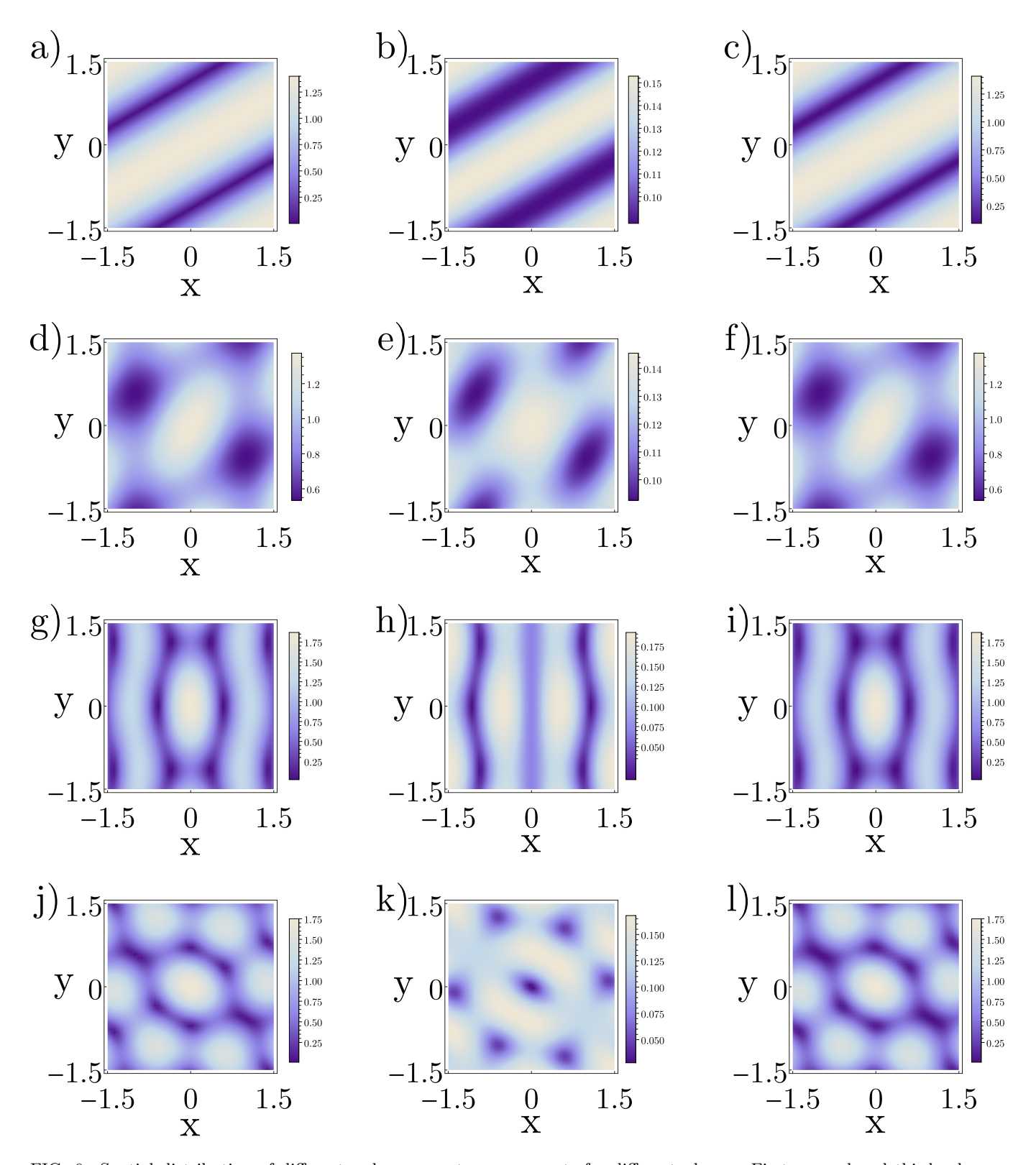


FIG. 6. Spatial distribution of different order parameter components for different phases. First, second and third columns represent $\eta_A(\mathbf{r})|, |\eta_E(\mathbf{r})|$ and $|\Psi(\mathbf{r})|$ for these phases. Figs.(a)-(c) show the order parameter amplitudes for **phase 2a** with the ground state $\frac{e^{i\theta}}{\sqrt{2}}\{1,1,0,0,0,0\}$. Figs.(d)-(f) show the order parameter amplitudes for **phase 3a** with the ground state $\frac{e^{i\theta}}{\sqrt{2}}\{\sqrt{1-u^2},\sqrt{2}u,\sqrt{1-u^2},0,0,0\}$ with u=0.3. Figs.(g)-(i) show the order parameter amplitudes for **phase 4a** with the ground state $\frac{e^{i\theta}}{\sqrt{10}}\{2,1,1,2,0,0\}$. Figs (j)-(l) show the order parameter amplitudes for **phase 4b** with the ground state $\frac{2e^{i\theta}}{5}\{1,1/2,1,0,2,0\}$. All ground state component values are chosen for illustrating the features in order parameter and are not chosen specific to any particular domain of GL parameters. All the in-plane $\{x,y\}$ coordinates are in units of π/k_0 , k_0 being the optimal momenta.

The corresponding supercurrent is given by [95]

$$\mathbf{J}_{s}(\mathbf{q}_{s}) = -\frac{d\mathcal{F}(\{\mathbf{Q}_{j} + \mathbf{q}_{s} - 2e\mathbf{A}\}, \{\alpha, \phi\})}{d\mathbf{A}} \bigg|_{\mathbf{A}=0}
= -\left[\sum_{\mathbf{Q}_{j} \in \mathcal{Q}_{6}} \frac{\partial \mathcal{F}[\{\mathbf{Q}_{j} + \mathbf{q}_{s}\}, \{\alpha, \phi\}]}{\partial \alpha_{j}} \frac{d\alpha_{j}}{d\mathbf{A}} + \frac{\partial \mathcal{F}[\{\mathbf{Q}_{j} + \mathbf{q}_{s} - 2e\mathbf{A}\}, \{\alpha, \phi\}]}{\partial \mathbf{A}} \right] \bigg|_{\mathbf{A}=0}
= -\sum_{\mathbf{Q}_{j} \in \mathcal{Q}_{6}} \frac{\partial \mathcal{F}_{min}[\{\mathbf{Q}_{j} + \mathbf{q}_{s} - 2e\mathbf{A}\}]}{\partial \mathbf{A}} \bigg|_{\mathbf{A}=0}
= 2e \sum_{\mathbf{Q}_{j} \in \mathcal{Q}_{6}} \partial_{\mathbf{q}_{s}} \mathcal{F}_{min}[\{\mathbf{Q}_{j} + \mathbf{q}_{s}\}].$$
(C2)

In the third equality, we used the fact that the α_j component for the ground state should satisfy the GL equation $\frac{\partial \mathcal{F}}{\partial \alpha_j} = 0$ so that the free energy is minimized, denoted as \mathcal{F}_{min} . With Eq.(B45), the expression for $\mathcal{F}_{min}[\{\mathbf{Q}_j + \mathbf{q}_s\}]$ can be further expanded as

$$\mathcal{F}_{min}[\{\mathbf{Q}_{j} + \mathbf{q}_{s}\}] = \sum_{j \in \mathbb{Z}_{6}} \Delta T(\mathbf{Q}_{j} + \mathbf{q}_{s}) \tilde{\alpha}_{i}^{2} + \left[c_{0} \left(\sum_{j \in \mathbb{Z}_{6}} \tilde{\alpha}_{i}^{2}\right)^{2} + c_{1} \sum_{j \in \mathbb{Z}_{6}} \tilde{\alpha}_{i}^{2} \tilde{\alpha}_{i+1}^{2} + c_{2} \sum_{j \in \mathbb{Z}_{6}} \tilde{\alpha}_{i}^{2} \tilde{\alpha}_{i+2}^{2} + c_{3} \sum_{j \in \mathbb{Z}_{6}} \tilde{\alpha}_{i}^{2} \tilde{\alpha}_{i+3}^{2}\right] (C3)$$

where $\tilde{\alpha}_i = \Delta_0 a_j$ with $\{\Delta_0, a\}$ to be different solutions discussed in Sec.B 2.

In Eq.(C3), the momentum shift \mathbf{q}_s only appears in the second order GL coefficient

$$\Delta T(\mathbf{Q}_i + \mathbf{q}_s) \approx T - T_c^{(0)}(\mathbf{k} = \mathbf{Q}_i + \mathbf{q}_s), \tag{C4}$$

with the critical temperature eigenvalue $T_c^{(0)}(\mathbf{k})$ given in Eq.(A48). Here we consider the isotropic approximation and neglect all anisotropic corrections, which is a good approximation when $|\mathbf{k}| < \sqrt{\frac{T_A}{\gamma_A'}}$ so that $T_c^{(0)}(\mathbf{k}) \gg \Delta T_c^{(1)}(\mathbf{k}), \Delta T_c^{(2)}(\mathbf{k})$.

Although the GL coefficient $\Delta T(\mathbf{Q}_j + \mathbf{q}_s)$ is isotropic in Eq.(C4), the spontaneous symmetry breaking in the SC ground state \mathcal{P} , namely $\tilde{\alpha}_i$ in Eq.(C3), can still induce the anisotropy in critical current along different directions. Using Eqs.(C2), (C3) and (C4), we find

$$|\mathbf{J}_{s}(\mathbf{q}_{s})| = \sum_{j \in \mathbb{Z}_{6}} 4 \left[T_{c,A} + T_{c,E} - |\mathbf{Q}_{j} + \mathbf{q}_{s}|^{2} (\gamma_{A}' + \gamma_{E}') + \sqrt{\left\{ T_{c,A} - T_{c,E} + |\mathbf{Q}_{j} + \mathbf{q}_{s}|^{2} (\gamma_{E}' - \gamma_{A}') \right\}^{2}} \right]$$

$$\times \left[|\mathbf{Q}_{j} + \mathbf{q}_{s}| (\gamma_{A}' + \gamma_{E}') - \frac{\left\{ T_{c,A} - T_{c,E} + |\mathbf{Q}_{j} + \mathbf{q}_{s}|^{2} (\gamma_{E}' - \gamma_{A}') \right\} 2 |\mathbf{Q}_{j} + \mathbf{q}_{s}| + 8 |\mathbf{Q}_{j} + \mathbf{q}_{s}| |\zeta_{1}'|^{2}}{\sqrt{\left\{ T_{c,A} - T_{c,E} + |\mathbf{Q}_{j} + \mathbf{q}_{s}|^{2} (\gamma_{E}' - \gamma_{A}') \right\}^{2}}} \right]$$

$$\times \left\{ -\frac{1}{2f_{\lambda}[\{c\}]} a_{\lambda,j}^{2} + \frac{1}{4(f_{\lambda}[\{c\}])^{2}} \left(c_{0} + c_{1} a_{\lambda,j}^{2} a_{\lambda,j+1}^{2} + c_{2} a_{\lambda,j}^{2} a_{\lambda,j+2}^{2} + c_{3} a_{\lambda,j}^{2} a_{\lambda,j+3}^{2} \right) \right\},$$
 (C5)

where λ labels the particular ground state we are interested in, $f_{\lambda}[\{c\}]$ is the corresponding optimizing functions and $\{a_{\lambda,j\in\mathbb{Z}_6}\}$ are the components of order parameter defined in B 2.

The critical current is defined by maximizing the magnitude of supercurrent $J_s(\mathbf{q}_s)$, which can be written as

$$J_c(\theta) = \max_{q_s} |\mathbf{J}_s(\mathbf{q}_s)|,\tag{C6}$$

for a certain momentum angle θ with $\mathbf{q}_s = q_s(\cos(\theta), \sin(\theta))$. We further define the normalized critical current,

$$\mathcal{J}(\theta) = \frac{J_c(\theta)}{J_c(0)},\tag{C7}$$

to characterize the anisotropy of critical current. The SDE efficiency η is then defined by

$$\eta = \frac{J_c(0) - J_c(\pi)}{J_c(0) + J_c(\pi)} = \frac{1 - \mathcal{J}(\pi)}{1 + \mathcal{J}(\pi)}.$$
 (C8)

We numerically evaluate $|\mathbf{J}_s(\mathbf{q}_s)|$ in Eq.(C5) and then maximize it with respect to q_s to compute the critical current $J_c(\theta)$ in Eq.(C6), from which we can extract the critical current anisotropy $\mathcal{J}(\theta)$ via Eq.(C7). The critical current anisotropy $\mathcal{J}(\theta)$ as a function of θ is shown in Fig.7 (a-g) for the **phases 1, 2a, 2c, 3a, 3d, 4a** and **4b**, respectively. Among these phases, we find $\mathcal{J}(\theta)$ remains isotropic for **phase 1**, but reveals anisotropy for all other phases (**phases 2a, 2c, 3a, 3d, 4a, 4b**). **Phase 2c** reveals a two-fold rotation symmetry. Thus, the SDE does not appear for the **phases 1** and **2c**, but exists for other phases. Among the phases with SDE, only **phase 3d** preserves three-fold rotation symmetry, while the other phases, including **phases 2a, 3a, 4a, 4b**, also break three-fold rotation. In the main text, we have discussed the normalized critical current $\mathcal{J}(\theta)$ and the SDE efficiency η for the **phase 3d**. Below we will address two questions about the features shown in Fig.7: (1) why does **phase 1a** show isotropic $\mathcal{J}(\theta)$, even though it breaks both C_{3z} and \mathcal{T} ? (2) Why does $\mathcal{J}(\theta)$ show additional mirror symmetry with the mirror line shown by red dashed lines in Fig.7, even though there is no mirror symmetry in the original free energy?

(1) The minimum free energy of the **phase 1a** is given by

$$\mathcal{F}_{min,1}(\mathbf{q}_s) = -\frac{\Delta T(\mathbf{Q}_0 + \mathbf{q}_s)^2}{4c_0},\tag{C9}$$

from which we can derive the supercurrent from Eq.(C5)

$$|\mathbf{J}_{s}(\mathbf{q}_{s})| = \frac{1}{c_{0}} \left[T_{c,A} + T_{c,E} - |\mathbf{Q}_{0} + \mathbf{q}_{s}|^{2} (\gamma'_{A} + \gamma'_{E}) + \sqrt{\left\{ T_{c,A} - T_{c,E} + |\mathbf{Q}_{0} + \mathbf{q}_{s}|^{2} (\gamma'_{E} - \gamma'_{A}) \right\}^{2}} \right]$$

$$\times \left[|\mathbf{Q}_{0} + \mathbf{q}_{s}| (\gamma'_{A} + \gamma'_{E}) - \frac{\left\{ T_{c,A} - T_{c,E} + |\mathbf{Q}_{0} + \mathbf{q}_{s}|^{2} (\gamma'_{E} - \gamma'_{A}) \right\} 2 |\mathbf{Q}_{0} + \mathbf{q}_{s}| + 8 |\mathbf{Q}_{0} + \mathbf{q}_{s}| |\zeta'_{1}|^{2}}{\sqrt{\left\{ T_{c,A} - T_{c,E} + |\mathbf{Q}_{0} + \mathbf{q}_{s}|^{2} (\gamma'_{E} - \gamma'_{A}) \right\}^{2}}} \right]. (C10)$$

The function $|\mathbf{J}_s(\mathbf{q}_s - \mathbf{Q}_0)|$ is isotropic across different directions θ of $\mathbf{q}_s - \mathbf{Q}_0$. Hence, one can say that the critical current for this particular shifted current is independent of θ , i.e.-

$$\tilde{J}_c = \max_{\mathbf{q}_s - \mathbf{Q}_0} |\mathbf{J}_s(\mathbf{q}_s - \mathbf{Q}_0)|. \tag{C11}$$

Here, we implicitly assume that the maximum occurs at some $|\mathbf{q}_s| > |\mathbf{Q}_0|$. Following the definition of $J_c(\theta)$ in Eq.(C6), we can see that

$$J_c(\theta) = \max_{q_s} |\mathbf{J}_s(\mathbf{q}_s)| = \max_{|\mathbf{q}_s - \mathbf{Q}_0|} |\mathbf{J}_s(\mathbf{q}_s - \mathbf{Q}_0)| = \tilde{J}_c$$
 (C12)

Thus, one see that $J_c(\theta)$, and subsequently $\mathcal{J}(\theta)$ is isotropic for **phase 1** in Fig.7a. For other phases, multiple \mathbf{Q}_j components contributing to the $\mathcal{F}_{min}(\mathbf{q}_s)$ so that the above argument is no longer valid and the critical current anisotropy generally exists.

(2) Next we will discuss the emergent mirror symmetry by the red dashed lines shown in Fig.7. Since the orientation of the mirror axis is different for different phases, we first give a general definition of the mirror symmetry. The mirror symmetry $\mathcal{M}_{\theta_{||}}^{||}$ is defined for a mirror plane perpendicular to our 2D system containing the axis parallel to an arbitrary azimuthal direction $\theta_{||}$ in the 2D plane. This acts on any general pairing momentum \mathbf{q} as

$$\mathcal{M}_{\theta_{\parallel}}^{\parallel} : \tilde{\mathbf{q}} = R_z[\theta_{\parallel} - \theta_{\mathbf{q}}]\mathbf{q} = q\{\cos(2\theta_{\parallel} - \theta_{\mathbf{q}}), \sin(2\theta_{\parallel} - \theta_{\mathbf{q}})\}; \quad \mathbf{q} = q\{\cos(\theta_{\mathbf{q}}), \sin(\theta_{\mathbf{q}})\},$$
(C13)

where $R_z(\phi)$ denotes the operation of rotation by angle ϕ along the z-axis. Let us take the example of **phase 2a** to demonstrate how it has this emergent symmetry for $\theta_{\parallel} = \frac{\pi}{6}$. First we write down the minimum energy for this phase,

$$\mathcal{F}_{min,2a}(\tilde{\mathbf{q}}_s) = \frac{(\Delta T(\mathbf{Q}_0 + \tilde{\mathbf{q}}_s))^2 + (\Delta T(\mathbf{Q}_1 + \tilde{\mathbf{q}}_s))^2}{8c_0 + 2c_1}.$$
 (C14)

We see the momentum dependence in this minimum free energy manifests in $\Delta T(\mathbf{Q}_j + \mathbf{q}_s)$ for j = 0, 1. Following

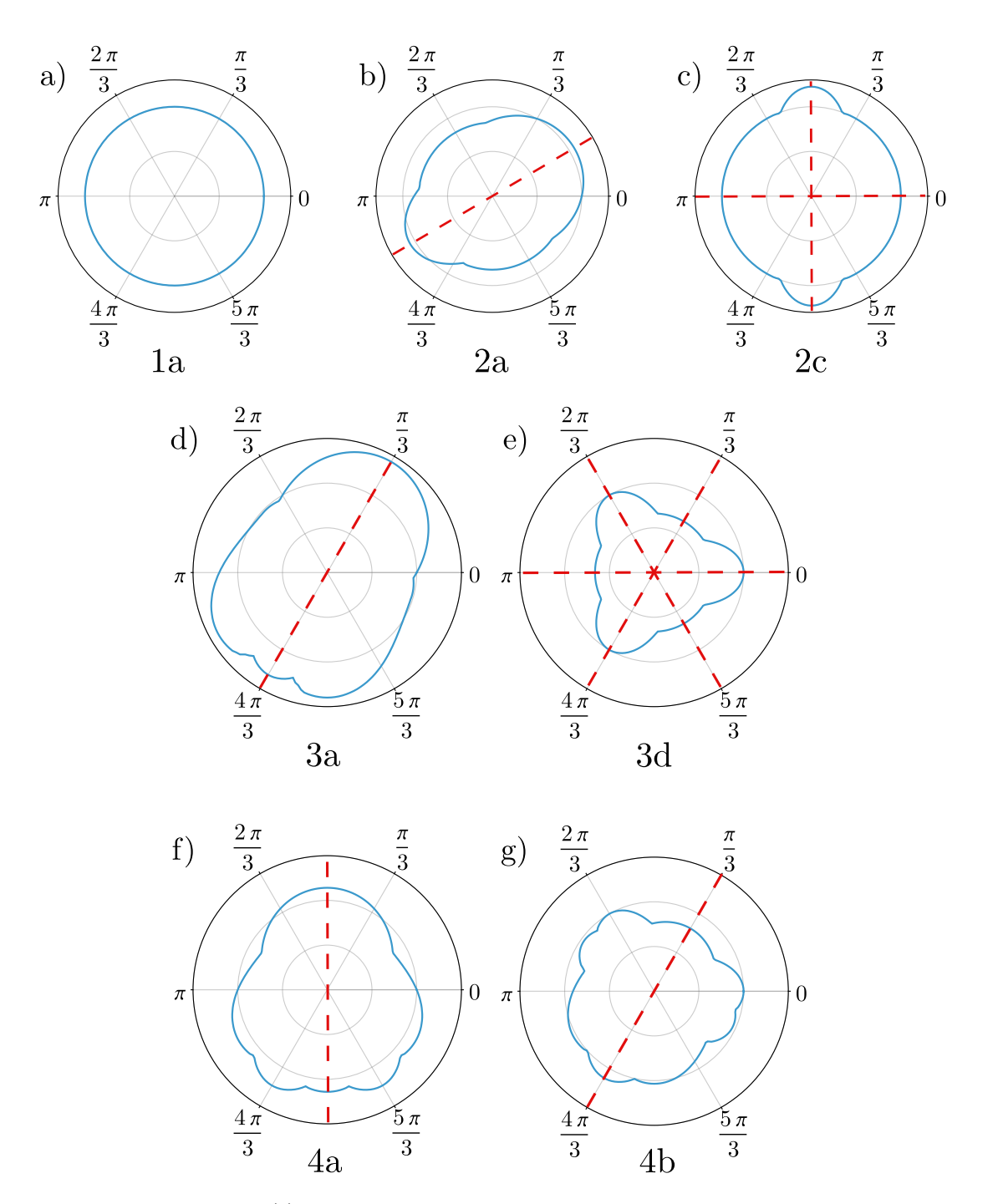


FIG. 7. Normalized critical current $\mathcal{J}(\theta)$ as a function of θ for different Superconductor phases. Each panel is labeled by the ansatze index $\lambda \in \mathcal{Y}$. The red dashed lines represent the additional mirror symmetry axes of $\mathcal{J}(\theta)$.

from Eq.(C4) and referring to the definition of $T_c^{(0)}(\mathbf{Q}_j + \mathbf{q}_s)$ in Eq.(A42), we see that $\Delta T(\mathbf{Q}_j + \mathbf{q}_s)$ is a polynomial function of quadratic terms $(\mathbf{Q}_j + \mathbf{q}_s)^2$. Expanding this expression gives

$$(\mathbf{Q}_j + \mathbf{q}_s)^2 = k_0^2 + q_s^2 + 2k_0 q_s \cos\left(\frac{j\pi}{3} - \theta_{\mathbf{q}_s}\right); \quad \mathbf{q}_s = q_s \{\cos(\theta_{\mathbf{q}_s}), \sin(\theta_{\mathbf{q}_s})\} \quad \forall j \in \mathbb{Z}_6.$$
 (C15)

With $\mathcal{M}_{\pi/6}^{||}$, $\mathcal{F}_{min,2a}(\mathbf{q}_s)$ becomes $\mathcal{F}_{min,2a}(\tilde{\mathbf{q}}_s)$, the transformation of this energy will be dictated by the transformation

of \mathbf{q}_s in $(\mathbf{Q}_j + \mathbf{q}_s)^2$ for j = 0, 1. From Eq.(C13), for $\theta_{\parallel} = \frac{\pi}{6}$, the transformations are

$$\mathcal{M}_{\pi/6}^{||}: (\mathbf{Q}_{0} + \tilde{\mathbf{q}}_{s})^{2} = k_{0}^{2} + q_{s}^{2} + 2k_{0}q_{s}(\pi/3 - \theta_{\mathbf{q}_{s}}) = (\mathbf{Q}_{1} + \mathbf{q}_{s})^{2} \Rightarrow \Delta T(\mathbf{Q}_{0} + \tilde{q}_{s}) = \Delta T(\mathbf{Q}_{1} + \tilde{q}_{s})$$

$$\mathcal{M}_{\pi/6}^{||}: (\mathbf{Q}_{1} + \tilde{\mathbf{q}}_{s})^{2} = k_{0}^{2} + q_{s}^{2} + 2k_{0}q_{s}(\theta_{\mathbf{q}_{s}}) = (\mathbf{Q}_{0} + \mathbf{q}_{s})^{2} \Rightarrow \Delta T(\mathbf{Q}_{1} + \tilde{q}_{s}) = \Delta T(\mathbf{Q}_{0} + \tilde{q}_{s}), \tag{C16}$$

and thus, we find

$$\mathcal{M}_{\pi/6}^{||}: \quad \mathcal{F}_{min,2a}(\tilde{\mathbf{q}}_s) = \frac{(\Delta T(\mathbf{Q}_0 + \tilde{\mathbf{q}}_s))^2 + (\Delta T(\mathbf{Q}_1 + \tilde{\mathbf{q}}_s))^2}{8c_0 + 2c_1}$$
 (C17)

$$= \frac{(\Delta T(\mathbf{Q}_1 + \mathbf{q}_s))^2 + (\Delta T(\mathbf{Q}_0 + \mathbf{q}_s))^2}{8c_0 + 2c_1} = \mathcal{F}_{min,2a}(\mathbf{q}_s).$$
 (C18)

Thus, we prove that the minimum free energy of **phase 2a** in Eq.(C17) remains invariant under this emergent mirror symmetry, which does not exist in our original free energy in Eq.(B45). From Eq.(C2), this $\mathcal{M}_{\pi/6}^{||}$ symmetry of $\mathcal{F}_{min,2a}(\mathbf{q}_s)$ gets inherited by the corresponding supercurrent $\mathbf{J}_s(\mathbf{q}_s)$ and consequently, shows up in $\mathcal{J}(\theta)$ shown in Fig.7(b) for **phase 2a**. Under similar arguments, **Phase 2c** will also show mirror symmetry $\mathcal{M}_{0,\frac{\pi}{2}}^{||}$ in Fig.7(c), **Phase 3a** and **Phase 4b** have the mirror $\mathcal{M}_{\frac{\pi}{3}}^{||}$ in Fig.7(d) and (g), respectively, **Phase 3d** shows three mirror axes, i.e.- $\mathcal{M}_{0,\frac{\pi}{3},2\frac{\pi}{3}}^{||}$ in Fig.7(e), and **Phase 4a** will have $\mathcal{M}_{\frac{\pi}{2}}^{||}$ symmetry in Fig.7(f). These different critical current patterns of $\mathcal{J}(\theta)$ will allow us to distinguish these different SC phases.